Molecular characterization of the lipidome by mass spectrometry

DISSERTATION

zur Erlangung des akademischen Grades

Doctor rerum naturalium

(Dr. rer. nat.)

vorgelegt

der Fakultät für Biologie und Naturwissenschaften
der Technische Universität Dresden

von

Master of Science,

Christer Stenby Ejsing

Geboren am 10. August 1976 in Gentofte, Dänemark

Gutachter: Prof. Dr. Kai Simons (Technische Universität Dresden)
Prof. Dr. Bernard Hoflack (Technische Universität Dresden)
Prof. Dr. Michael Karas (Johann Wolfgang Goethe-Universität)

Eingereicht am: 16. October 2006
Tag der Verteidigung: 13. Februar 2007

SUMMARY

Cells, whether bacterial, fungal or mammalian, are all equipped with metabolic pathways capable of producing an assortment of structurally and functionally distinct lipid species. Despite the structural diversity of lipids being recognized and correlated to specific cellular phenomena and disease states, the molecular mechanisms that underpin this structural diversity remain poorly understood. In part, this is due to the lack of adequate analytical techniques capable of measuring the structural details of lipid species in a direct, comprehensive and quantitative manner. The aim of my thesis study was to establish methodology for automated and quantitative analysis of molecular lipid species based on mass spectrometry. From this work a novel high-throughput methodology for lipidome analysis emerged. The main assets of the methodology were the structure-specific mass analysis by powerful hybrid mass spectrometers with high mass resolution, automated and sensitive infusion of total lipid extracts by a nanoelectrospray robot, and automated spectral deconvolution by dedicated Lipid Profiler software. The comprehensive characterization and quantification of molecular lipid species was achieved by spiking total lipid extracts with unique lipid standards, utilizing selective ionization conditions for sample infusion, and performing structure-specific mass analysis by hybrid quadrupole time-of-flight and ion trap mass spectrometry. The analytical routine allowed the comprehensive characterization and quantification of molecular glycerophospholipid species, molecular diacylglycerol species, molecular sphingolipid species including ceramides, glycosphingolipids and inositol-containing sphingolipids, and sterol lipids including cholesterol.

The performance of the methodology was validated by comparing its dynamic quantification range to that of established methodology based on triple quandrupole mass spectrometry. Furthermore, its efficacy for lipidomics projects was demonstrated by the successful quantitative deciphering of the lipid composition of T cell receptor signaling domains, mammalian tissues including heart, brain and red blood cells, and the yeast *Saccharomyces cerevisiae*.

TABLE OF CONTENTS

LIST OF ABBREVIATIONS

Cer/$[Cer]^-$	- used for the annotation of ceramide species or designating ceramide-specific fragment ions
$[CerP]^-$	- used to designate ceramide phosphate-specific fragment ions
Da	- Dalton
FA	- fatty acid
FWHM	- Full Width at Half Maximum,
-I	- used to designate fragment ions produced by neutral loss of inositol
$[IP]^-$	- inositolphosphate fragment ion
IPC	- inositolphosphoceramide
$[LCBP]^-$	- used for designating long chain base phosphate-specific fragment ions
LPC	- lysophosphatidylcholine
LTQ Orbitrap	- hybrid linear ion trap Orbitrap mass spectrometer.
m/z	- mass per charge ratio
MS	- mass spectrometry
MS/MS	- tandem mass spectrometry
MS^n	- multi-stage mass spectrometry
MIPC	- mannosyl-inositolphosphoceramide
$[MIP]^-$	- mannosyl-inositolphosphate fragment ion
$M(IP)_2C$	- mannosyl-diinositolphosphoceramide
$[M(IP)_2]^{2-}$	- doubly charged mannosyl-diinositolphosphate fragment ion
MPIS	- multiple precursor ion scanning
MRM	- multiple reaction monitoring
-P	- used to designate fragment ions produced by neutral loss of phosphate
PA	- phosphatidic acid
PC	- phosphatidylcholine
PE	- phosphatidylethanolamine
PG	- phosphatidylglycerol
PI	- phosphatidylinositols
PIS	- precursor ion scanning; PIS *m/z* 281.3 stands for scanning for precursor ions that produce a fragment ion with *m/z* 281.3 upon collision-induced dissociation
PLA_2	- phospholipase A_2
ppm	- parts per million
PS	- phosphatidylserine
PX FA_i/FA_j	- PX molecule with FA_i moiety on the *sn*-1 position of the glycerol phosphate backbone, and FA_j moiety on the *sn*-2 position
PX FA_i-FA_j	- PX molecule (or a mixture of isomeric molecules) comprising FA_i-FA_j on unidentified positions of the glycerol phosphate backbone
QqTOF	- quadrupole time-of-flight mass spectrometer, “q” stands for a RF-only quadrupole of the collision cell
SM	- sphingomyelin
TLC	- thin-layer chromatography
TOF	- time-of-flight

INDEX OF FIGURES

INDEX OF TABLES

1. INTRODUCTION

1.1. LIPIDOMICS

The crucial role of lipids in cell, tissue and organ physiology is evident by their unique membrane organizing properties that provide cells with functionally distinct subcellular membrane compartments (*e.g.* endoplasmatic reticulum, Golgi apparatus, secretory vesicles, plasma membrane, etc.), their functional role in cell signaling (*e.g.* phospholipase C and phospholipase A_2 in modulating immunological responses), their endocrine actions (*e.g.* steroid hormones), and their essential role for energy production and energy storage (Vance and Vance, 1996). Cells, whether bacterial, fungal or mammalian, are all equipped with metabolic pathways capable of producing an assortment of structurally and functionally distinct lipid species by combining a variety of apolar fatty acid (FA) or fatty alcohol moieties with different backbone structures (*i.e.* glycerol phosphate and long chain bases) and various head groups. In mammalian cell membranes the total number of molecular lipid species may well exceed thousands (van Meer, 2005).

Although the chemical diversity of lipids is well appreciated and has been correlated to specific cellular phenomena and disease states (Casserly and Topol, 2004; Ikonen and Holtta-Vuori, 2004; Serhan and Savill, 2005; Simons and Ehehalt, 2002), the molecular mechanisms that underpin this diversity remain poorly understood. In part, this is due to the lack of adequate analytical techniques capable of measuring the structural details of lipid species in a direct, comprehensive and quantitative manner. Novel analytical approaches, in particular the mass spectrometry-based techniques, are emerging for the system-level analysis of lipid species and are set to define the cell biological and physiological functions of the lipid species heterogeneity.

Lipidomics can be defined as the system-level analysis and characterization of lipids and their interaction partners (van Meer, 2005; Wenk, 2005). A "lipidome" is the comprehensive and quantitative description of a set of lipid species; for example constituting a cell (thereby termed cellular lipidome). Lipidomics is a subgroup within the field of metabolomics. Furthermore, lipidomics can be subdivided into membrane-lipidomics and mediator-lipidomics (Serhan, 2005) which address either the comprehensive and quantitative description of membrane lipid constituents, or the structural characterization and quantification of low abundant bioactive lipid species, respectively.

1.1.1. Classification and chemistry of lipids

Lipids can be classified into 8 classes based on their chemical structure: fatty acyls, glycerolipids, glycerophospholipids, sphingolipids, sterol lipids, prenol lipids, saccharolipids, and polyketides (Fahy *et al.*, 2005). Pertinent to this thesis work are the three main classes of membrane lipids: glycerophospholipids, sphingolipids and sterol lipids.

Glycerophospholipids are the major components of biological membranes, and have inherent biological activities by acting as second messengers themselves or as precursors for the generation of second messengers (Vance and Vance, 1996). Glycerophospholipids consist of a glycerol phosphate backbone with a head group attached at the *sn*-3 position, and FA or fatty alcohol moieties attached to the remaining two positions via ester or ether bonds, respectively. Seven classes of glycerophospholipids are commonly recognized based on the chemical structure of the head group: phosphatidic acid (PA), phosphatidylserine (PS), phosphatidylglycerol (PG), cardiolipin, phosphatidylcholine (PC), phosphatidylethanolamine (PE), and phosphatidylinositol (PI) (Figure 1).

Glycerophospholipids with an ether or vinyl-ether linked fatty alcohol moiety at the *sn-1* position are subdivided into plasmanyl species and plasmenyl species (also termed plasmalogens), respectively (Figure 1) (IUPAC-IUB, 1978; Nagan and Zoeller, 2001). In mammalians, ether linkages occur predominantly in PCs and PEs. Plasmanyl species typically exist as PC species, whereas plasmenyl species mainly exist as PE species with the exception of the heart where plasmenyl PC species predominate (Vance and Vance, 1996). The main significance of ether species relate to the production of platelet activating factor (1-alkyl-2-acetyl-PC) and its concomitant implication in blood coagulation and inflammatory responses. Lysospecies exist having only one FA or fatty alcohol moiety attached to the glycerol phosphate backbone (Figure 1). Lysospecies occur as intermediates in glycerophospholipid biosynthesis, and function as second messengers.

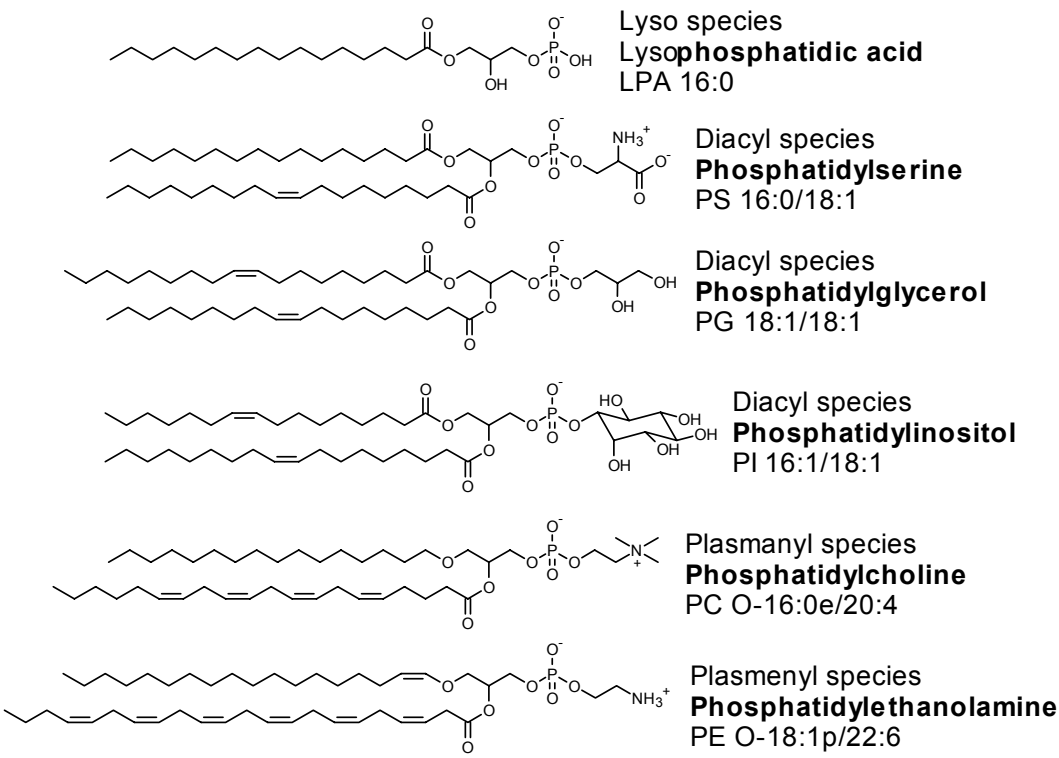

Figure 1. Chemical structures of glycerophospholipid species.

Sphingolipids are found in essentially all animals, plants and fungi. This lipid class can be divided into several classes. Pertinent to this thesis are the long chain bases (also termed sphingoid bases) which are the common structural feature of all sphingolipids, ceramides (Cers), phosphosphingolipids (including sphingomyelin (SM)), neutral glycosphingolipids and acidic glycosphingolipids (Figure 2). More than 300 different types of acidic glycosphingolipids have been reported, and this does not include the structural heterogeneity of the ceramide backbone. Members of this lipid class play vital roles in membrane organization, biological recognition and signal transduction. SMs and the glycosphingolipids contribute to the formation of membrane microdomains (also termed lipid rafts) based on their interaction with sterols (Simons and Vaz, 2004). The structure of the carbohydrate moieties of the complex glycosphingolipids serve as signature for cell types, mediate specific interactions with extracellular matrix proteins and receptors, and are used by viruses, bacteria and bacterial toxins to attach and enter cells (Vance and Vance, 1996). Finally, long chain bases and long chain base phosphates, as well as ceramide and ceramide phosphates, can serve as first and second messengers in signal transduction cascades (Futerman and Hannun, 2004).

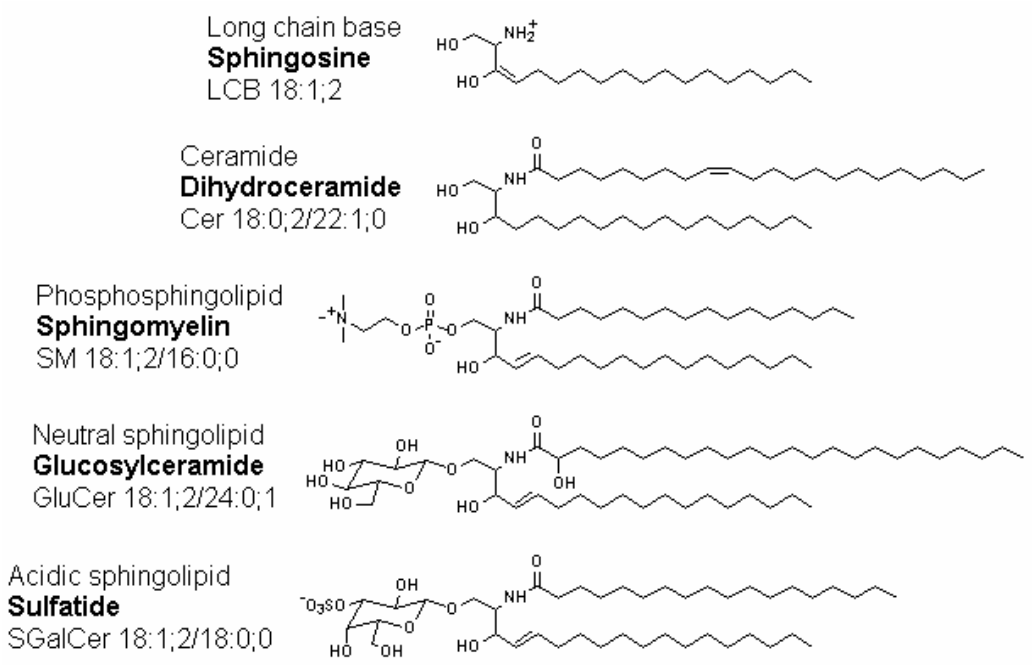

Figure 2. Chemical structure of common sphingolipids.

Sterol lipids (Figure 3), of which cholesterol and its derivatives are the most widely studied in mammalian systems, constitute an important component of membrane lipids. In addition, this structurally complex lipid class is implicated in numerous physiological functions including hormonal actions (steroid hormones), digestive processes (bile acids), tissue development (Eaton, 2006) and regulating cell membrane permeability (Haines, 2001). In addition to cholesterol, there are many unique sterols in plant, fungal and marine sources (Vance and Vance, 1996).

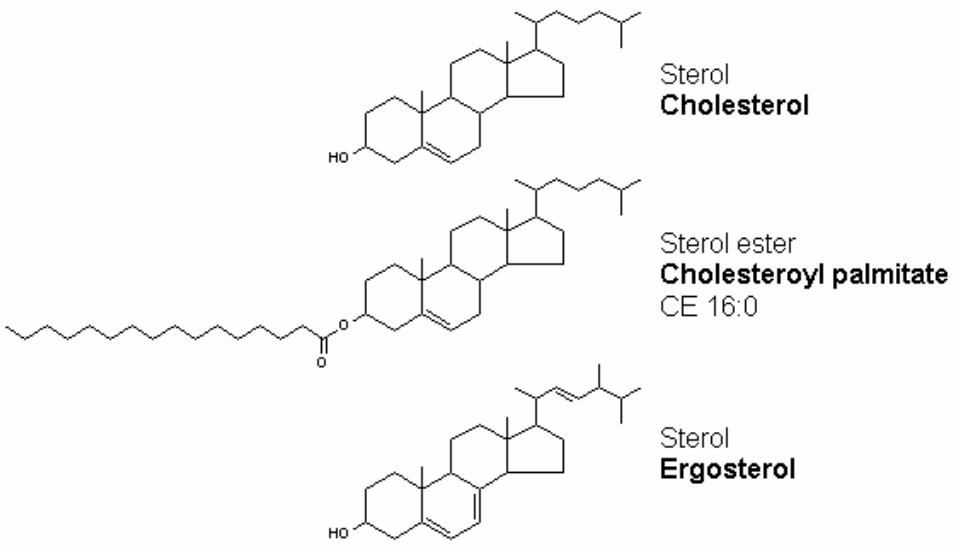

Figure 3. Chemical structure of common sterol lipids.

1.2. MASS SPECTROMETRIC LIPID ANALYSIS

In order to gain further insights into the molecular mechanisms that underpin the lipid species diversity of biological membranes, the application of analytical methodology capable of measuring the structural details of lipid species in a direct, comprehensive and quantitative manner is required. Conventional analytical technologies for lipid analysis such as high-performance liquid chromatography, thin-layer chromatography (TLC), and gas chromatography are only applicable for the characterization of global perturbations of lipid composition or target analysis of radioactively or fluorescently labeled species (Blank *et al.*, 1984; Connor *et al.*, 1997; Kuypers *et al.*, 1991). These techniques are time-consuming, labor-intensive, require relatively large amount of sample, and can be prone to biased losses of certain types of lipids (DeLong *et al.*, 2001). Improvements in mass spectrometric technology have proved highly efficient for the characterization and quantification of molecular lipid species in total lipid extracts (Reviewed by Griffiths, 2003; Han and Gross, 2005; Merrill *et al.*, 2005; Murphy *et al.*, 2001; Pulfer and Murphy, 2003). This methodology is less time-consuming compared to that of conventional methods, and requires less sample amount because of its higher sensitivity and specificity.

1.2.1. Fundamentals of mass spectrometry

Mass spectrometry is a method that measures the mass-to-charge ratio (*m/z*, can be measured in Dalton (Da)) of molecular ions and detects their intensity. The data generated by a mass spectrometer is represented by a mass spectrum having the *m/z* of molecular ions on the abscissa and their intensity on the ordinate (Figure 17A page 42). By mass spectrometry, the accurate mass estimate of a given molecular ion, the abundance, and, in the case of tandem or multiple-stage (MS^n) mass spectrometry, structural information can be obtained.

There are three main components of a mass spectrometer: an ion source, mass analyzers, and an ion detector (Figure 4). The ion source serves to generate molecular ions in gas phase (*e.g.* by electron impact, electrospray ionization). The molecular ions are focused and transported by ion optics into the mass analyzers which separate the ions according to their *m/z* prior to their final registration by an ion detector. All components are operated by dedicated electronics and a computer. The mass analyzer and ion detector sections are operated at low pressures to allow unperturbed transmission and detection of the gas phase ions (*i.e.* in the range of 10^{-2} to 10^{-7} Torr).

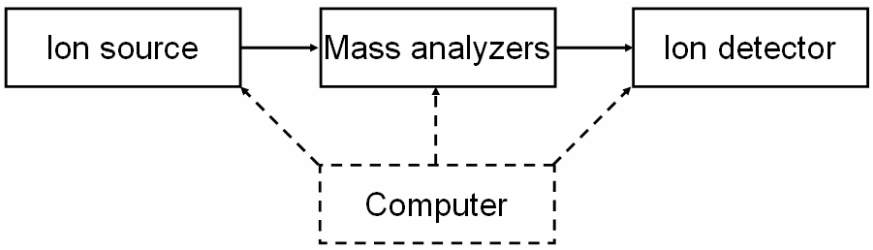

Figure 4. Typical components of a mass spectrometer include an ionization source, a section of mass analyzers, and an ion detector. The components are operated by electronics and a computer.

Electrospray ionization is a commonly used method for the mass spectrometric analysis of glycerophospholipids and sphingolipids. The basics of electrospray ionization are reviewed by Cole (2000). Electrospray ionization generates molecular ions at atmospheric pressure by passing a sample in solution through a small capillary at a low flow rate (1-300 μl/min). The application of a strong electric field (1-4 kV) results in electrolytic processes within the capillary and an electrical field at the apex of the capillary, which produces a fine spray of charged droplets. A series of fission events ultimately leads to the production of smaller droplets that bear an excess charge and a single molecule. Inevitably, single molecules will become charged as the remaining solvent evaporates (Figure 5). The electrospray ionization process produces ions primarily *via* protonation (in positive ion mode) or deprotonation (in negative ion mode), or *via* the formation of adduct cations (*e.g.* Li^+) or adduct anions (*e.g.* Cl^-).

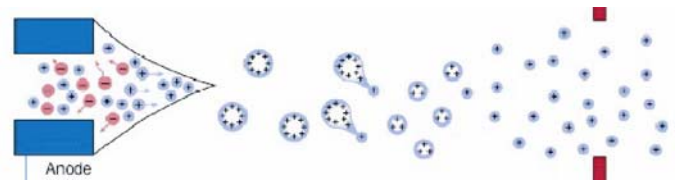

Figure 5. Schematic of electrospray ionization in positive ion mode.

Electrospray ion sources can be combined with mass spectrometers having distinct types of mass analyzers such as quadrupole, ion trap, time-of-flight (TOF), Fourier transform ion cyclotron resonance and orbitrap. Each type of mass analyzer and concomitant ion detector has its specific analytical advantages. Importantly, all analyzers differ in the speed by which they produce mass spectra, their mass accuracy (the error of the estimated *m/z* value compared to the calculated *m/z* value) and mass resolution (which can be defined as Δm being the full width of a peak at half its maximum (FWHM) height).

Quadrupole mass analyzers are ion beam analyzers. These devices are usually composed of four rods with cylindrical geometry arranged in a specific three-dimensional

orientation (Figure 6A). By applying a combination of direct current and relative frequency voltages to the rods, ions can be transmitted through the quadrupole mass analyzer. The analyzer can be operated in three modes, depending on the selection of voltages and frequencies: (i) all ions with *m/z* within a certain interval (*e.g.* 200 to 1000) can be transmitted simultaneously, (ii) ions of a given *m/z* ratio can traverse the analyzer, whereas ions with different *m/z* ratios collide with the rods and are lost, or (iii) ions of increasing *m/z* can be made to pass successively through the analyzer in small intervals (*e.g.* 0.1 to 0.2 Da). In the last mentioned operation mode, the quadrupole mass analyzer is said to be scanning, and is the basis of precursor ion scanning (PIS) technology (*q.v.* additional details below).

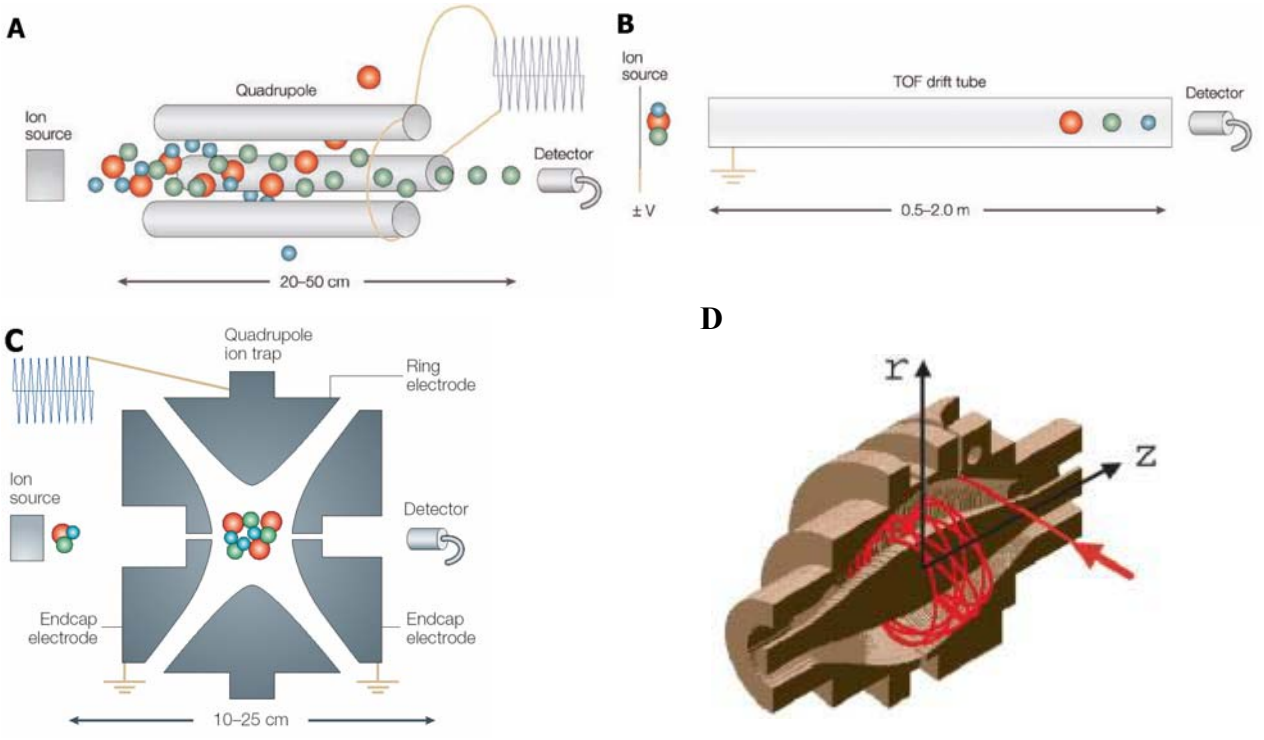

Figure 6. Schematic overview of mass analyzers. **(A)** Quadrupole mass analyzer. The top rod is not shown since the view is from above. **(B)** TOF analyzer. **(C)** Quadrupole ion trap mass spectrometer. The ion trap analyzer is composed of the two end-cap electrodes and the ring electrode. **(D)** Cutaway view of the orbitrap mass analyzer. Picture is adapted from (March, 1997) and (Hu *et al.*).

The **TOF analyzer** is a relatively simple device (Figure 6B). In this type of analyzer, ions are pulse-accelerated into a TOF drift tube. Based on difference in obtained velocity, ions will be separated according to *m/z*. Since all ions acquire the same energy during the pulse, ions of lower *m/z* ions achieve higher velocities than the higher *m/z* ions. Thus, the *m/z* of ions can be determined by measuring the time it takes for the ions to travel a fixed distance.

Quadrupole ion trap mass analyzers are composed of two end-cap electrodes and one ring electrode (Glish and Vachet, 2003; March, 1997) (Figure 6C). Ions are injected in the trap over a short period of time and are then maintained in stable orbits within the trap by

means of electrostatic fields. By changing the voltages on the electrodes, and thereby the electric fields, the orbits of ions can be made unstable in an *m/z* selective manner. By correct choice of voltages, ions can be ejected for either detection, or the isolation of ions of a given *m/z*. Isolated ions can subsequently be subjected to collision-induced dissociation, and produce fragment ions that can then be trapped in the analyzer (MS^2). Fragment ions can be ejected for either detection or for another round of ion isolation and collision-induced dissociation (MS^3). This operational feature, termed multi-stage mass spectrometry, can be repeated virtually an unlimited number of times (MS^n), and therefore makes the quadrupole ion trap mass analyzer suitable for detailed structural characterization of analyte ions. **Linear quadrupole ion trap analyzers** are similar to the quadrupole ion trap, but traps ions in a two dimensional quadrupole field, instead of the three dimensional quadrupole field.

The **Fourier transform ion cyclotron resonance mass analyzer** measures mass by detecting the image current produced by ions cyclotroning in a magnetic field. Ions are injected (guided by a quadrupole or ion trap mass analyzer) and trapped in a so-called Penning trap where an oscillating electric field perpendicular to the magnetic field excites them to cyclotron in phase (in a ion packet). Detectors at fixed positions measure the electric image of the ion packets which pass in time and produce a cyclical signal. Since the signal frequency of ions is determined by the *m/z* ratio, this signal can be deconvoluted by performing a Fourier transform on the signal. Fourier transform ion cyclotron resonance mass spectrometry is a high mass accuracy and resolution technique. Molecular ions can be measured with a mass resolution of 500.000 (FWHM) and provides a mass accuracy in the low ppm range.

The **orbitap** is the most recently introduced mass analyzer (commercially available since 2005). In the orbitrap, ions are trapped in an orbit around a central, spindle-shaped electrode (Figure 6D). The electrode confines the ions so that they both orbit around the central electrode and oscillate back and forth along the axis of the electrode. This oscillation generates an image current in the detectors. Since the frequencies of these image currents depends on the *m/z* ratio, mass spectra can be obtained by Fourier transformation of the recorded signals. Similar to the Fourier transform ion cyclotron resonance mass analyzer, the orbitrap measure ions with high mass accuracy and resolution (100.000 FWHM).

1.2.2. Lipid analysis by electrospray ionization mass spectrometry

Electrospray ionization mass spectrometry is an established and powerful tool for the characterization and quantification of molecular lipid species in total lipid extracts (Han and Gross, 1994; Han and Gross, 1995; Kerwin *et al.*, 1994). The specificity and reliability of this

methodology was improved by the use of PIS and neutral loss scanning technology (Brugger *et al.*, 1997). Applying this technology allowed the specific detection of molecular ions (precursor ions) that upon collision-induced dissociation release characteristic fragment ions. In positive ion mode PCs and SMs are readily detected as protonated molecular cations. Upon collision-induced dissociation these ions generate a characteristic fragment ion of the phosphorylcholine head group having *m/z* 184.07. Performing PIS *m/z* 184.1 on a triple quadrupole mass spectrometer allowed the quantitative profiling of molecular PC and SM species at the low nM concentration range (Brugger *et al.*, 1997). Collision-induced dissociation of cationic molecular PE and PS species promote the specific neutral loss of their head group moiety (*e.g.* neutral loss of 141 by PE species) which prompted their quantitative profiling by neutral loss scanning (Brugger *et al.*, 1997). Notably, all glycerophospholipids except for PCs are preferentially ionized as negatively charged molecular anions. Upon collision-induced dissociation in negative ion mode, anionic glycerophospholipid species produce acyl anions corresponding to the FA moieties attached to the glycerol phosphate backbone (Hsu and Turk, 2000a; Hsu and Turk, 2000b; Hsu and Turk, 2000c; Hsu and Turk, 2001). This prompted the use of PIS technology for quantitative and direct profiling of the FA constituents molecular glycerophospholipid species (Beckedorf *et al.*, 2002; Ekroos *et al.*, 2002; Han *et al.*, 2004). Similar approaches have been applied for the molecular characterization and quantification of sphingolipids (Gu *et al.*, 1997; Han, 2002; Liebisch *et al.*, 1999).

Electrospray ionization mass spectrometry has been successfully applied in studies of lipid composition (Blom *et al.*, 2001; Brugger *et al.*, 1999; Brugger *et al.*, 2006; Brugger *et al.*, 2004; Fridriksson *et al.*, 1999; Rodemer *et al.*, 2003; Schneiter *et al.*, 1999), lipid trafficking (Heikinheimo and Somerharju, 2002), and lipid metabolism (Boumann *et al.*, 2003; Boumann *et al.*, 2004; Brooks *et al.*, 2002; DeLong *et al.*, 1999; Hunt *et al.*, 2002). Interestingly, the studies on lipid metabolism allowed the monitoring of enzyme substrate specificity and FA remodelling *in vivo.* The use of stable isotope labeled precursors of PC metabolism was used to demonstrate that the two pathways for PC synthesis produce different molecular species in both mammalians and yeast (Boumann *et al.*, 2003; Boumann *et al.*, 2004; DeLong *et al.*, 1999).

1.2.3. The hybrid quadrupole time-of-flight (QqTOF) mass spectrometer

Mass spectrometric lipid analysis has been developed successfully using triple quadrupole and ion trap mass spectrometers. However, novel hybrid instrumentations which combine the analytical advantages of different mass analyzers are emerging as powerful tools

for lipid analysis due to their higher sensitivity, mass accuracy and mass resolution. Recently, a hybrid QqTOF mass spectrometer (Chernushevich *et al.*, 2001) combined with a nanoelectrospray ion source was successfully applied for comprehensive lipidome analysis (Ekroos *et al.*, 2002). Contrary to triple quadrupole mass spectrometers which only allow the acquisition of a single precursor ion scan at the time, QqTOF mass spectrometers can acquire a virtually unlimited number of precursor ion spectra due to the TOF analyzer. This multiple precursor ion scanning (MPIS) technology was demonstrated to be an efficient tool for the simultaneous and quantitative profiling of the FA composition of molecular glycerophospholipid in total lipid extracts (Ekroos *et al.*, 2002; Kuerschner *et al.*, 2005). Furthermore, the sensitivity of this instrumentation was similar to that of conventional triple quadrupole mass spectrometers (Brugger *et al.*, 1997; Liebisch *et al.*, 2004).

The basic components the QqTOF mass spectrometers are three consecutively aligned quadrupole mass analyzers, a reflecting TOF analyzer, and a multiple anode detector combined with a multichannel time-to-digital converter (Figure 7) (Chernushevich *et al.*, 2001). The configuration of the mass analyzers can be regarded as the replacement of the third quadrupole mass analyzer in a triple quadrupole mass spectrometer by a TOF analyzer. The three quadruples of the QqTOF mass spectrometer have independent functions. The first quadrupole (Q0) serves to focus and transfer ions originating from the ion source, the second (Q1) is a mass filter quadrupole that can separate ions, and the third quadrupole (Q2) function as a collision cell where ions can be fragmented by collision-induced dissociation through collision with neutral gas molecules (*i.e.* N_2 or Ar).

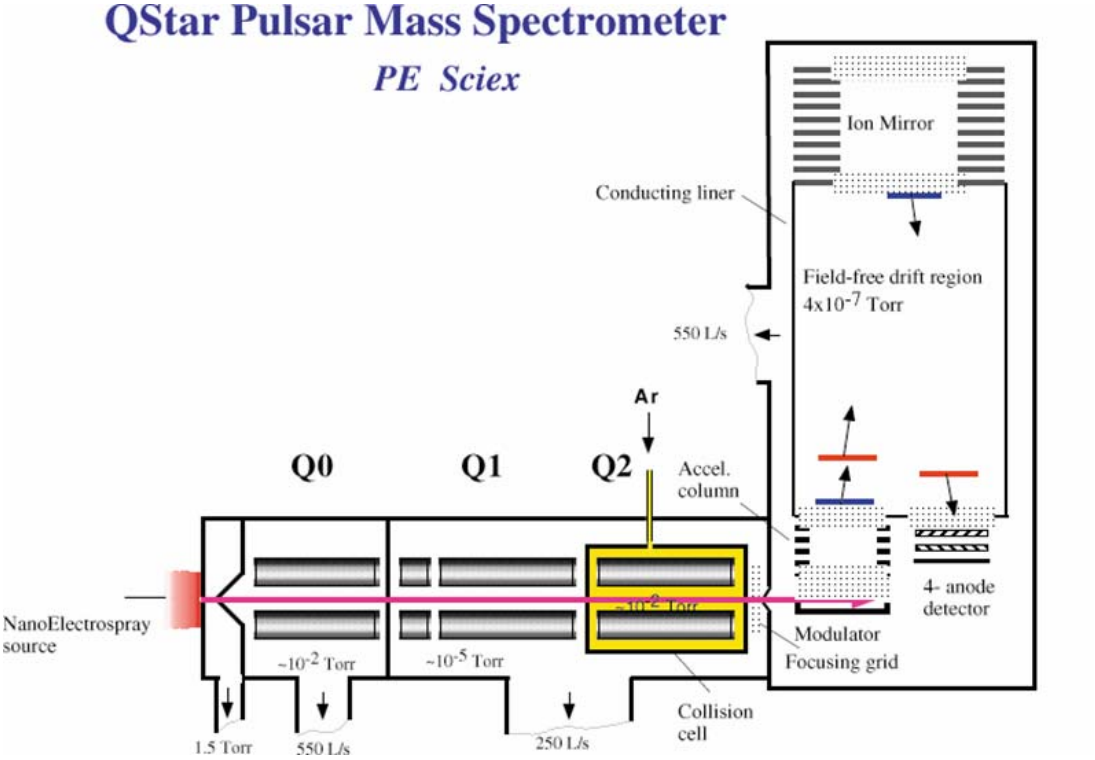

Figure 7. Overview of the QqTOF mass spectrometer. From the Operator Manual of QSTAR Pulsar-*i*

Ions entering from Q2 are detected in the TOF analyzer. The basic components of the TOF analyzer are an ion accelerator, an ion mirror, and the ion detector. The ion accelerator serves to accelerate ions, which are then separated in the drift tube based on difference in velocity. The ion reflector functions to reverse the direction of the ion. This instrumental feature improves the mass resolution by reducing variation in the kinetic energy ions pulsed out of the ion accelerator.

The QqTOF mass spectrometer can be operated in three acquisition modes: (i) TOF mass spectrometry (TOF MS) mode, (ii) tandem mass spectrometry (MS/MS) mode, and (iii) (M)PIS mode. In TOF MS mode, the mass filter quadrupole (Q1) is operated as a transmission element, *i.e.* all ions having a broad range of *m/z* are transmitted simultaneously, and the TOF analyzer records the mass spectrum. This yields a mass spectrum of all ionized molecules present in the electrosprayed solvent. The TOF MS spectrum provides information regarding molecular mass (*m/z*) and number of charges of a given analyte ion (*q.v.* Figure 17A page 42). Limited information about the molecular structure of the analyte ion can be derived.

In MS/MS mode, the Q1 is operated in the mass filter mode to transmit only a precursor ion of interest within a certain mass window (typically of 1-3 Da). Precursor ions are then accelerated into the collision cell (Q2) where they undergo collision-induced dissociation through multiple collisions with gas molecules. Resulting product ions (and remaining precursor ions) then pass into the TOF analyzer for detection. The recorded MS/MS spectrum reflects a set of structure specific fragment ions that provide structural

information about the precursor ion (*q.v.* Figure 17B page 42). Multiple reaction monitoring (MRM) and data-dependent acquisition are two additional acquisition modes based on MS/MS analysis. By data-dependent acquisition an initial survey TOF MS spectrum is recorded, which is used to automatically select abundant precursor ions for subsequent MS/MS analysis. The MS/MS analysis of each selected precursor ion is performed only once during the sample acquisition, and typically requires 30 seconds for recording each MS/MS. This technology was recently applied for comprehensive lipidome analysis (Schwudke *et al.*, 2006). MRM analysis allows the targeted MS/MS analysis of a defined set of precursor ions. This acquisition mode is independent of the abundance of the precursor ions detected by TOF MS, and is performed by the repeated 1 second MS/MS analysis of each of the targeted precursor ions for several minutes. Quantitative analysis of targeted precursor ions is readily performed by monitoring the intensities of fragment ions.

In (M)PIS mode, precursor ions that generate one or a set of specific fragment ions are detected. In this mode, the Q1 scans over a defined mass range (*e.g. m/z* 600-900) in small steps (0.1 or 0.2 Da). Precursor ions with increasing *m/z* values are sequentially transmitted and accelerated into the collision cell where they undergo collision-induced dissociation. The fragment ions generated at the defined precursor *m/z* are transmitted into the TOF analyzer for detection. By this technology a Q1 mass spectrum is generated that specifically shows only the precursor ions producing the monitored fragment ions. Importantly, the TOF analyzer allows a virtually unlimited number of PIS to be simultaneously recorded and monitored with high mass accuracy (0.1 Da). In comparison, conventional triple quadrupole mass spectrometers only allow the monitoring of a single fragment ion with a relatively poor mass accuracy (1 Da).

2. AIM OF THE THESIS

The aim of the thesis study was to develop mass spectrometric methodology for automated and quantitative lipid analysis. It was desired that the methodology allowed the characterization and absolute quantification of molecular glycerophospholipid, sphingolipid and sterol lipid species. The methodology should be designed for high-throughput oriented lipid analysis by integrating robotic sampling, lipid species-specific mass analysis and software-assisted deconvolution of spectral data. Furthermore, the methodology should be applicable for biochemical and cell biological studies of cellular membranes.

3. RESULTS AND DISCUSSION

3.1. AUTOMATED IDENTIFICATION AND QUANTIFICATION OF GLYCEROPHOSPHOLIPID MOLECULAR SPECIES BY MPIS

To understand how the full cellular lipid complement (also termed cellular lipidome (Han and Gross, 2003; Han and Gross, 2005)) controls diverse cellular processes, it is important to characterize and quantify lipids as individual molecular species. This means that, for glycerophospholipid species, the head group and moieties of fatty alcohol and/or FA(s) should be determined for each lipid molecule.

Collision-induced dissociation of molecular anions of glycerophospholipids produces abundant acyl anions of their FA moieties (Han and Gross, 1994; Hsu and Turk, 2000a; Hsu and Turk, 2000b; Hsu and Turk, 2000c; Hsu and Turk, 2001; Kerwin *et al.*, 1994). By selecting their *m/z* for MPIS on a hybrid QqTOF mass spectrometer (Chernushevich, 2000; Chernushevich *et al.*, 2001), the FA composition of a large number of molecular species could be simultaneously determined in total lipid extracts (Ekroos *et al.*, 2002; Ekroos *et al.*, 2003) (*q.v.* section 3.2. page 39). Thus, MPIS advanced the characterization of lipidomes compared to the conventional analysis by PIS and/or neutral loss scanning that annotates lipid species by their lipid class and sum formula (the total number of carbon atoms and double bonds) of their FA moieties (Brugger *et al.*, 1997; Han and Gross, 1994; Koivusalo *et al.*, 2001; Liebisch *et al.*, 2004; Wenk *et al.*, 2003). The specificity arising from the accurate selection of *m/z* of fragment ions by the high mass resolution TOF analyzer enhanced the dynamic range of precursor ion scans (Ekroos *et al.*, 2002; Steen *et al.*, 2001) and enabled the identification of low abundant molecular species from various classes of glycerophospholipids comprising unique FA moieties (Kuerschner *et al.*, 2005).

However, MPIS spectra acquired from total lipid extracts are exceedingly complex and hardly amenable to manual interpretation under high-throughput settings (Ekroos *et al.*, 2002). The identification of molecular species of glycerophospholipids typically required manual reviewing, matching and annotation of more than 40 simultaneously acquired precursor ion spectra, which, considering a large number of detected precursors and a more than ten-fold difference in their abundance was extremely laborious. Furthermore, only relative quantification of individual species was possible since no methods for absolute quantification (including the selection of internal standards and isotope intensity correction

algorithms (Han and Gross, 2005)) were available. This severely limited the scope and impact of MPIS-driven lipidomics and prompted the development of algorithms and their software implementation for rapid, quantitative and automated interpretation of large amounts of MPIS data.

This section describes the methodology developed for the identification and quantification of molecular glycerophospholipid species by automated interpretation of MPIS spectra which has been implemented in dedicated software termed Lipid Profiler. Endogenous species of common lipid classes could be simultaneously quantified using a set of synthetic lipid class-specific diheptadecanoyl (17:0/17:0) internal standards, and applying a novel algorithm for the isotopic correction of peak intensities adjusted to the specific features of MPIS spectra.

3.1.1. Identification of lipid species by MPIS

Figure 8 shows how MPIS for acyl anions of FAs and a head group-specific fragment ion identified glycerophospholipid molecular species. An equimolar mixture of synthetic PE 18:0/18:2, PE 18:1/18:1, PE 18:0/18:1 and PE 18:0/18:0 was directly infused into a hybrid QqTOF mass spectrometer. MPIS analysis was performed in negative ion mode by simultaneously acquiring precursor ion spectra for the PE head group fragment ion (PIS *m/z* 196.0, Figure 8A), and acyl anions corresponding to FA 18:2 (PIS *m/z* 279.2, Figure 8B), FA 18:1 (PIS *m/z* 281.3, Figure 8C) and FA 18:0 (PIS *m/z* 283.3, Figure 8D), respectively. The PE head group scan detected three precursor ions at *m/z* 742.6, 744.6 and 746.6, corresponding to PE species with the sum formulae PE 36:2, PE 36:1 and PE 36:0, respectively (Figure 8A). Cross-correlation of peak profiles in the PE head group scan, and the three FA scans, revealed that PE 36:2 was comprised of two individual molecular species, *i.e.* asymmetric PE 18:0-18:2 species, as determined by the simultaneous detection of the precursor ion with *m/z* 742.6 by FA 18:2 scan (PIS *m/z* 279.2, Figure 8B) and by FA 18:0 scan (PIS *m/z* 283.3, Figure 8D), and symmetric PE 18:1-18:1 species detected by FA 18:1 scan (PIS *m/z* 281.3, Figure 8C). Similarly, MPIS identified PE 36:1 (*m/z* 744.6) and PE 36:0 (*m/z* 746.6) species as PE 18:0-18:1 and PE 18:0-18:0, respectively (Figure 8C,D).

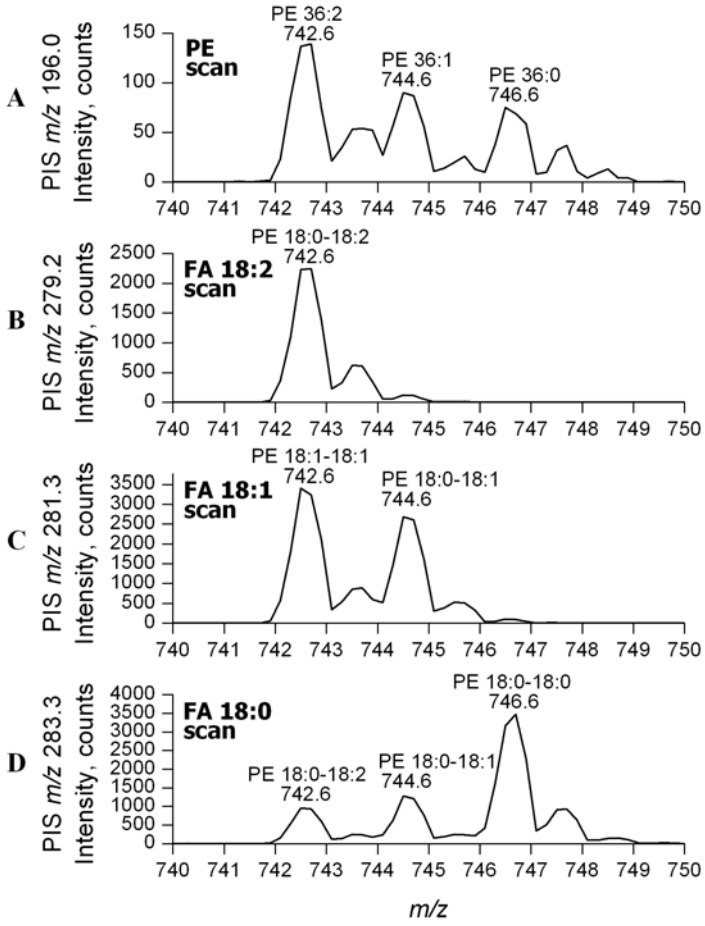

Figure 8. Identification of individual molecular species of PE standards by MPIS. The equimolar mixture of PE 18:0/18:2 (*m/z* 742.6), PE 18:1/18:1 (*m/z* 742.6), PE 18:0/18:1 (*m/z* 744.6) and PE 18:0/18:0 (*m/z* 746.6) was analyzed by MPIS. **(A)** PIS *m/z* 196.0 spectrum (PE head group scan). **(B)** PIS *m/z* 279.2 spectrum (FA 18:2 scan). **(C)** PIS *m/z* 281.3 spectrum (FA 18:1 scan). **(D)** PIS *m/z* 283.3 spectrum (FA 18:0 scan). Detected lipid precursors are designated by their sum formulas in the panel A and by their molecular composition in other panels.

Asymmetric glycerophospholipid species occur as positional isomers, *i.e.* species with the inverted position of FA moieties on the glycerol phosphate backbone (*e.g.* PE 18:0/18:2 *vs* PE 18:2/18:0). Previous studies demonstrated that, in the MS/MS and MPIS spectra of asymmetric PE and PC species, the acyl anion of the *sn*-2 FA moiety was two to three-fold more abundant than that of the *sn*-1 FA moiety (Ekroos *et al.*, 2003; Han and Gross, 1995; Hsu and Turk, 2000c; Hvattum *et al.*, 1998). The ratio of precursor ion intensities at *m/z* 742.6 (identified as PE 18:0-18:2) differed by two-fold in the PIS *m/z* 279.2 spectrum (FA 18:2 scan) and in the PIS *m/z* 283.3 spectrum (FA 18:0 scan), respectively (Figure 8B,D). This indicated that the major PE species with *m/z* 742.6 comprised FA 18:0 and FA 18:2 moieties at the *sn*-1 and *sn*-2 position, respectively (*i.e.* PE 18:0/18:2). Similarly, the relative abundance of the precursor peaks detected in the PIS *m/z* 281.3 spectrum (FA 18:1 scan) and PIS *m/z* 283.3 spectrum (FA 18:0 scan) indicated that the PE species at *m/z* 744.6 was PE 18:0/18:1. On the contrary, in the MS/MS and MPIS spectra of anionic glycerophospholipids

(*i.e.* PA, PS, and PG), the relative intensity of acyl anions is reversed – the acyl anion of the *sn-1* FA moiety is more abundant than the acyl anion of the *sn-2* FA moiety (Hsu and Turk, 2000b; Hsu and Turk, 2001).

If required, the relative amount of positional isomers could be estimated by correlating the precursor ion intensity ratio to a response function determined by MPIS analysis of a set of synthetic positional isomers identical or similar to the endogenous species in question (*e.g.* PE 18:0/18:2 and PE 18:2/18:0). However, due to the vast number of molecular species in total lipid extracts this approach is practically impossible since it requires determining response functions for each pair of potential positional isomers. To circumvent this limitation of MPIS analysis, methodology was developed to accurately determine the relative amount of positional isomers by the direct MS^3 analysis of lipid precursors on an ion trap mass spectrometer (*q.v.* section 3.2, page 39).

3.1.2. Identification of lipid species by Lipid Profiler software

Lipid Profiler software was developed for automated identification and quantification of molecular lipid species detected by TOF MS and MPIS. Lipid Profiler deciphered MPIS spectra and identified molecular species of glycerophospholipids, essentially as outlined above. The identification of an asymmetric glycerophospholipid species required that the same precursor ion was detected by two complementary FA scans (*e.g.* the detection of precursor ions with *m/z* 742.6 by scans for FA 18:0 and FA 18:2, Figure 8B,D). In addition, the precursor ion *m/z* should equal, within a specified tolerance, the *m/z* expected for a lipid species of a given class, whose sum formula matches the total number of carbon atoms and double bonds in the corresponding FA scans. In the example above, the precursor ions with *m/z* 742.6 matched the *m/z* expected for the sum formula of PE 36:2 (*i.e. m/z* 742.54), since it was detected by PIS *m/z* 283.3 and PIS *m/z* 279.2 for the acyl anions of FA 18:0 and FA 18:2, respectively. The identification of symmetric glycerophospholipid species relied on the detection of a precursor ion by a single FA scan, however, both matching criteria equally applied. Hence, the precursor ion with *m/z* 742.6 should match the sum formula of PE 36:2, since it was detected by PIS *m/z* 281.3 for the acyl anion of FA 18:1 (Figure 8C).

In some glycerophospholipid species the hydrocarbon moiety is attached to the *sn*-1 position of the glycerol phosphate backbone through an ether bond (plasmanyl species) or vinyl ether bond (plasmenyl species or plasmalogens) (Figure 1 page 10) (Nagan and Zoeller, 2001). Collision-induced dissociation of molecular anions of both plamanyl and plasmenyl species produces abundant acyl anions of the *sn-2* FA moieties, along with relatively low abundant head group fragments and, for the plasmenyl species, also a low abundant

alkenoxide fragment ions is produced from the *O*-alk-1'-enyl moiety. Acyl anions were typically 20- to 100-fold more abundant compared to alkenoxide fragments. Alkenoxide fragments and acyl anions that differ by a single methylene group are isobaric ($\Delta m = 0.0364$ Da), and therefore robust assignment of precursor ions as ether or diacyl species relied upon the abundance difference between *sn*-2 and *sn*-1 related fragments: to recognize a precursor ion as an ether species, more than a 20-fold difference in abundance was typically required. Otherwise, this precursor was considered as a diacyl species. Ambiguous assignments could be verified by direct MS/MS analysis of the corresponding precursors (Schwudke *et al.*, 2006; Zemski Berry and Murphy, 2004)

The lipid species identification was further supported by the concomitant detection of the same precursor ions in confirmatory and/or supplementary precursor ion scans. Confirmatory scans use *m/z* of lipid class-specific fragment ions, such as PIS *m/z* 196.0 - the PE head group scan. For example, the identification of PE 18:0-18:2 detected at *m/z* 742.6 by scans specific for FA 18:0 and FA 18:2 moieties (Figure 8B,D), was validated by detecting the same precursor by the PE head group-specific scan (Figure 8A). Supplementary scans utilize fragment ions that are common for lipids of all classes comprising specific FA moieties. For example, upon collision-induced dissociation, acyl anions of polyunsaturated FAs lose CO_2. Corresponding *m/z* of neutral loss products were included in the MPIS experiment and supported the identification of lipid species containing a polyunsaturated FA moiety, independently of the lipid class (*q.v.* section 3.1.5 page 29).

A typical MPIS analysis utilized 41 simultaneously acquired precursor ion scans and recognized *ca.* 200 lipid precursors in a total lipid extract. The spectra were interpreted by Lipid Profiler within 30 seconds on a conventional (Pentium 4) desktop computer. Within this time period the software accessed the MPIS data file, produced a peak list with a user-defined threshold intensity, performed isotopic correction (see below), annotated precursor ions and created the identification report. Details on the quantification routines are presented in section 3.1.7 page 32.

3.1.3. MPIS enhances the identification specificity of lipid molecular species

The performance of MPIS in identifying molecular species of glycerophospholipids was evaluated by comparing it to the conventional lipid-class specific precursor- and neutral loss scans commonly applied in lipidomics. To this end, a commercially available PC extract from bovine heart was analyzed by PIS *m/z* 184.1 in positive ion mode. This scan specifically detects PC and SM species, yet it only annotates them with the sum formula (Brugger *et al.*, 1997; Liebisch *et al.*, 2004). The same extract was analyzed by MPIS in negative ion mode by

selecting *m/z* of 41 acyl anions of common FAs, as well as several lipid class-specific fragments (*q.v.* Appendix Table 1A page 102). Notice that including ammonium salts in the electrosprayed analyte enabled sensitive detection of PC species as anionic adducts (*q.v.* section 3.2. page 39). The PIS *m/z* 184.1 and MPIS spectra were processed by Lipid Profiler software, which identified and annotated plausible PC precursors (Figure 9A). Among other peaks, PIS *m/z* 184.1 scan detected abundant diacyl PC 34:2 at *m/z* 758.6 and putative ether species PC *O*-34:3 at *m/z* 742.7 (Figure 9A). The MPIS profile was in a full agreement with the PIS *m/z* 184.1 spectrum, but also provided important details on the chemical structure of the identified lipids. The diacyl PC 34:2 was detected as an acetate adduct at *m/z* 816.7 by precursor ion scans specific for FA 16:1, FA 16:0, FA 18:2 and FA 18:1 moieties (Figure 9B). The relative abundance of the precursor peaks in the corresponding FA scans determined the predominant location (*sn-1* and *sn-2*) of FA moieties in both molecular species. Its major and minor isobaric components were identified as PC 16:0/18:2 and PC 16:1/18:1 with peak intensity ratios equal to 3 and 5, respectively. The ether PC *O*-34:3 was detected by scans for FA 18:2 and FA 15:1/*O*-16:1 moieties at *m/z* 800.7 (Figure 9B). However, because of the peak intensity ratio of 100, it was annotated as the plasmenyl species PC *O*-16:1/18:2, where the *O*-alk-1'-enyl moiety was 16:1 and the *sn*-2 moiety was FA 18:2. The fully automated interpretation recognized 30 isobaric PCs in the PIS *m/z* 184.1 spectrum, whereas 48 individual molecular species were revealed by MPIS (Table 1).

To further validate the automated interpretation of MPIS profiles, we analyzed, in the same way (however, in negative ion mode), commercially available extracts of PAs, PEs, PGs, PSs, and PIs. The lipid class specific scans (PIS *m/z* 153.0 for PAs, PGs and PSs; PIS *m/z* 196.0 for PEs and PIS *m/z* 241.0 for PIs) were acquired simultaneously with FA scans in the same MPIS experiments (*q.v.* Appendix Table 1A page 102) and deciphered by Lipid Profiler. We compared the number of species detected by the respective lipid class-specific scans (as annotated by the sum formula) and the number of species detected in FA scans (as annotated by the molecular composition). Altogether, MPIS method increased the number of detected species in all classes, on average, by a factor of 1.8, compared to the conventional lipid class-specific precursor ion scans (Table 1).

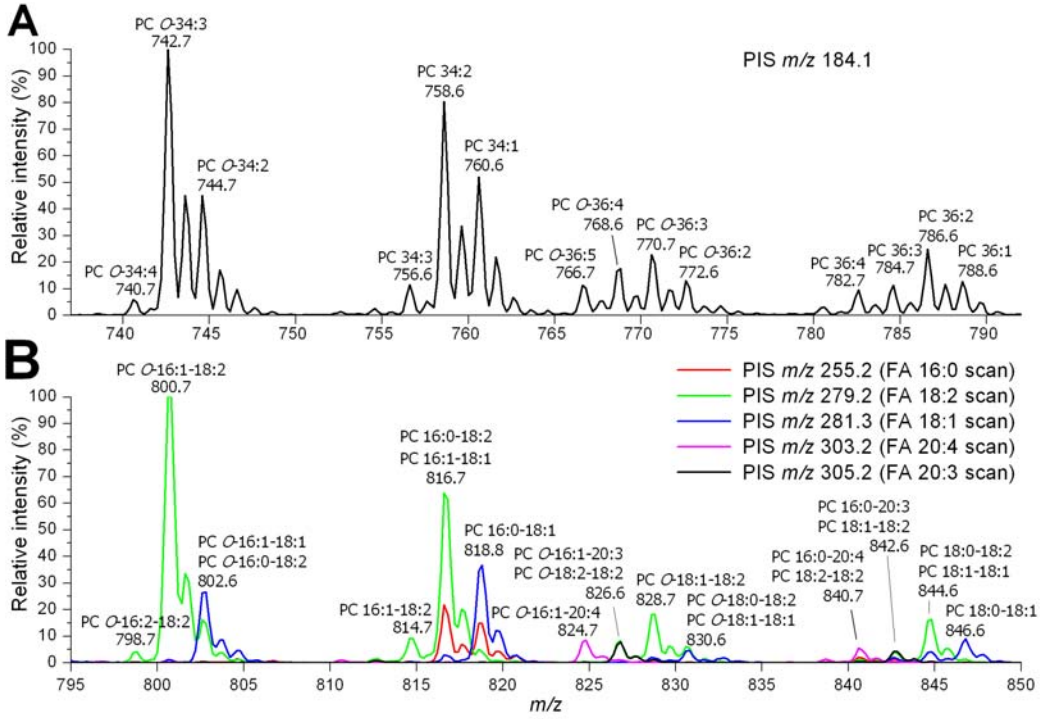

Figure 9. Spectral profiles obtained by lipid class specific PIS and lipid species specific MPIS. **(A)** PIS *m/z* 184.1 spectrum of bovine heart PC extract acquired in positive ion mode. Detected precursors are annotated as diacyl or ether species using a sum formula. Note that PIS *m/z* 184.1 is not capable of distinguishing isobaric diacyl species and ether species. Identified PC species are annotated assuming that the major constituent of the detected precursor contains even numbered acyl, alkyl, or alkenyl chains. **(B)** FA profile of bovine heart PC extract obtained by MPIS analysis. In negative ion mode PC precursors were detected as acetate adducts. For clarity only 5 precursor ion spectra (out of 41 acquired) are presented. Identified precursor ions are annotated using molecular formula that describes the FA moieties of the detected lipid species.

The identification specificity of species with long and unsaturated FA moieties was noticeably improved. Thereby, MPIS revealed that PE *O*-38:6 detected at *m/z* 748.7 by PE-specific head group scan PIS *m/z* 196.0 comprised of at least three individual species: PE *O*-18:2/20:4, PE *O*-18:1/20:5 and PE *O*-16:1/22:5. At the same time, PE 34:1 detected at *m/z* 716.6 was single species PE 16:0/18:1 (data not shown). Similar results were obtained by the analysis of extracts of other lipid classes.

Table 1. The number of lipid species identified by lipid class-specific scans and by MPIS analysis[1]

Lipid source	Lipid class-specific scan	Number of species identified by lipid class-specific scan	Number of species identified by FA-specific scans	Factor difference[4]
Chicken egg PA extract	PIS *m/z* 153.0[2]	15	24	1.6
Bovine heart PE extract	PIS *m/z* 196.0[2]	27	60	2.2
Porcine brain PS extract	PIS *m/z* 153.0[2]	15	24	1.6
Chicken egg PG extract	PIS *m/z* 153.0[2]	14	26	1.9
Bovine heart PC extract	PIS *m/z* 184.1[3]	30	48	1.6
Bovine liver PI extract	PIS *m/z* 241.0[2]	20	37	1.9

[1]Detected precursor ions were identified by Lipid Profiler software using isotope correction (see below)
[2]Performed in negative ion mode. Detected species were annotated by sum formula
[3]Performed in positive ion mode. Detected species were annotated by sum formula
[4]The ratio between the numbers of identified lipid species detected by MPIS and the respective lipid class scan

3.1.4. High mass resolution of the TOF analyzer improves the specificity of MPIS

The identification of lipid species by Lipid Profiler relies on the specificity of precursor ion scans. Here we demonstrate that because of the high mass resolution of the TOF analyzer, MPIS distinguishes lipid species whose specific fragments, potentially suitable for precursor ion scan profiling, are isobaric. Collision-induced dissociation of PIs yields the class-specific head group fragment ion with *m/z* 241.01 ($C_6H_{10}O_8P$)(Hsu and Turk, 2000a). However, it is isobaric with the acyl anion of FA 15:0 having *m/z* 241.22 ($C_{15}H_{29}O_2$), which, despite having the odd number of carbon atoms, is common in mammalian glycerophospholipids (Connor *et al.*, 1997; Ekroos *et al.*, 2003).

A total lipid extract of MDCK II cells was analyzed by MPIS as described above. As anticipated, PIS *m/z* 241.0 revealed a profile of PI species (Figure 10A), but did not overlap with the PIS *m/z* 241.2 profile (Figure 10B) that is specific for glycerophospholipids with FA 15:0 moieties. The detected species were identified by Lipid Profiler by considering other FA scans that were acquired in parallel. One of these scans, specific for glycerophospholipids containing FA 16:0 moieties, is presented in Figure 10C as a reference. The ratio of intensities of the precursor peaks detected by FA 16:0 and FA 15:0 scans was equal to 1 thus indicating that the precursor at *m/z* 778.7 was an equimolar mixture of PC 15:0/16:0 and PC 16:0/15:0. In other lipid species the FA 15:0 moiety was mostly located at the *sn-1* position: PC 15:0/18:1 (*m/z* 804.7, peak intensities ratio = 5), PE 15:0/16:0 (*m/z* 764.8; peak intensities ratio = 3) and PE 15:0/18:1 (*m/z* 790.9, peak intensities ratio = 6). Interestingly, the FA 16:0 scan identified another lipid with the odd numbered FA moiety PC 16:0/17:1 (Figure 10C), which was confirmed by the cross-correlation with the FA 17:1 scan (data not shown).

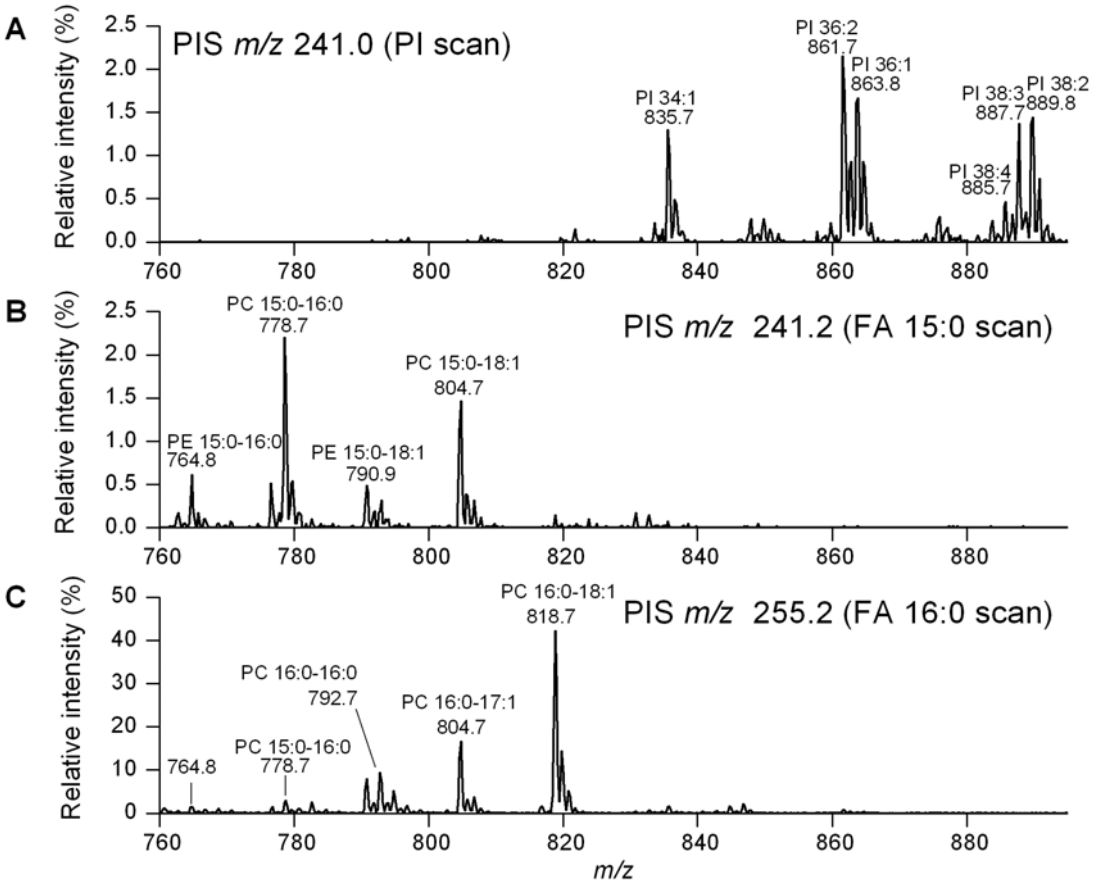

Figure 10. Specific precursor ion scans distinguish PI species from glycerophospholipids comprising FA 15:0 moieties, despite their characteristic fragments are isobaric. A lipid extract of MDCK II cells was analyzed by MPIS in negative ion mode. (A) PI species were detected by PIS *m/z* 241.0 and annotated by sum formula. (B) FA 15:0 containing lipids of all classes were detected by PIS *m/z* 241.2 and annotated by molecular formulas. (C) FA 16:0 containing lipids of all classes were detected by PIS *m/z* 255.2 Note that PC 15:0-16:0 (*m/z* 778.7) was detected both in FA 15:0 and FA 16:0 scans. Peak intensities are normalized to the most abundant precursor ion at *m/z* 742.7 (PE 18:1-18:1).

3.1.5. MPIS identification of lipid species having a polyunsaturated FA moiety

Acyl anions of polyunsaturated FAs, produced by the collision-induced dissociation of molecular anions of diacyl and ether glycerophospholipids, yield additional satellite fragments by neutral loss of CO_2 (Griffiths, 2003; Lu *et al.*, 2005). Their *m/z* were included into the list of fragments for MPIS (*q.v.* Appendix Table 1A page 102) as a supplementary means to validate the identification of corresponding molecular species. For example, MPIS profiling of a bovine heart PE extract revealed four low abundant PE species containing FA 20:5 moiety, which were simultaneously detected in scans specific for FA 20:5 and FA 20:5-CO_2 (Figure 11), which increased their identification confidence (Kuerschner *et al.*, 2005).

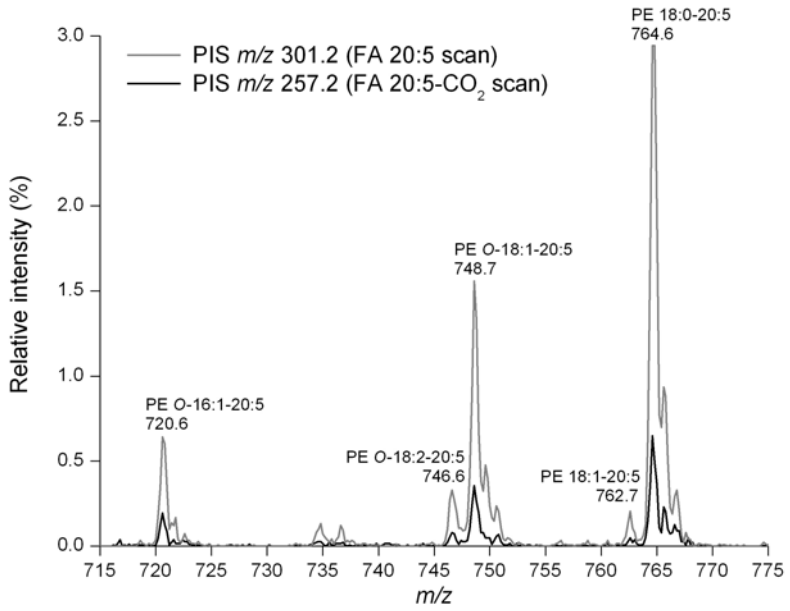

Figure 11. Validating the identification of lipid species containing a FA 20:5 moiety by supplementary scan for FA 20:5-CO2 fragment. Bovine heart PE extract was subjected to MPIS analysis. Scans acquired for FA 20:5 (PIS *m/z* 301.2) and FA 20:5-CO2 (PIS *m/z* 257.2) allowed the specific identification of FA 20:5 containing PE species. Peak intensities were normalized to the most abundant peak with *m/z* 766.6 detected by FA 20:4 scan (PIS *m/z* 303.2) that corresponded to PE 18:0-20:4.

Neutral loss of CO_2 from polyunsaturated acyl anions has two important implications for lipid profiling. First, loss of CO_2 from the acyl anion of docosahexaenoic acid FA 22:6 yields a fragment ion with *m/z* 283.2431 ($[FA\ 22{:}6\text{-}CO_2]^-$) that is isobaric with the acyl anion *m/z* 283.2642 of abundant stearic acid FA 18:0 and, therefore, additional caution should be taken when using *m/z* of this fragment in supplementary PIS. However, most importantly, loss of CO_2 directly affects the quantification accuracy of docosahexaenoic acid FA 22:6 containing glycerophospholipid species, which, as we demonstrate below, can be improved by using a specific correction factor together with MPIS profiles.

Here we define the correction factor α_{PX} as a ratio of the peak intensities of the precursor from the lipid class PX (*i.e.* PA, PE, PG, PS, PC, PI) detected by PIS *m/z* 283.3 (FA 22:6-CO_2 scan) and PIS *m/z* 327.2 (FA 22:6 scan). Correction factors were determined in a separate experiment using available synthetic standard(s), such as PC 16:0/22:6, PE *O*-16:1/22:6, PA 16:0/22:6 and PG 16:0/22:6, under the fixed instrument settings (most importantly, the collision energy offset). We observed that the intensity ratio of the acyl anion of FA 22:6 and its neutral loss fragment FA 22:6-CO_2 was mainly dependent on the lipid class (data not shown). The lipid class-specific correction factors were then used to adjust the intensities of the corresponding endogenous lipid precursors detected by PIS *m/z* 283.3 (FA 18:0 and FA 22:6-CO_2 scan):

$$I_{FA\ 18:0} = I_{PIS\ m/z\ 283} - \alpha_{PX} \cdot I_{PIS\ m/z\ 327.2},$$

The same correction factors also adjusted the intensity of the precursor peak at PIS *m/z* 327.2 (FA 22:6 scan):

$I_{FA\ 22:6} = (1+\alpha_{PX}) \cdot I_{PIS\ m/z\ 327.2}$,

As a test bed, we analyzed an equimolar mixture of synthetic isobaric plasmenyl PE *O*-16:1/22:6 (*m/z* 746.5130) and diacyl PE 18:0/18:0 (*m/z* 746.5705) species by MPIS. The correction factor α_{PE} was estimated as 0.56 (±0.05) by separately analyzing PE *O*-16:1/22:6 under the same instrument settings (Table 2). Applying the correction factor to the reference peak intensity of PE *O*-16:1/22:6 at PIS *m/z* 327.2 (FA 22:6 scan) allowed us to distinguish the contributions of the two species to the intensity at PIS *m/z* 283.3 (FA 18:0 and FA 22:6-CO_2 scans) and, thereby, correctly determine their molar ratio (Table 2). Analysis of PE 18:0/18:0 did not produce any signal in the PIS *m/z* 327.2 spectrum (FA 22:6 scan)(data not shown).

Table 2. Quantification of the isobaric species PE O-16:1/22:6 and PE 18:0/18:0 by PIS *m/z* 283.3 and the pre-determined correction factor

Analyte	PIS *m/z* (scan)	Rel. Int.[3]	α_{PE} estimate[4]
[1]PE O-16:1/22:6	327.2 (FA 22:6)	1	0.56 (±0.05)
	283.3 (FA 18:0/FA 22:6-CO_2)	0.56	
[2]PE O-16:1/22:6+ PE 18:0/18:0 (1:1)	327.2 (FA 22:6)	1	
	283.3 (FA 18:0/FA 22:6-CO_2)	2.22	
Accurate quantification of species by applying the correction factor			
	Scan (PIS *m/z*)	Rel. Int.[3]	Molar ratio
PE O-16:1/22:6	FA 22:6 (327.2)	1	$\frac{1+0.56}{1.66} = 0.938\ (\pm 0.002)$
	FA 22:6-CO_2 (283.3)	0.56	
PE 18:0/18:0	FA 18:0 (283.3)	1.66	

[1]Synthetic plasmenyl species PE O-16:1/22:6 (*m/z* 746.51) was analyzed three times by MPIS to estimate α_{PE} correction factor.
[2]Equimolar mixture of synthetic isobaric PE O-16:1/22:6 and PE 18:0/18:0 (*m/z* 746.57) was analyzed three times by MPIS.
[3]Precursor ion intensity was normalized to the intensity of the lipid precursor with *m/z* 746.5 detected by PIS *m/z* 327.2 (FA 22:6 scan).
[4]α_{PE} was calculated as the intensity ratio of precursor ions with *m/z* 746.5 detected by PIS *m/z* 283.3 and PIS *m/z* 327.2.

3.1.6. Isotope correction of peak intensities for MPIS quantification

Correction of peak intensities within overlapping isotopic clusters improves the confidence of identification of low abundant lipid species and the quantification accuracy (Han and Gross, 2005; Liebisch *et al.*, 2004). It is demonstrated here that a dedicated isotope peak intensity correction algorithm enabled reconstruction of the *bona fide* isotopic

distributions of lipid species in MPIS experiments. An extensive description of the isotope correction algorithms employed by Lipid Profiler software is provided in Ejsing *el al.* (2006).

TOF MS and MPIS spectra of synthetic PE 18:1/18:1 are presented here as an example. The isotope profile observed in TOF MS spectrum was in good agreement with the profile computed from its elemental composition $C_{41}H_{77}NO_8P$ (Figure 12). However, in PIS spectra the isotope profiles were perturbed because only a subset of the isotopic population of the intact precursor was detected. For example, the PIS *m/z* 281.3 (FA 18:1 scan) spectrum matched the isotope distribution calculated for the neutral fragment of the PE 18:1/18:1 that lost the acyl anion of FA 18:1 ($C_{23}H_{44}NO_6P$). The isotope profiles of the precursor in the PIS *m/z* 282.3 spectrum and PIS *m/z* 283.3 spectrum (FA 18:0 scan) also differed from the profile of the intact species, but agreed with the calculated isotopic abundances. Importantly, summing up the isotopic peak intensities in the PIS *m/z* 281.3, PIS *m/z* 282.3 and PIS *m/z* 283.3 spectra (Figure 12B,C,D) recreated the isotopic profile of the intact molecule (Figure 12A). For further quantitative analysis and reports, Lipid Profiler software operated with the total intensities of isotopic clusters computed using the ρ correction factor (type I isotope correction factor (Han and Gross, 2005)) as described in the Materials and Methods section (*q.v.* section 5.1.13. page 93).

3.1.7. Quantification of glycerophospholipid species by MPIS

Han *et al* (Han and Gross, 2005; Han *et al.*, 2004) demonstrated that quantification of lipid species in total lipid extracts could rely upon a single internal standard per analyzed lipid class, if applied together with the isotope correction of intensities of their monoisotopic peaks. The internal standards were selected such that their *m/z* was out of the range, typical for endogenous species, and the analysis was performed using an “intrasource separation” method that stimulated preferential ionization of certain lipid classes (Han *et al.*, 2006).

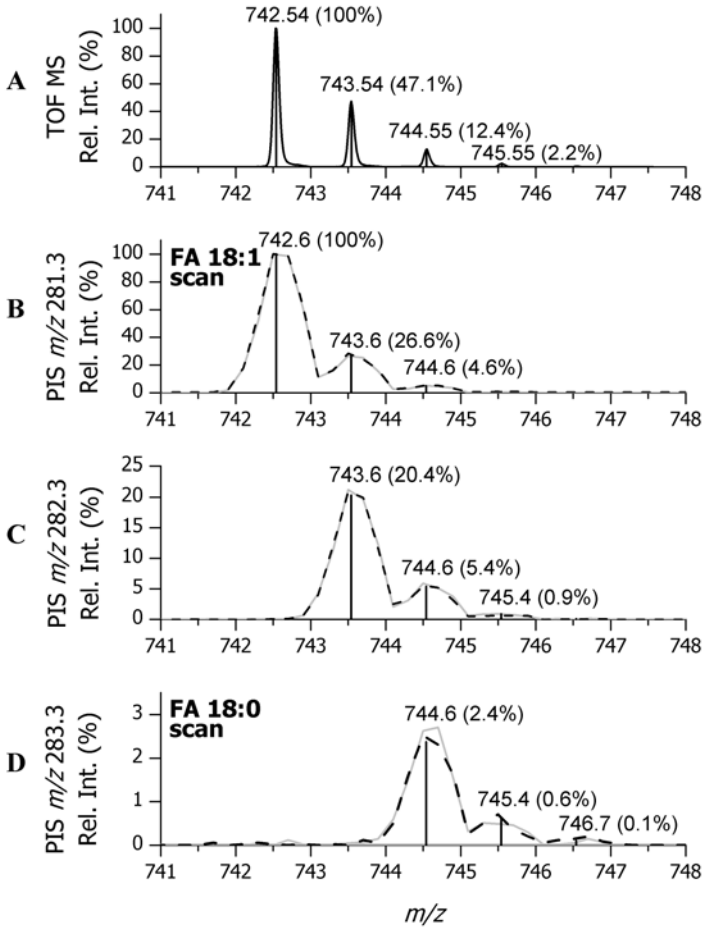

Figure 12. Comparison of isotopic profiles of the synthetic standard PE 18:1/18:1 in TOF MS and PIS spectra. Peak intensities in all precursor ion scans (panel B, C and D) were normalized to the intensity of the monoisotopic peak at *m/z* 742.6 in the PIS m/z 281.3 spectrum. MPIS spectra of two independent analyses are shown in grey line and black dots. The calculated isotopic distributions are presented as vertical bars and respective values are in parenthesis. **(A)** TOF MS spectrum. **(B)** PIS m/z 281.3 spectrum (FA 18:1 scan). **(C)** PIS *m/z* 282.3 spectrum. **(D)** PIS m/z 283.3 spectrum (stands for FA 18:0 scan). Note that summing up the intensities of isotopic peaks in precursor ion spectra (panels B, C, D) recreates the isotopic profile of the intact PE 18:1/18:1 detected by TOF MS (panel A).

Here, it is demonstrated that molecular species of glycerophospholipids of various classes could be simultaneously quantified by MPIS using a one-class/one-standard approach, combined with the collision energy ramping and the dedicated isotope correction algorithm. Synthetic diheptadecanoyl species of major glycerophospholipid classes: PA 17:0/17:0, PE 17:0/17:0, PG 17:0/17:0, PS 17:0/17:0, PC 17:0/17:0 and PI 17:0/17:0 were employed as internal standards. All of them were detectable by PIS *m/z* 269.3 (FA 17:0 scan) (Figure 13A) and their mixture was spiked at nM concentration into total lipid extracts. Ramping the collision energy compensated for *m/z*-dependent differences in the yield of acyl anions (Figure 13B). The PIS profile of these 6 diheptadecanoyl species (Figure 13A) was reproducible and served as an internal quality control for the efficiency of lipid extraction and ionization. None of them were detectable in total lipid extracts from *E. coli*, *S. cerevisiae* and

mammals, although pronounced levels of PE 17:0/17:0 were detected in *C. elegans* total lipid extracts (data not shown). Importantly, these standards (except PI 17:0/17:0) are commercially available and since they are not isotopically labeled, their precursor and fragment peaks have natural isotopic profiles.

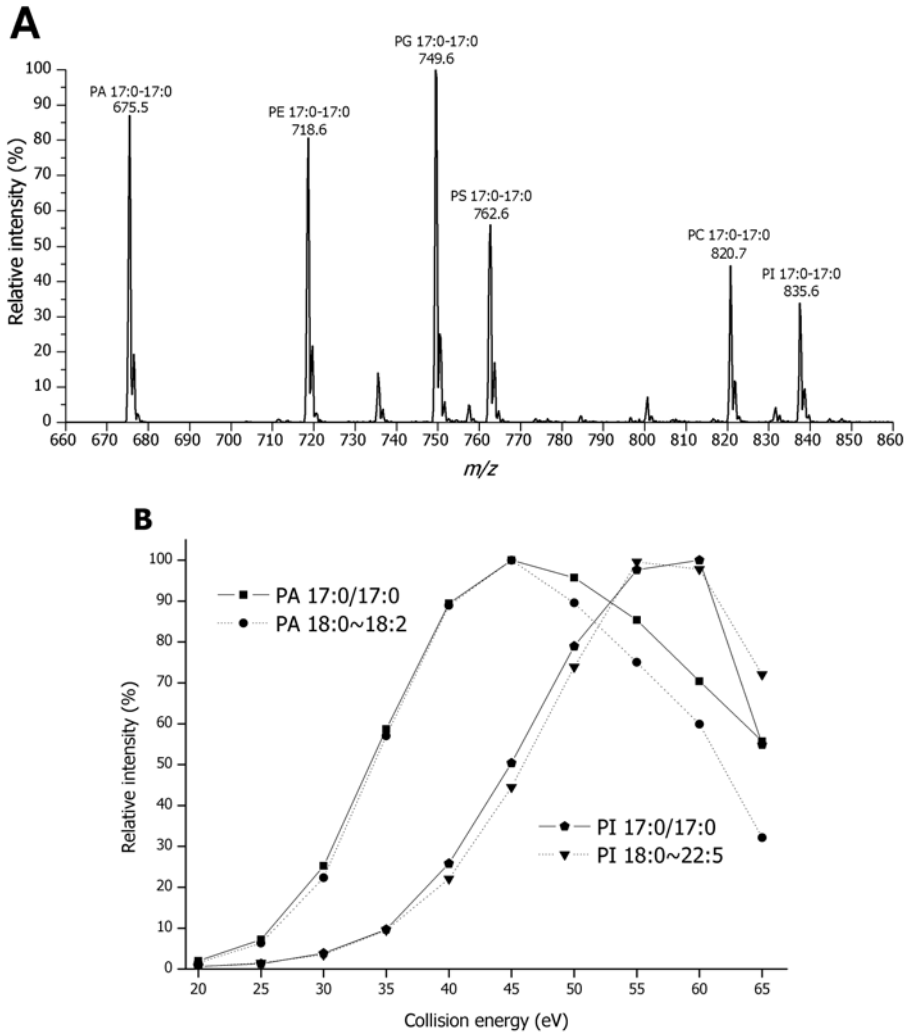

Figure 13. **(A)** PIS *m/z* 269.3 (FA 17:0 scan) spectrum of an equimolar mixture of PA 17:0/17:0, PE 17:0/17:0, PG 17:0/17:0, PS 17:0/17:0, PC 17:0/17:0 and PI 17:0/17:0. Each lipid species was spiked to a final concentration of 250 nM. Collision energy was ramped from 45 eV at *m/z* 620 to 60 eV at *m/z* 920 for optimal signal response. **(B)** Relative intensity of peaks of acyl anions produced at different collision energy offsets. Precursor ions of PA 17:0/17:0 (*m/z* 675.5, squares), PA 18:0-18:2 (*m/z* 699.5, circles), PI 17:0/17:0 (*m/z* 837.6, pentagons) and PI 18:0-20:5 (*m/z* 911.6, triangles). Total intensity of acyl anions at the indicated collision energy was normalized to the total intensity at the optimal collision energy. The average intensity determined in two independent experiments, performed under the same instrument settings, are presented.

To evaluate the quantification dynamic range, we analyzed the solutions of individual synthetic standards of lipids that are common in biological membranes (*e.g.* PE 18:1/18:1) within the concentration range of 1 nM to 100 μM, whereas the concentration of each of the six diheptadecanoyl standards was fixed at 250 nM. Within this range, the instrument

response was linear for all analyzed species with a slope value of approximately one, independently of their lipid class (data not shown).

To test if the quantification method was applicable for analyzing complex mixtures of endogenous lipids, we analyzed a dilution series of an *E. coli* polar lipid extract spiked with the fixed concentration of the same diheptadecanoyl standards and quantified the absolute amounts of PE 16:0/17:1 and PG 16:0/19:1 - the two most abundant species among all detectable PEs and PGs. To this end, their total peak intensity (the sum of intensities of the precursor peaks detected in the two complementary FA scans) were subjected to isotopic correction, divided by the intensity of the peak of the internal standards PE 17:0/17:0 and PG 17:0/17:0, respectively, and multiplied by the concentration of the internal standard and the ρ correction factor (*q.v.* equation in section 5.1.13. page 93). The concentrations of PE 16:0/17:1 and PG 16:0/19:1 were plotted as a function of the total lipid concentration in the extract (in mg/L) and total concentration of phosphate (in μM), as was determined by phosphate analysis (Figure 14). Similar to the results obtained with synthetic standards, the signal intensity of both quantified species changed linearly within approximately 10 nM to 100 μM of the total sample phosphate with a Limit of Quantification (Schwudke *et al.*, 2006) better than 1 nM and 30 nM for PE 16:0/17:1 and PG 16:0/19:1, respectively. The total molar concentration of all identified PE and PG species equaled 89% of the total sample phosphate content, with the remaining 11% corresponding to cardiolipins, which are poorly ionizable under the applied infusion conditions (data not shown). The PE and PG class species equaled 78% and 11% of the total sample phosphate content, respectively, which was in good agreement with previous reports (Vance and Vance, 1996).

Using MPIS, together with the set of diheptadecanoyl internal standards, we profiled commercially available polar lipid extracts from porcine brain and bovine heart. Automated identification, annotation, isotopic correction and quantification of lipid species were performed using Lipid Profiler software. The absolute concentration of each species (*e.g.* PE 18:0/20:4) was determined and converted to mol% by normalizing to the sum of the concentrations of all identified glycerophospholipid species (Figure 15A). The comparative analysis of brain and heart lipid extracts suggested multifaceted differences in their molecular lipid composition. The most abundant species in the brain tissue were PC 16:0/18:1, PS 18:0/18:1, PE *O*-18:2/18:1 and PC 18:1/18:1, compared to PC *O*-16:1/18:2, PE 18:0/20:4, PC 16:0/18:2, PC 16:0/18:1 and PE *O*-16:1/18:2 in the heart tissue (Figure 15A).

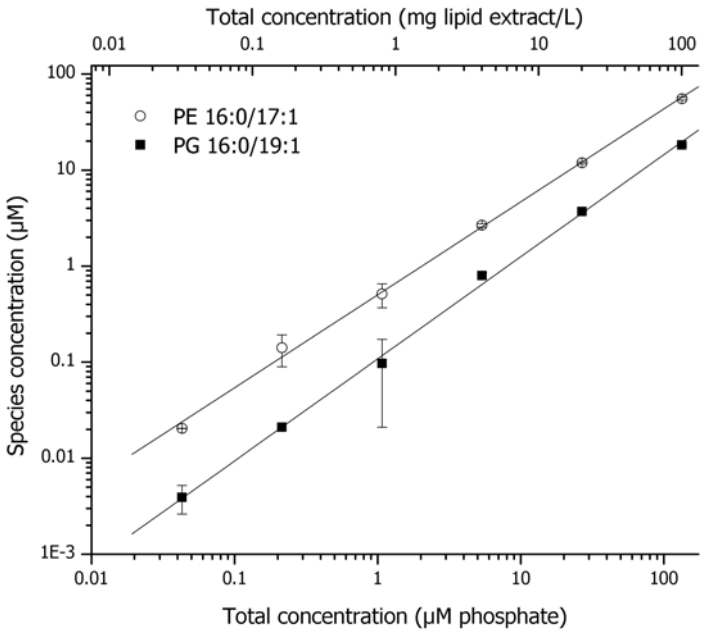

Figure 14. Dynamic range of MPIS quantification in the *E.coli* polar lipid extract. The set of synthetic internal standards (each at a final concentration of 250 nM) was spiked into an *E. coli* polar lipid extract. MPIS spectra were acquired as described in Materials and Methods and individual species identified and quantified using Lipid Profiler software. The estimated concentrations of the abundant PE 16:0/17:1 (*m/z* 702.5) and PG 16:0/19:1 (*m/z* 761.5) were plotted as a function of the total lipid concentration in mg/L (upper *x*-axis) and total sample phosphate content (lower *x*-axis).

MPIS methodology provided comprehensive and quantitative description of the glycerophospholipidome, which can be processed, displayed and compared in several ways – such as the direct quantitative species-to-species comparison (Figure 15A), or emulated total FA profile (Figure 15B) (typically obtained by gas chromatography - mass spectrometry) or lipid class profile (Figure 15C) (typically obtained by thin layer chromatography or normal phase liquid chromatography). For example, the emulated FA profile showed that brain glycerophospholipids were enriched in FA 18:1, and contained similar amounts of FA 18:0 and FA 16:0. They also comprised a diverse pool of polyunsaturated FA 22:6, FA 22:5, FA 22:4 and FA 20:4 that, taken together, equaled 15 mol% of all FA moieties (Figure 15B). In comparison, heart glycerophospholipids were enriched in FA 18:2 (low abundant in brain glycerophospholipids) and FA 20:4, and contained similar amounts of FA 18:1, FA 18:0 and FA 16:0 (Figure 15B). At the same time, the lipid class-specific profiling showed that PEs were equally abundant in brain and heart, whereas the two tissues showed noticeable differences in the amounts of PCs, PSs and PIs (Figure 15C).

Despite being a sensitive, versatile and robust analytical tool, the MPIS approach requires optimization of the sample preparation protocol and several instrument control settings. In particular, it is important to minimize in-source fragmentation of lipid precursors, adjust the collision energy ramping and collision gas pressure for best signal response, optimize the enhancement (q_2 ion trapping) settings (Chernushevich, 2000) and control the

intensities of detected peaks to avoid saturation of the TOF analyzer. Settings of the ion source (NanoMate HD System) must allow stable and reproducible spray with the flow injection rate of 200 to 300 nL/min. Sample preparation should minimize the content of chloride anions in the sprayed analyte to avoid the enhanced abundance of chloride adducts with PCs (in addition to the desired acetate adducts) complicating the identification of PC species. If MPIS fails to achieve unequivocal identification of certain molecular species, it is worth reducing the sample complexity by preparative TLC or liquid chromatography (DeLong *et al.*, 2001; Sommer *et al.*, 2006).

3.1.8. Discussion

We developed an analytical routine for the automated deciphering of MPIS spectra, which includes the identification, annotation, isotopic correction of peak intensities and quantification of molecular species of glycerophospholipids. The quantification relied upon a set of six diheptadecanoyl (17:0/17:0) synthetic internal lipid standards, covering common glycerophospholipid classes, and was linear within a concentration range of 10 nM to 100 μM. The MPIS methodology produced a comprehensive and quantitative description of the complex ensemble of glycerophospholipid species by the direct analysis of total lipid extracts of cells and tissues. The analysis time was 30 minutes per sample and lent itself to high throughput lipidomics.

Quantification of glycerophospholipids in total lipid extracts typically relies on spiked internal standards, representing lipids of the quantified lipid classes, and the acquisition of lipid class-specific precursor or neutral loss scans (Brugger *et al.*, 1997; Liebisch *et al.*, 2004). This methodology is straightforward and powerful, yet it fails to distinguish isobaric species often present in lipid extracts (e.g. PC 18:0/18:2 and PC 18:1/18:1). By applying a combination of multiple FA-specific, lipid class-specific and supplementary precursor ion scans bundled in a single MPIS experiment, it has become possible to distinguish and quantify isobaric diacyl and ether species. The specificity and quantification capabilities of the MPIS approach were supported by the linearity of calibration curves of individual lipid species, acquired from a total lipid extract (Figure 14); by matching MPIS and conventional PIS profiles acquired from the same sample in independent experiments, (Schwudke *et al.*, 2006) and Figure 9, and, finally, by a good agreement between the composition and relative abundance of endogenous lipid species detected by MPIS and a mass spectrometry independent approach (Connor *et al.*, 1997; Ekroos *et al.*, 2003).

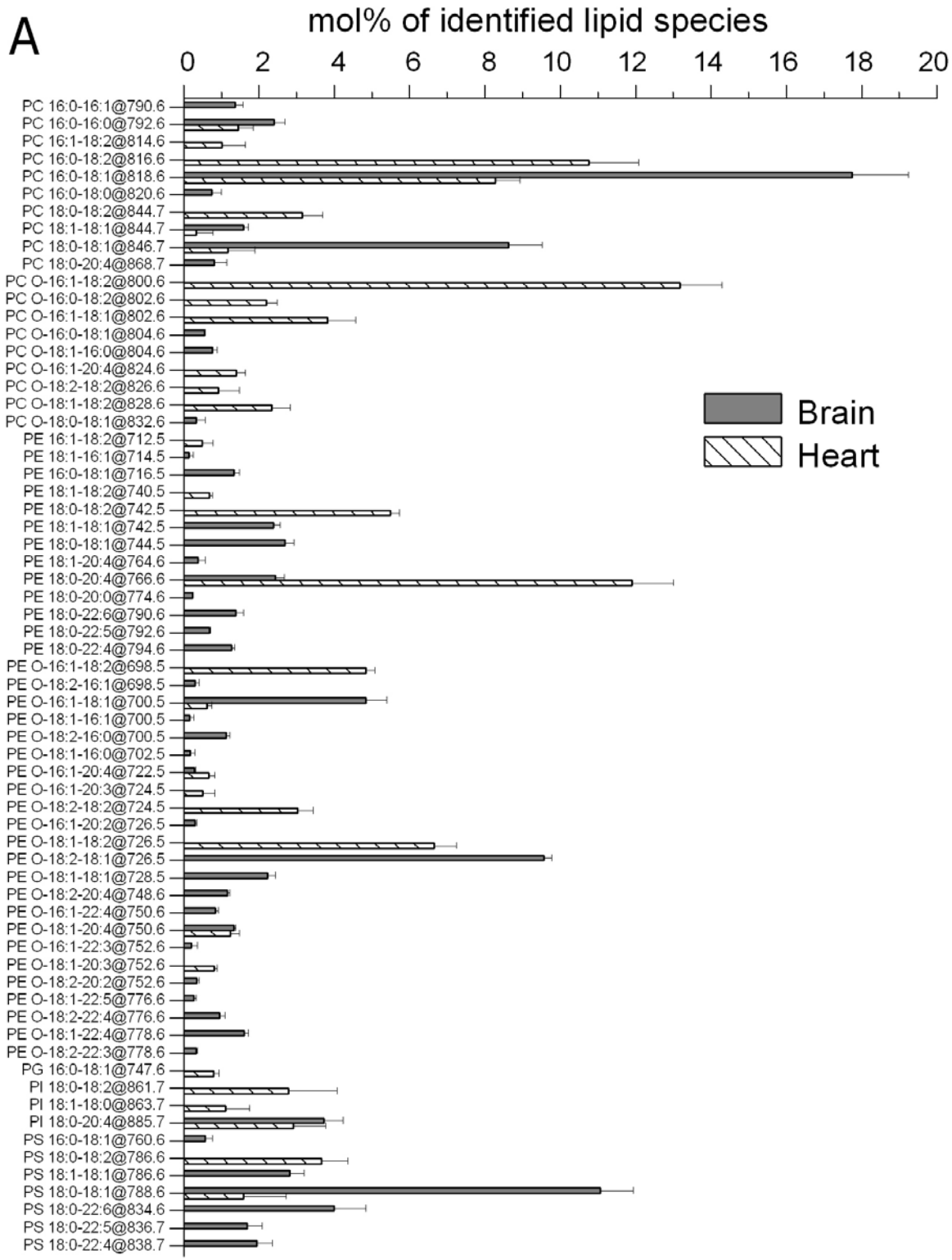
A
mol% of identified lipid species
0
2
4
6
8
10
12
14
16
18
20
PC 16:0-16:1@790.6
PC 16:0-16:0@792.6
PC 16:1-18:2@814.6
PC 16:0-18:2@816.6
PC 16:0-18:1@818.6
PC 16:0-18:0@820.6
PC 18:0-18:2@844.7
PC 18:1-18:1@844.7
PC 18:0-18:1@846.7
PC 18:0-20:4@868.7
PC O-16:1-18:2@800.6
PC O-16:0-18:2@802.6
PC O-16:1-18:1@802.6
PC O-16:0-18:1@804.6
PC O-18:1-16:0@804.6
PC O-16:1-20:4@824.6
PC O-18:2-18:2@826.6
PC O-18:1-18:2@828.6
PC O-18:0-18:1@832.6
PE 16:1-18:2@712.5
PE 18:1-16:1@714.5
PE 16:0-18:1@716.5
PE 18:1-18:2@740.5
PE 18:0-18:2@742.5
PE 18:1-18:1@742.5
PE 18:0-18:1@744.5
PE 18:1-20:4@764.6
PE 18:0-20:4@766.6
PE 18:0-20:0@774.6
PE 18:0-22:6@790.6
PE 18:0-22:5@792.6
PE 18:0-22:4@794.6
PE O-16:1-18:2@698.5
PE O-18:2-16:1@698.5
PE O-16:1-18:1@700.5
PE O-18:1-16:1@700.5
PE O-18:2-16:0@700.5
PE O-18:1-16:0@702.5
PE O-16:1-20:4@722.5
PE O-16:1-20:3@724.5
PE O-18:2-18:2@724.5
PE O-16:1-20:2@726.5
PE O-18:1-18:2@726.5
PE O-18:2-18:1@726.5
PE O-18:1-18:1@728.5
PE O-18:2-20:4@748.6
PE O-16:1-22:4@750.6
PE O-18:1-20:4@750.6
PE O-16:1-22:3@752.6
PE O-18:1-20:3@752.6
PE O-18:2-20:2@752.6
PE O-18:1-22:5@776.6
PE O-18:2-22:4@776.6
PE O-18:1-22:4@778.6
PE O-18:2-22:3@778.6
PG 16:0-18:1@747.6
PI 18:0-18:2@861.7
PI 18:1-18:0@863.7
PI 18:0-20:4@885.7
PS 16:0-18:1@760.6
PS 18:0-18:2@786.6
PS 18:1-18:1@786.6
PS 18:0-18:1@788.6
PS 18:0-22:6@834.6
PS 18:0-22:5@836.7
PS 18:0-22:4@838.7
Brain
Heart

Figure 15

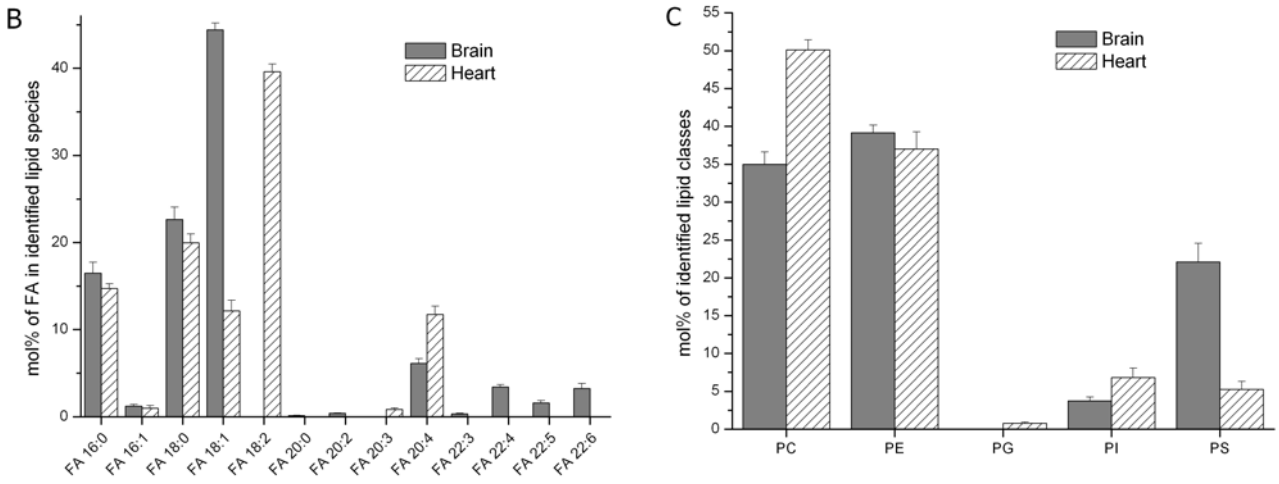

Figure 15. Comparative lipid analysis of total polar lipid extracts from porcine brain and bovine heart. **(A)** Species-to-species comparison. The mol% of identified lipid species were calculated as outlined in Materials and Methods. **(B)** Emulated total FA profile. The mol% of FA moieties were calculated as the sum of molar concentrations of lipid species in panel A containing the respective FA moiety, followed by normalization to the total molar concentration of all FA moieties. The FA concentration corresponding to symmetric lipid species was multiplied by a factor of two to account for two identical FA moieties. **(C)** Lipid class profile. The mol% of lipid classes were calculated as the sum of the mol% of lipid species (in panel A) of the respective lipid class. The MPIS analysis was repeated four times.

3.2. CHARTING MOLECULAR COMPOSITION OF PC SPECIES BY MPIS AND ION TRAP MS^3 FRAGMENTATION

Phosphatidylcholines are the most abundant glycerophospholipids in mammalian cells, accounting for more than 30% of the total lipid content (Kawai *et al.*, 1974). In mammalian cells, PCs are synthesised *via* the CDP-choline pathway or *via* the phosphatidylethanolamine methylation pathway (Cui *et al.*, 1993; Kent, 1995; Walkey *et al.*, 1998). Further metabolism involves remodelling processes, which are controlled by a coordinated action of acyltransferases, transacylases, and lipases (Yamashita *et al.*, 1997). Inhibiting the CDP-choline pathway is lethal (Baburina and Jackowski, 1998; Cui *et al.*, 1996) and is not compensated by the alternative PE methylation pathway, presumably because different PC species are produced (DeLong *et al.*, 1999; Waite and Vance, 2000). The majority of *de novo* synthesized PCs are believed to comprise saturated FAs at the *sn*-1 position and unsaturated FAs at the *sn*-2 position (Akesson *et al.*, 1970; Arvidson, 1968), although they might be altered by subsequent remodeling (Lands and Hart, 1965; Okuyama *et al.*, 1975; van Heusden *et al.*, 1981).

Electrospray ionisation mass spectrometry is a sensitive and specific tool for the characterization of PCs in total lipid extracts (Brugger *et al.*, 1997; Han and Gross, 1994; Han

and Gross, 1995; Kerwin *et al.*, 1994). Because of the positively charged quaternary amine of the choline head group, PCs are readily detected in positive ion mode with the femtomole sensitivity (Brugger *et al.*, 1997). Collision-induced dissociation of cations of PCs yields a characteristic fragment of the phosphorylcholine moiety having *m/z* 184.1, which enables their quantitative profiling in unprocessed lipid extracts by PIS (Brugger *et al.*, 1997). Since the fragmentation of SMs yields the same fragment, PIS *m/z* 184.1 simultaneously detects both PCs and SMs. Mono-protonated molecular ions of PCs have even nominal masses, whereas ions of SMs have odd nominal masses, which necessitate isotope correction of peak intensities for accurate quantification (Liebisch *et al.*, 2004; Ejsing *et al.*, 2006). Despite being sensitive and specific, PIS *m/z* 184.1 does not determine the FA composition of PC directly, but only allows the total number of carbon atoms and double bonds in both FA chains to be inferred from the masses of the PC precursors (the same applies for SMs). Hence, PIS *m/z* 184.1 fails to distinguish and estimate the relative amount of PC species having equal mass but different composition of FA moieties (*i.e.* isobaric and isobaric PC species) (Figure 16).

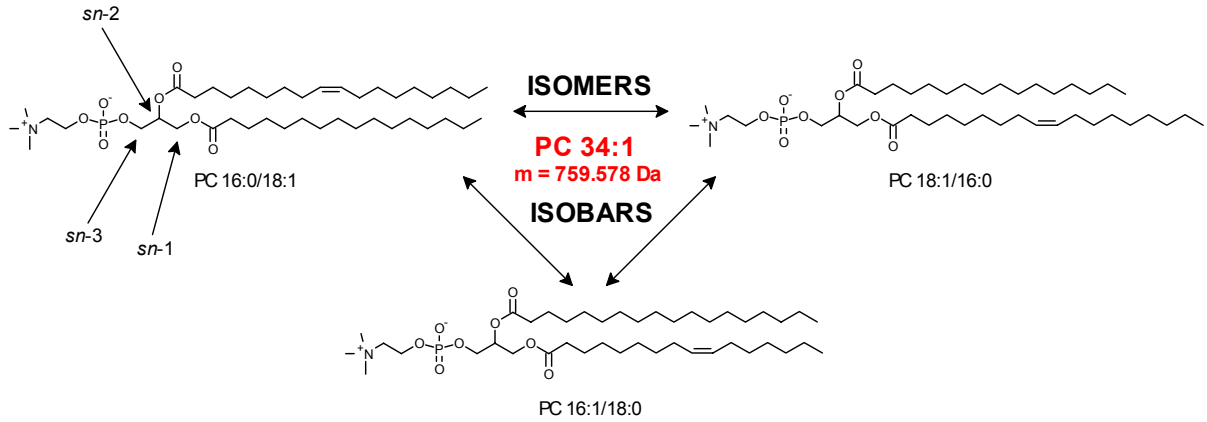

Figure 16. Chemical structures of isomeric and isobaric PC species. PIS *m/z* 184.1 only allows detected PC (and SM) precursors to be annotated by a sum formula indicating the total number of carbon atoms and double bonds in the FA moieties (*e.g.* PC 34:1).

MPIS methodology is an efficient tool for charting the FA composition of glycerophospholipids detectable in negative ion mode (Ekroos *et al.*, 2002) (*q.v.* section 3.1). However, MPIS is not directly applicable for the analysis of PCs species because of their positively charged quaternary amine. MPIS allows specific determination of the FA composition of a particular lipid, and the position of FA moieties (*sn*-1 or *sn*-2) could be inferred from the ratio of intensities of peaks of acyl anions (*q.v.* section 3.1.1. page 22). However, the relative quantification becomes ambiguous if a fragmented precursor is a mixture of isobaric species, which might belong to the same class, or to different classes of lipids.

This section outlines an analytical strategy for quantitative profiling of PC species by a combination of MPIS on a QqTOF mass spectrometer and MS^3 fragmentation on an ion trap mass spectrometer. Millimolar concentrations of ammonium salts in the electrosprayed analyte enabled sensitive detection of PCs as negatively charged adducts, which can be directly analysed by MPIS. MS^3 fragmentation of adducts on an ion trap mass spectrometer allowed us to quantify the relative abundance of positional isomers. The analysis of lipid extracts from human red blood cells characterized the pool of PCs as a complex mixture of isobaric and isomeric species.

3.2.1. Quantification of positional isomers of synthetic PC standards

To quantify positional isomers of endogenous PCs, we first established the isomeric purity of available synthetic standards. Phospholipase A_2 (PLA_2) hydrolyses the *sn*-2 ester bond in PCs, yielding 2-lysoPCs. We tested PLA_2 specificity by hydrolysing 15 mg of synthetic PC 16:0/18:1 standard and analysing the reaction mixture by ^{1}H-NMR. We only detected the signal from hydrogen atoms of the secondary alcohol and not from the primary alcohol, which indicated that *sn*-1 ester bond was not hydrolysed to any noticeable extent (data not shown). We therefore concluded that under the applied reaction conditions the hydrolysis of the *sn*-2 ester bond by PLA_2 is specific.

Mass spectrometric analysis of PLA_2-treated PC standards on a QqTOF mass spectrometer by TOF MS and by PIS *m/z* 184.1 suggested that they contained a noticeable amount of positional isomers as presented in Table 3 (mol% determined by MPIS and ion trap MS^3 fragmentation of the same standard PCs are also presented in Table 3 and discussed below).

Table 3. Isomeric purity of synthetic PC standards

	Abundance of Isomeric Species, mol%[a,b]			
	PLA_2 Hydrolysis and QqTOF MS			
Lipid Standard	TOF MS	PIS *m/z* 184.1	MPIS	Ion Trap MS^3[c]
16:0/18:1	88/12	87/13	88/12	83/17
18:1/16:0	83/17	82/18	81/19	79/21
16:0/18:0	88/12	85/15	88/12	83/17
18:0/16:0	94/6	95/5	93/7	93/7
18:0/18:1	96/4	96/4	95/5	89/11
18:1/18:0	81/19	81/19	84/16	75/25

[a] mol% of the indicated lipid standard/mol% of the related isomer, *e.g.* PC 16:0/18:1 vs. PC 18:1/16:0
[b] coefficient of variation for QqTOF MS measurements was 1.6 % and for ion trap MS^3 measurements 3.6%
[c] MS^3 fragmentation of chloride adducts in negative ion mode

3.2.2. MS/MS fragmentation of anion adducts of PCs on a QqTOF mass spectrometer

Since phosphorylcholine moiety comprises a quaternary amino group, high sensitivity detection of PCs in negative ion mode is problematic. Spiking 5 mM ammonium acetate or chloride into an electrosprayed solution of PCs produced the anion adducts $[M+CH_3COO]^-$ and/or $[M+Cl]^-$, respectively (Han and Gross, 1995; Kerwin *et al.*, 1994; Larsen *et al.*, 2001) (Figure 17). Upon collision-induced dissociation, anion adduct of PC ions lose both a methyl group from the choline moiety and the counter ion, yielding a fragment ion (designated as $[M–15]^-$) with *m/z* 15 Da smaller than the mass of the zwitterionic form of the intact PC (Figure 17). The $[M–15]^-$ ions undergo further fragmentation either *via* formation of low abundant intermediates by neutral loss of free FA $[M–15–R'CH_2COOH]^-$ or by neutral loss of ketene $[M–15–R'CH=C=O]^-$, or yielding acyl anions of FAs directly. Similar pattern of fragment ions was observed in MS/MS analysis of PCs (Han and Gross, 1995) as well as other glycerophospholipids on a triple quadrupole instrument (Hsu and Turk, 2000a; Hsu and Turk, 2000b; Hsu and Turk, 2000c; Hsu and Turk, 2001). Acyl anion fragment of *sn*-2 FA was more abundant than the FA at *sn*-1 position.

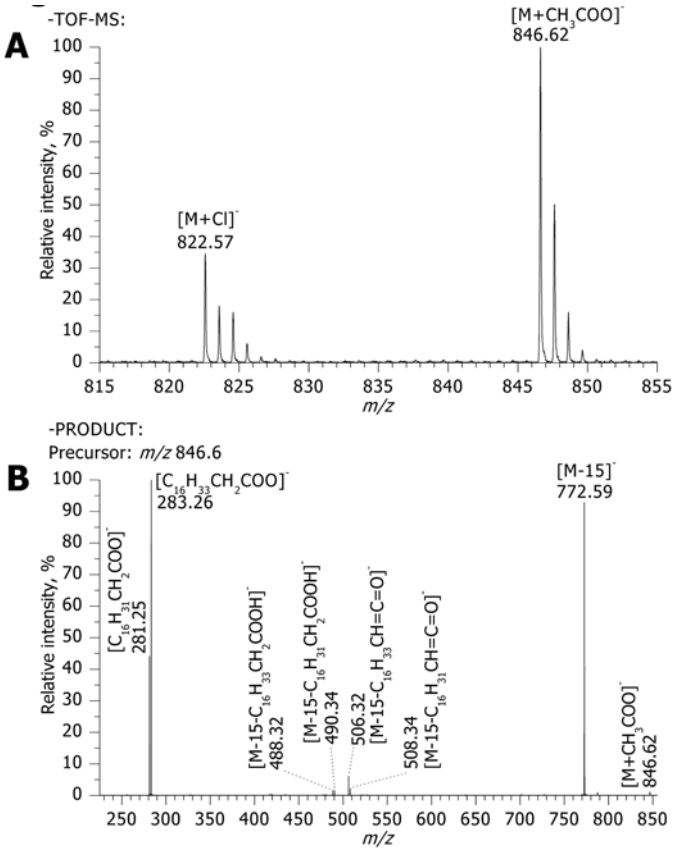

Figure 17. **(A)** TOF MS spectrum of synthetic PC 18:1/18:0 standard (note that the standard contained 19% of the isomeric PC 18:0/18:1, Table 3). PC was detected as anions of acetate and chloride adducts at *m/z* 846.62 and *m/z* 822.57, respectively. **(B)** MS/MS spectrum of the acetate adduct at *m/z* 846.62 acquired at collision energy 40 eV. Peaks at *m/z* 772.59, 283.26, and 281.25 correspond to the fragment ion of demethylated PC ([M - 15]$^-$) and acyl anions of stearic and oleic acid, respectively. Low abundant fragments were produced by the loss of FAs as ketenes [M - 15 - C16H31CH=C=O]$^-$ (*m/z* 508.34) and [M - 15 - C16H33CH=C=O]$^-$ (*m/z* 506.32) and by neutral loss of free FAs [M - 15 - C16H31CH2COOH]$^-$ (*m/z* 490.34) and [M - 15 - C16H33CH2COOH]$^-$ (*m/z* 488.32).

We further examined how the intensity of fragments depends on the applied collision energy (Figure 18). At low collision energy (~ 30 eV) MS/MS spectra were dominated by the intact precursor ion and $[M–15]^-$ fragment of the de-methylated PC. With increasing collision energy the intensity of both precursor and $[M–15]^-$ ions decreased, with concomitantly increasing intensity of acyl anion fragments. The intensity of acyl anions peaked at ~50 eV and then decreased, presumably because high collision energy compromised focusing and steering of the ion beam in the mass spectrometer. In the range of 40-60 eV, altering the collision energy had almost no impact on the yield of acyl anions and, consequently, no tuning of the collision energy was required for optimising the sensitivity.

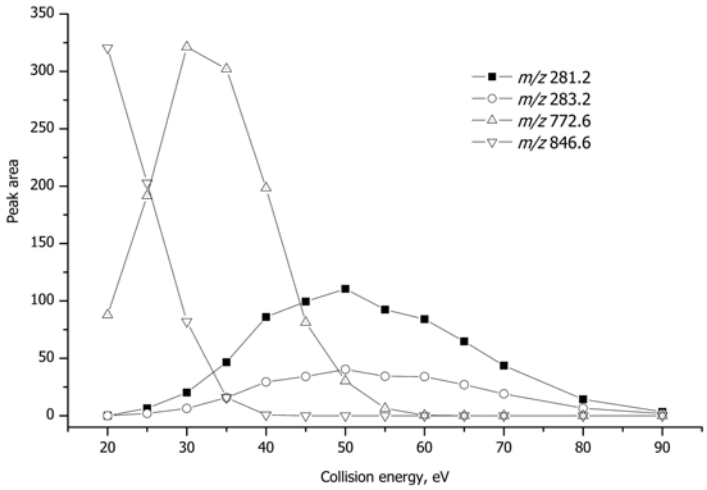

Figure 18. Intensity of peaks of fragments of the acetate adduct of PC 18:1/18:0 change with increasing the collision energy. *m/z* 846.6 - $[M+CH_3COO]^-$; *m/z* 772.6 - $[M–15]^-$; *m/z* 281.2 and *m/z* 283.2 - acyl anions of stearic and oleic acids, respectively.

3.2.3. Profiling of PCs by MPIS

Since acyl anions of FA moieties are efficiently produced by collision-induced dissociation of anion adducts of PCs they could be directly profiled by MPIS, similar to other classes of glycerophospholipids (Ekroos *et al.*, 2002). MPIS analysis of PC 16:0/18:1 and PC 18:1/16:0 standards was performed by selecting *m/z* 255.2 and 281.2, corresponding to acyl anions of palmitic acid (16:0) and oleic acid (18:1), respectively, and precursor ions of acetate and chloride adducts were detected (Figure 19). As expected, the fragment patterns in MS/MS spectra of adducts (Figure 17), the peak of the precursor ion was more abundant in precursor ion scans for the acyl anion fragment of *sn*-2 FA, than of *sn*-1 FA. The ratio of their intensities did not depend on the mode of analysis and delineated the major component in the mixture of positional isomers.

PLA_2-treated PC standards were subjected to MPIS, which demonstrated that LPCs were also detectable as acetate and chloride adduct ions (data not shown). Further analysis of

precursor ion peak areas demonstrated that MPIS produced a quantitatively consistent estimation of the mol% of related positional isomers (Table 3).

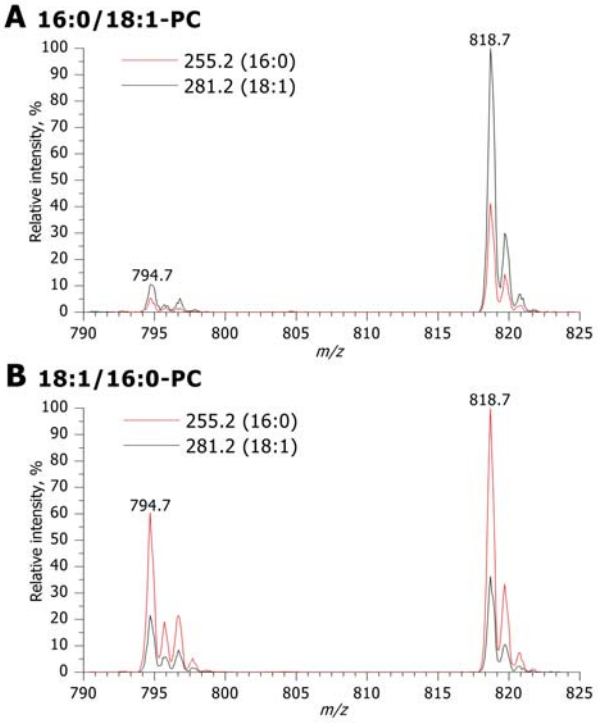

Figure 19. **(A)** MPIS spectra of synthetic PC 18:0/18:1 standard. Acyl anions of stearic and oleic acid (*m/z* 283.25 and *m/z* 281.25) were selected as fragment ions identifying precursor ions of acetate (*m/z* 818.9) and chloride (*m/z* 794.9) adducts. **(B)** MPIS spectra of synthetic PC 18:1/18:0 standard, acquired in the same way as the spectrum in panel A. Note reversed intensities of peaks of the precursor, compared to panel A. Isomeric purity of the standards is presented in Table 3.

3.2.4. MS^n fragmentation of PC adducts on an ion trap mass spectrometer

Regardless of the applied collision energy, fragmentation of anion adducts of PCs on the QqTOF mass spectrometer did not produce ions which could directly characterize the relative abundance of isomeric PC species (Figure 17). In contrast with tandem mass spectrometers equipped with a linear collision cell (*e.g.* triple quadrupole or QqTOF instruments), ion trap mass spectrometers fragment a precursor ion by applying an *m/z*-dependent resonance excitation voltage, which leaves product ions unaffected. If necessary, any product ion can be further trapped and fragmented in another cycle of the tandem mass spectrometric experiment (MS^n experiments) (reviewed in (March, 1997)).

We tested if fragmenting anion adducts of PCs in an ion trap mass spectrometer would enable direct quantification of positional isomers. MS^2 fragmentation of the chloride adduct of PC 16:0/18:1 standard produced abundant ion of a de-methylated fragment of PC $[M–15]^-$ at *m/z* 744 (Figure 20). Subsequently, MS^3 fragmentation of $[M–15]^-$ resulted in neutral loss of the FAs as ketene $[M–15–R'CH=C=O]^-$ thereby producing fragment ions of intermediate de-

methylated LPCs at *m/z* 480 and 506, with the *m/z* 480 being most abundant. Acyl anion fragments $[R'CH_2COO]^-$ were observed at *m/z* 255 and 281, although they were less abundant than in QqTOF spectra. Minor fragments formed by neutral loss of free FA $[M–15–R'CH_2COOH]^-$ from $[M–15]^-$ were detected at *m/z* 462 and 488. As expected, MS^4 fragmentation of the de-methylated LPCs produced the acyl anion fragment and corresponding products of ketene and free FA losses at *m/z* 242 and 224, respectively (data not shown). Ion trap MS^n analysis of other PC standards followed the same fragmentation pathways (data not shown).

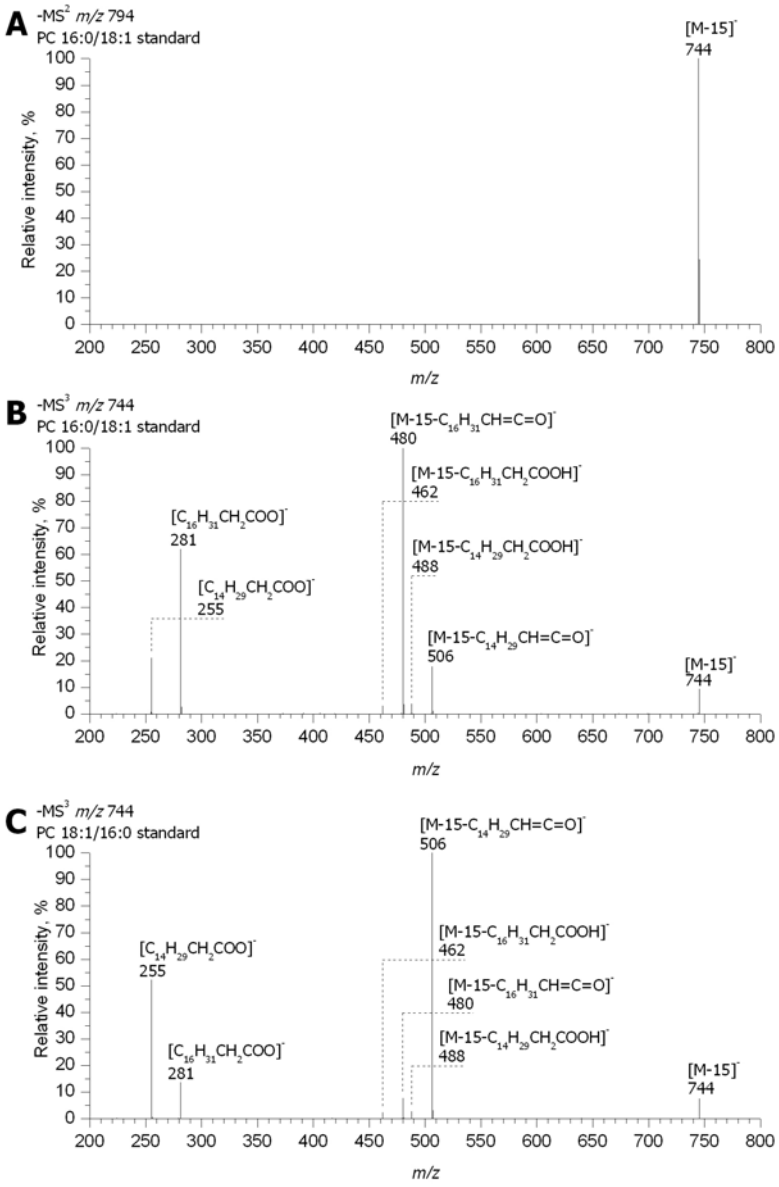

Figure 20. **(A)** MS^2 spectrum of a chloride adduct of the synthetic PC 16:0/18:1 standard. Abundant fragment at *m/z* 744 corresponds to de-methylated PC $[M–15]^-$. **(B)** MS^3 spectrum of *m/z* 744 ($[M-15]^-$). The observed fragments are the products of ketene loss $[M–15–C_{14}H_{29}CH=C=O]^-$ (*m/z* 506) and $[M–15–C_{16}H_{31}CH=C=O]^-$ (*m/z* 480), corresponding to ions of de-methylated LPC 18:1 and LPC 16:0, respectively; acyl anions of oleic (*m/z* 281) and palmatic *(m/z* 255) acids; loss of free FA $[M–15–C_{14}H_{29}CH_2COOH]^-$ (*m/z* 488) and $[M–15–C_{16}H_{31}CH_2COOH]^-$ (*m/z* 462). **(C)** MS^3 spectrum of $[M–15]^-$ ion (*m/z* 744) obtained by MS^2 fragmentation of a chloride adduct of synthetic PC 18:1/16:0 standard. The spectrum is similar to the one in panel B, but the intensities of fragments at *m/z* 506 and 480, as well as at *m/z* 281 and 255 are reversed.

MS^3 fragmentation of the isomeric standard PC 18:1/16:0 produced a spectrum, in which the intensities of fragment ions were reversed compared to the spectrum of PC 16:0/18:1 standard (Figure 20), suggesting that fragmentation pathways in ion trap and QqTOF mass spectrometers are similar (Figure 21), implying that release of FAs as either acyl anions or as neutral ketenes are position-dependent processes.

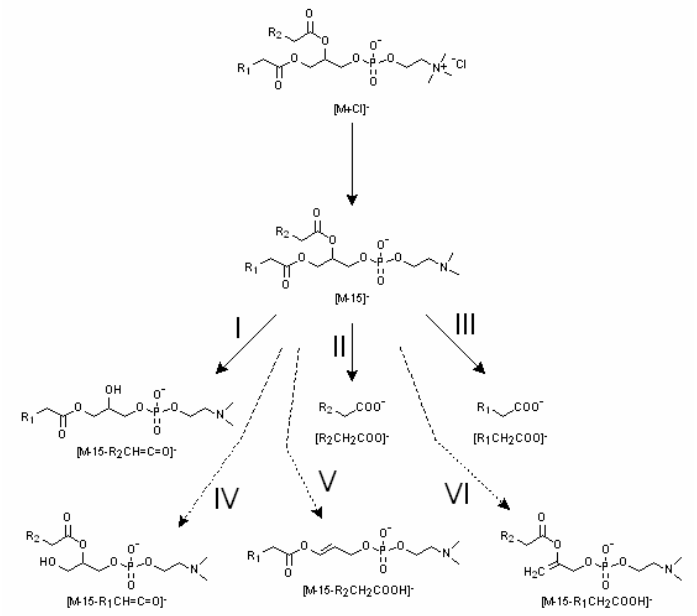

Figure 21. Fragmentation pathways of anion adduct of PC under low-energy collision-induced dissociation. In the first step of collision-induced dissociation of the PC adduct anion (*e.g.*. $[M+Cl]^-$) the de-methylated fragment ion $[M–15]^-$ is produced. Fragmentation of the $[M–15]^-$ ion proceeds along three major pathways: (I) loss of *sn*-2 FA as a ketene yields a de-methylated 2-LPC; (II) and (III) - formation of acyl anions of *sn*-2 and *sn*-1 FAs; and three minor pathways: (IV) loss of *sn*-1 FA as a ketene; (V) and (VI) - loss of neutral FA from *sn*-2 and *sn*-1 positions.

3.2.5. Quantitative analysis of positional isomers by MS^3 fragmentation

MS^3 fragmentation of PC adducts yielded abundant de-methylated LPC fragment ions matching the neutral loss of *sn*-2 FA as ketene, which might be employed in direct quantification of isomeric and isobaric species. We therefore evaluated if the relative intensity of these ions correlated with the estimates of mol% of isomeric species determined by PLA_2 hydrolysis of synthetic standards. The ratio of intensities of de-methylated LPCs fragment ions produced *via* neutral loss of FAs as ketenes (*i.e.* $[M–15–R'CH=C=O]^-$) correlated with the estimates of mol% determined by the other three independent methods of detection (Table 3). To further validate the method, we mixed pairs of isomeric standards in various molar ratios, digested the mixtures by PLA_2 and determined the content of positional isomers on the QqTOF mass spectrometer. Aliquots of the mixtures of standards were analysed directly by MS^3 fragmentation, and the results were compared. Linear regression demonstrated a statistically confident correlation between the obtained mol% estimates (Figure 22). The same

experiment was performed using other pairs of isomeric standards: PC 16:0/18:0 and PC 18:0/16:0, and PC 14:0/18:0 and PC 18:0/14:0, and produced similar results (data not shown). Taken together, the data indicated that neutral loss of FA as ketene predominantly occurs at the *sn*-2 position.

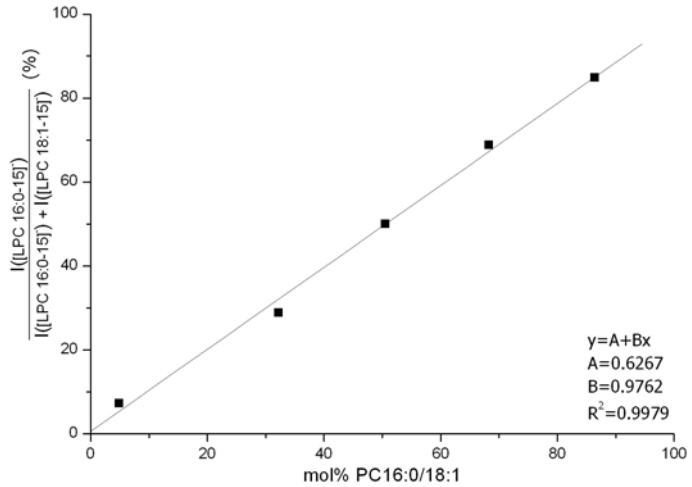

Figure 22. Quantification of mixtures of PC 18:1/16:0 and PC 16:0/18:1 standards by ion trap MS^3 fragmentation. X-axis: mol% of PC 18:1/16:0 in the mixture determined by PLA_2 hydrolysis and PIS *m/z* 184.1; Y-axis: the peak intensity of de-methylated $[LPC\ 16:0\text{-}15]^-$ (*i.e.* $[M–15–C_{16}H_{31}CH=C=O]^-$, *m/z* 480) divided by the sum of peak intensities of de-methylated $[LPC\ 16:0\text{-}15]^-$ and $[LPC\ 18:1\text{-}15]^-$ (*i..e.* $[M–15–C_{14}H_{29}CH=C=O]^-$, *m/z* 506) and in acquired MS^3 spectra.

The intensity of other fragments, or a combination of intensities of fragments, observed in MS^3 spectra did not correlate well with the mol% of the isomers, possibly due to the yield of fragments from other fragmentation pathways being less position-specific than that of ketene loss. Further supporting this notion, we found that lysophosphatidic acid fragments formed by loss of ketene from *sn*-2 position enabled accurate estimates of mol% in mixtures of PA 16:0/18:1 and PA 18:1/16:0, although they were much less abundant than fragment ions produced by neutral loss of free FA (data not shown).

3.2.6. Validation of the mass spectrometric approach

The lipid composition and major molecular species of glycerophospholipids of human red blood cells were previously rigorously characterized (Connor *et al.*, 1997) by a sophisticated analytical routine that involved several TLC separations, hydrolysis of lipids by phospholipase C, derivatization of diradylglycerols by benzoic anhydride followed by quantification of diradylglycerolbenzoates by reversed-phase HPLC (Blank *et al.*, 1984). Diradylglycerolbenzoates were separated into 20 chromatographic peaks (some of them contained a few co-eluted species), however separation of positional isomers was not achieved (Blank *et al.*, 1984).

To further validate our mass spectrometric approach, we determined the molecular composition of PCs from human red blood cells (Table 4) and compared it with the results previously reported by Connor *et al* (Connor *et al.*, 1997). Connor *et al* identified 26 molecular species of PCs by HPLC and 22 species were identified in the present work by a combination of PIS *m/z* 184.1 and MPIS. We note that we did not acquire precursor ion spectra for acyl anions of a few minor FAs (*e.g*. 22:6) although Connor *et al* found corresponding lipids. Within the datasets independently obtained by Connor et al and by us (Table 4) 14 molecular species overlapped. All non-overlapping species were of low abundance and their relative content was less than 3 mol%. All 8 major PC species with relative content > 3 mol%, which were reported by Connor *et al*, were also detected by mass spectrometry with very similar relative abundance. Furthermore, ion trap MS^3 analysis of major PC species suggested that positional isomers (remained undetected by Connor *et al*) are common in human red blood cells (Table 4). For example PC 20:4/16:0, having a highly unsaturated arachidonic acid at *sn*-1 position, constitutes about 13 mol% of the total PC 36:4.

Connor *et al* detected one PC species comprising a FA with odd number of carbon atoms: PC 17:0/18:1. Mass spectrometry confirmed that 17:0 and 17:1 are major FAs with odd number of carbons that are present in PCs from red blood cells and we also detected them in three other molecular species (Table 4). We note here that *m/z* of PC species with FAs having an odd number of carbon atoms might coincide with *m/z* of ether PCs in which an alkyl chain is linked to the glycerol phosphate backbone *via* an ether, rather than an ester, bond. However, in MS/MS spectrum of synthetic 1-O-hexadecyl-2-arachidonoyl-*sn*-glycerol-3-PC standard, no corresponding alkoxide ion at *m/z* 241.25 was observed (data not shown). Therefore alkoxide anions of ether lipids will not be detectable by MPIS and will not compromise the confidence of peak assignment in MPIS spectra. PC peaks in which only a single acyl anion was identified and the confirmatory FA with odd number of carbon atoms was not detected will indicate the presence of ether species. Taken together, PIS *m/z* 184.1, MPIS for acyl anion of FA moieties, and ion trap MS^3 fragmentation revealed high complexity of the molecular composition of PCs, represented by a variety of isomeric and isobaric species. We concluded that qualitative and quantitative concordance of the molecular composition of PCs determined by us and independently by Connor *et al* validates the mass spectrometry-based approach.

Table 4. The molecular composition of PCs from human red blood cells

PIS *m/z* 184.1			MPIS		Ion Trap MS³		
+Precursor Ion	Relative Content	Brutto Composition[a]	−Precursor Ion[b]	Fatty Acid Moieties	−Precursor Ion[c]	Molecular Species	
m/z	%		*m/z*		*m/z*		*mol %*
706.6	1	30:0	764.8	14:0;16:0			
732.6	2	32:1	790.6	16:0;16:1			
734.6	5	32:0	792.6	16:0/16:0			
746.6	1	33:1	804.8	16:0;17:1			
748.6	<1	33:0	806.8	16:0;17:0			
756.6	<1	34:3	814.8	16:1;18:2			
758.6	20	34:2	816.8	16:0;18:2	792	16:0/18:2	94
						18:2/16:0	6
760.6	22	34:1	818.8	16:0;18:1	794	16:0/18:1	85
						18:1/16:0	15
762.6	3	34:0	820.8	16:0;18:0			
772.6	1	35:2	830.8	17:0;18:2			
774.6	<1	35:1	832.8	17:0;18:1			
782.6	7	36:4	840.8	16:0;20:4	816	16:0/20:4	87
						20:4/16:0	13
784.6	4	36:3	842.8	18:1;18:2	818	18:1/18:2	42
				16:0;20:3		18:2/18:1	16
				18:0;18:3		16:0/20:3	31
						20:3/16:0	6
						18:3/18:0	5
786.6	8	36:2	844.8	18:0;18:2	820	18:0/18:2	71
				18:1/18:1		18:2/18:0	7
						18:1/18:1	23
788.6	6	36:1	846.8	18:0;18:1			
				16:0;20:1			
790.6	<1	36:0	848.8	18:0/18:0			
808.6	1	38:5	866.8	18:1;20:4			
810.6	2	38:4	868.8	18:0;20:4			

[a] Total number of carbon atoms:total number of double bonds.
[b] Detected as acetate adduct.
[c] Detected as chloride adduct.

3.2.7. Discussion

PCs can be detected at the low μM – nM sensitivity as anionic acetate and chloride adducts, which produce structure-specific ions upon tandem mass spectrometric fragmentation. Regardless of the type of the instrument, collision-induced dissociation of an anionic adduct first generates abundant $[M–15]^-$ fragment, whose subsequent fragmentation pathways are common for negatively charged glycerophospholipids (Hsu and Turk, 2000a; Hsu and Turk, 2000b; Hsu and Turk, 2000c; Hsu and Turk, 2001; Larsen *et al.*, 2001) (Figure 21).

The difference of fragment patterns observed in QqTOF MS/MS and ion trap MS^2, MS^3 and MS^4, originate from mechanisms by which the collision energy is transmitted to selected precursor ions and affects the yield of unstable intermediates. It is therefore not surprising that the fragmentation of PC adducts in a QqTOF instrument at high collision

energy predominantly yielded acyl anion fragments of the FA moieties, whereas abundant peaks of the de-methylated LPCs were observed in MS^3 ion trap spectra.

The inspection of fragmentation pathways by ion trap MS^3 revealed that they have different positional specificity (Figure 20 and Figure 21). Neutral loss of FA as ketene accounts for ~58 % of the total intensity of fragment ions and occurs almost exclusively *via* the cleavage of *sn*-2 FA (~99% of ketene fragment ions), thus generating de-methylated 2-LPC. Its yield does not depend on the FA moieties, as is evident from the accurate estimation of mol% of isomeric species comprising different combinations of FAs (Table 3 and Figure 22). Acyl anion fragments are abundant in MS^3 spectra (~39% of the total fragment ion intensity) and are mostly (although not exclusively!) produced from the *sn*-2 FA (80% of intensity of acyl anion fragments). Neutral loss of free FA appears to be a relatively minor process that accounts for about 2% of the total fragment ion intensity.

Relative (in mol%) quantification of isobaric and isomeric PC species by ion trap MS^3 fragmentation is direct and does not require internal standards. The determination is very specific because of the accurate selection of precursor masses at MS^2 and MS^3 stages, and therefore is reliable even if applied to total lipid extracts. Furthermore, matching pairs of de-methylated 2-LPCs and acyl anion fragments of *sn*-2 FA additionally verify the peak assignment. At the same time, MS^3 fragmentation is poorly suited for the detection of PC precursors in lipid mixtures, as well as for the quantification of PC species with different molecular mass. Since no efficient PIS is possible on ion trap mass spectrometers, complementary analysis by QqTOF mass spectrometry and by ion trap mass spectrometry should be performed.

We applied MPIS on a QqTOF mass spectrometer and MS^3 fragmentation on the ion trap mass spectrometer, to characterize the molecular composition of PCs. MPIS complemented the previously established method of PIS *m/z* 184.1 and not only increased the specificity and the dynamic range of detection, but also allowed us to identify the FA moieties and their relative localization on the glycerol phosphate backbone of the individual PC molecules. MS^3 fragmentation of precursor ions detected by MPIS independently enabled quantitative estimation of the relative amount of their positional isomers. Since a combination of mass spectrometric methods could account for individual molecular species of PCs, we assumed that this is currently the most comprehensive approach for their characterization.

The combination of MPIS and MS^3 was applied to profile PCs in a total lipid extract from human red blood cells (Table 4) and MDCK II cells (data not shown). Although PCs of human red blood cells have been extensively characterized, no indication of the possible presence of positional isomers has been reported (Renooij *et al.*, 1976). Biochemical studies

have shown that FA remodelling is a common phenomenon in eukaryotic organisms (Yamashita *et al.*, 1997), which potentially accounts for the observed presence of isomeric lipid species. Biophysical studies have demonstrated that positional isomers display different types of phase behaviour and have differences in phase transition temperatures (Cunningham *et al.*, 1998; Keller *et al.*, 2000). Importantly, positional isomers differ in their ability to interact with sterols thus affecting the dynamics of membrane microdomains.

3.3. COLLISION-INDUCED DISSOCIATION PATHWAYS OF YEAST SPHINGOLIPIDS AND THEIR MOLECULAR PROFILING IN TOTAL LIPID EXTRACTS

Wild type *S. cerevisiae* synthesizes three classes of inositol-containing sphingolipids: inositolphosphoceramides (IPCs), mannosyl-inositolphosphoceramides (MIPCs) and mannosyl-diinositolphosphoceramides ($M(IP)_2Cs$) (Figure 23) (Dickson and Lester, 1999a; Funato *et al.*, 2002; Schneiter, 1999; Sims *et al.*, 2004). Numerous genetic, biochemical and cell biological studies have implicated the yeast sphingolipids in several cellular processes, such as heat-stress responses, calcium homeostasis, protein sorting and cell surface polarization (Bagnat *et al.*, 2001; Bagnat *et al.*, 2000; Bagnat and Simons, 2002; Dickson and Lester, 2002; Eisenkolb *et al.*, 2002; Schneiter, 1999).

The inositol-containing sphingolipids consist of three structural elements: a long chain base and an amide-linked FA form that the apolar ceramide backbone, to which a polar head group is attached *via* a phosphate moiety (Figure 23). The structural diversity of yeast sphingolipids stems from the variability of their head groups, as well as the number of carbon atoms and the number and position of hydroxyl groups and double bonds in their ceramide backbone (Funato *et al.*, 2002; Garton *et al.*, 2003). In *S. cerevisiae,* long chain bases typically contain 16 to 20 carbon atoms and two (in dihydrosphingosines) or three (in phytosphingosines) hydroxyl groups, which, in combination with various amide-linked FA moieties, give rise to sphingolipids with a dihydroceramide or phytoceramide backbone, respectively (Figure 23). The amide-linked FA moiety is typically composed of 26 carbon atoms and can be mono or di-hydroxylated or contain no hydroxyl groups.

Methods for the analysis of yeast glycerophospholipids by mass spectrometry have been developed and successfully used in yeast lipid biochemistry (Boumann *et al.*, 2003; Boumann *et al.*, 2004; Schneiter *et al.*, 1999). In comparison, few attempts have been made to establish methodology for the analysis of the yeast sphingolipids. Traditional methods such as chemical derivatization (Smith and Lester, 1974), gas chromatography - mass spectrometry

(Oh *et al.*, 1997) and magnetic sector mass spectrometry (Hechtberger *et al.*, 1994) have provided valuable information about the structural diversity of yeast sphingolipids. However, these methods are laborious and offer low sensitivity which severely limits their efficacy for high-throughput oriented lipidomics studies of *S. cerevisiae* and other organisms synthesizing inositol-containing sphingolipids (Dickson and Lester, 1999b; Sperling and Heinz, 2003).

This sections outlines the use of QqTOF (Chernushevich *et al.*, 2001) and linear ion trap-orbitrap (LTQ Orbitrap)(Hu *et al.*, 2005; Olsen *et al.*, 2005) mass spectrometers to elucidate the fragmentation pathways of inositol-containing sphingolipids and the identification of specific fragment ions for each lipid class and the ceramide backbone of individual lipid species. Subsequent QqTOF analysis using the method of MPIS, based on *m/z* of class-specific fragments, enabled simultaneous profiling of sphingolipids and glycerophospholipids in total yeast lipid extracts.

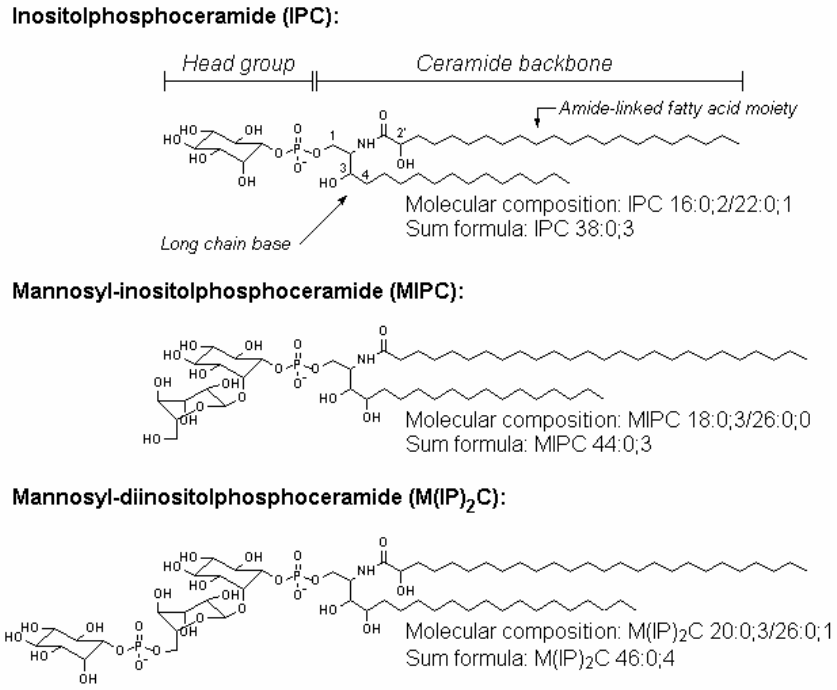

Figure 23. Structure of yeast sphingolipids. Inositol-containing sphingolipids consist of a long chain base and an amide-linked FA that together consitute a ceramide backbone, to which a polar head group is attached *via* a phosphate moiety. The long chain base and the FA moiety typically comprise 16 to 20 and 20 to 26 carbon atoms, respectively. The long chain base might comprise two (dihydrosphingosine) or three (phytosphingosine) hydroxyl groups at positions 1, 3 and 4 that form dihydroceramides or phytoceramides, respectively. The amide-linked FA moiety can be non-, mono-, or di-hydroxylated, with one hydroxyl group at position 2' (α-hydroxyl group) and other groups elsewhere between positions 9' and 16'. In this work, yeast sphingolipids were annotated either by their molecular composition or by sum formula. The molecular composition indicates the number of carbon atoms, double bonds and hydroxyl groups separately in the long chain base and in the FA moiety, whereas the sum formula provides the total number of carbon atoms, double bonds and hydroxyl goups in the entire ceramide backbone. The species annotation convention is explained in the Material and Methods (page 93).

3.3.1. Fragmentation pathways of IPCs

To elucidate the fragmentation pathways of the three inositol-containing sphingolipid classes - IPC, MIPC and $M(IP)_2C$, we isolated them by preparative TLC from the lipid extracts of wild type *S. cerevisiae* (Hechtberger *et al.*, 1994) and from three mutants (*i.e. scs7Δ*, *sur2Δ* and *scs7Δsur2Δ*), which are known to synthesize sphingolipids having altered structures of their ceramide backbones. Individual species within the same lipid class were subjected to tandem mass spectrometry on the QqTOF and LTQ Orbitrap mass spectrometers.

The most abundant ions in the IPC fraction isolated from wild type strain of *S. cerevisiae* were detected at *m/z* 952.70, 968.70, and 980.73, corresponding to IPC 44:0;4, IPC 44:0;5 and IPC 46:0;4, respectively (data not shown), as was previously observed (Gaigg *et al.*, 2001; Hechtberger *et al.*, 1994). Tandem mass spectra of all species acquired on a QqTOF instrument were dominated by two fragment ions at *m/z* 259.02 ($[IP]^-$) and 241.01 ($[IP - H_2O]^-$), both originating from the inositolphosphate head group (Figure 24A, D). These fragments are also typical for tandem mass spectra of phosphatidylinositols (Hsu and Turk, 2000a). Since *m/z* of IPC species do not overlap with *m/z* of phosphatidylinositols that comprise common FA moieties, the fragment ion with *m/z* 241.0 was previously used for profiling IPC species by PIS (Young *et al.*, 2002). Two very low abundant fragment ions, detected at *m/z* 790.65 and 772.63, were produced *via* neutral loss of the head group as dehydroinositol (Δm = 162.05 Da) followed by the loss of H_2O, corresponding to the two ceramide phosphate fragments $[CerP]^-$ and $[CerP - H_2O]^-$, respectively (Figure 24D). Efficient fragmentation of IPCs was achieved at the collision energy offset of 65-75 eV, compared to the 40-55 eV that was typically required for the fragmentation of glycerophospholipids (Ekroos *et al.*, 2003). Although the ratio of intensities of the two fragment ions *m/z* 259.02 and 241.01 was collision energy dependent, both fragments were always observed simultaneously, contrary to a typical fragmentation pattern of phosphatidylinositol species, in which *m/z* 241.0 fragment was most abundant (Hsu and Turk, 2000a).

We further investigated if the fragmentation of IPC species could yield abundant ions that were specific to their ceramide backbone. To this end we acquired MS^n spectra from their molecular anions on a hybrid linear ion trap - orbitrap mass spectrometer (Hu *et al.*, 2005). orbitrap is a novel Fourier transform orbital trapping mass analyzer (Hardman and Makarov, 2003; Makarov, 2000). To acquire MS^n spectra with high mass accuracy, precursor ions were isolated and fragmented in the linear trap, and spectra were acquired using either the orbitrap analyzer (for higher mass accuracy) or the linear ion trap detector (for better sensitivity). In contrast to instruments equipped with a linear collision cell, such as QqTOF or triple quadrupole mass spectrometers, the collision induced dissociation of precursor ions in an ion

trap usually leaves fragment ions intact, since they fall off the excitation resonance frequency. Therefore, labile intermediate products could be identified and the entire sequence of fragmentation events established *via* successive fragmentation by MS^n (Ekroos *et al.*, 2003; Larsen *et al.*, 2001). Continuous nanoflow infusion of lipid extracts offered ample time to acquire MS^n spectra with reliable ion statistics. Higher than 30.000 (FWHM) mass resolution, together with mass accuracy more than 3 ppm, achieved by the orbitrap analyzer, allowed us to unequivocally determine the elemental composition of detected fragment ions.

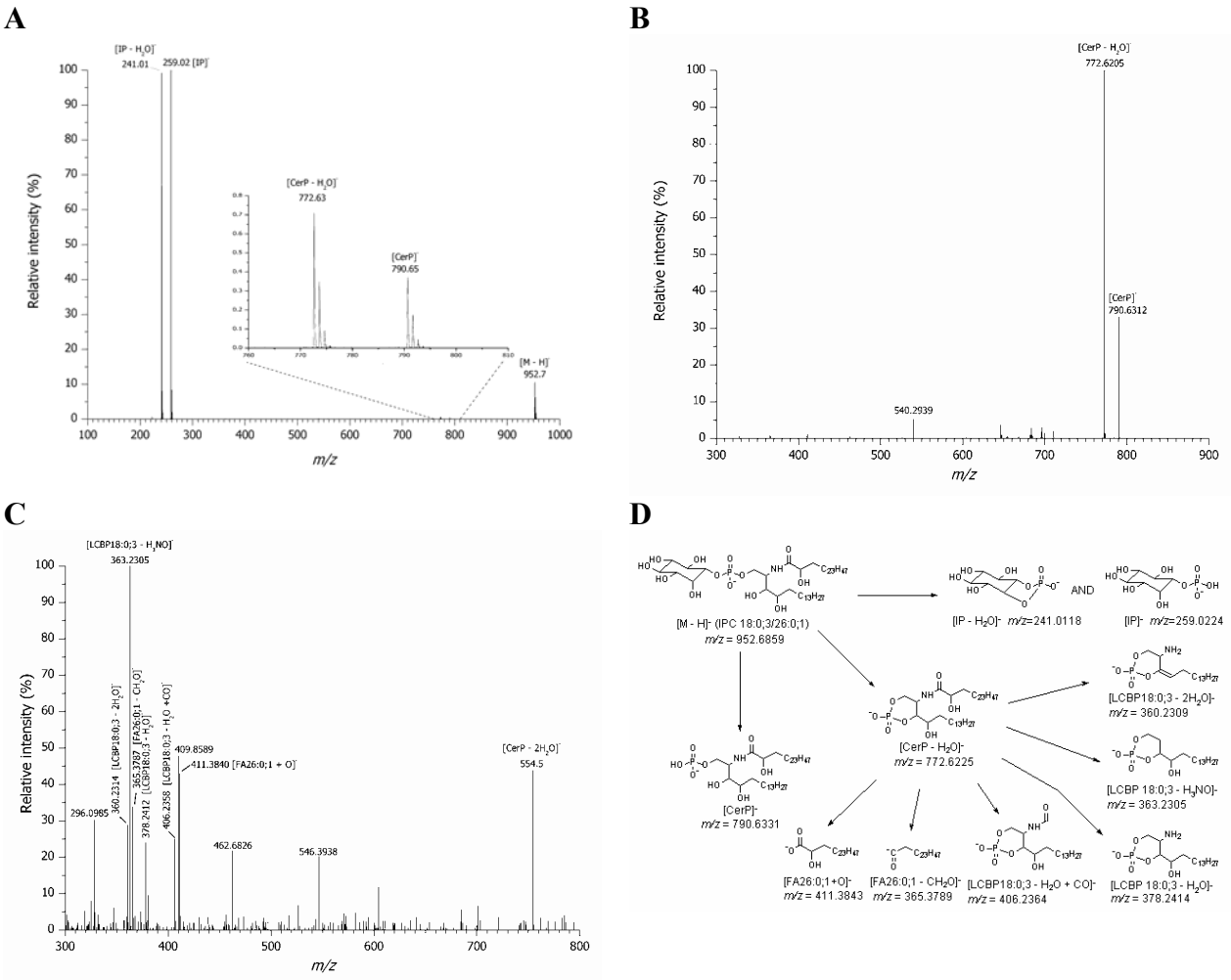

Figure 24. Fragmentation pathways of IPC species. **(A)** QqTOF MS/MS spectrum of IPC 44:0;4 ion of *m/z* 952.7 ([M - H]-) acquired at the collision energy of 68 eV. **(B)** Orbitrap MS^2 spectrum acquired from the same precursor **(C)** Orbitrap MS^3 spectrum acquired from the precursor ion *m/z* 772.6205 ([CerP - H2O]$^-$) at the relative collision energy of 24%. Peaks with *m/z* 462.6826, 409.8589, 365.5548, 296.0985 originated from background and were not detectable in the corresponding ion trap MS^3 spectrum (data not shown). **(D)** Major fragmentation pathways of IPC 18:0;3/26:0;1 elucidated by QqTOF MS/MS and LTQ Orbitrap MS^n analysis. The structure of the [CerP - H2O]$^-$ fragment ion with *m/z* 772.6225 is presented with a cyclic phosphate residue between the hydroxyl groups at positions 1 and 3 of the long chain moiety, however isomer structures are possible.

Orbitrap MS^2 analysis of the abundant IPC 44:0;4 species with *m/z* 952.6897, yielded intense ceramide phosphate fragments [CerP - H_2O]$^-$ and [CerP]$^-$ with *m/z* 772.6205 and *m/z* 790.6312, respectively (Figure 24B). The identification of fragment ions was supported by

their accurately determined *m/z* that deviated by less than 3 ppm from the corresponding calculated values, as well as by their further MS^3 analysis (see below). In general, similar patterns of fragment ions were observed in MS^2 spectra, acquired from the same precursors on the linear ion trap and on the orbitrap (data not shown). However, MS^2 spectra did not reveal the exact chemical structure of both ceramide-specific fragments. It was unclear, if the loss of H_2O produced a double bond elsewhere within their molecules, or yielded a cyclic phosphate moiety. For clarity we present the structure of (dehydro)ceramide phosphate fragment ions, with a cyclic phosphate moiety between the hydroxyl groups at positions 1 and 3 of the long chain base (Figure 24D), however alternative isomeric molecular structures are also possible.

Further orbitrap MS^3 analysis of *m/z* 772.6205 ($[CerP - H_2O]^-$) elucidated the composition of its ceramide backbone (Figure 24C). The fragmentation produced an acyl anion of the FA moiety $[FA26:0;1 + O]^-$ with *m/z* 411.3840 (mass accuracy 0.7 ppm). Another fragment ion, related to the FA moiety was detected at *m/z* 365.3787 and was produced *via* subsequent loss of CH_2O, *i.e.* $[FA26:0;1 - CH_2O]^-$ (mass accuracy 0.6 ppm). These fragments were previously detected in tandem mass spectra of ceramides acquired in negative ion mode on a triple quadrupole instrument (Han, 2002; Hsu and Turk, 2002). Fragments with *m/z* 378.2412, 363.2305 and 360.2314 were produced *via* neutral loss of the amide-linked FA, yielding the long chain base phosphate fragment ions $[LCBP18:0;3 - H_2O]^-$ (mass accuracy 0.5 ppm), $[LCBP18:0;3 - H_3NO]^-$ (mass accuracy 0.1 ppm) and $[LCBP18:0;3 - 2H_2O]^-$ (mass accuracy 1.4 ppm), respectively (Figure 24C, D). The fragment ion with *m/z* 406.2358 was produced by internal cleavage of the FA moiety resulting in neutral loss of the hydrocarbon chain with secondary α-hydroxyl ($[LCBP18:0;3 - H_2O + CO]^-$ (mass accuracy 1.5 ppm).

Although we could only speculate on the exact chemical structure of these fragment ions, the orbitrap mass accuracy allowed us to unequivocally determine the number of carbon atoms, hydroxyl groups and double bonds separately in the long chain base and in the amide-linked FA of their ceramide backbone. Once fragment ions in MS^3 spectra were identified, further structural analysis of low abundant IPC species was performed by MS^3 analysis on the linear ion trap, which improved the sensitivity and reduced the analysis time (data not shown).

Thus, the combination of QqTOF MS/MS and orbitrap MS^2 and MS^3 fragmentation allowed us to elucidate the chemical composition of the head group and both cleavable parts of the ceramide backbone, *i.e.* the long chain base and the amide-linked FA (Figure 24D). Interestingly, no fragments were observed in the MS^3 spectrum that pointed to alternative ceramide structures having different numbers of either methylene or hydroxyl groups. This indicated that the precursor ion IPC 44:0;4 at *m/z* 952.7 contained a ceramide backbone composed of a long chain base with 18 carbon atoms and three hydroxyl groups

(phytosphingosine), together with an amide linked FA moiety with 26 carbon atoms and one hydroxyl group, *i.e.* IPC 18:0:3/26:0;1, which agreed well with the previously reported GC-MS identification of amide-linked FAs in sphingolipids from wild type *S. cerevisiae* (Oh *et al.*, 1997).

To further substantiate the structural assignment of fragment ions, we performed orbitrap MS^2 and MS^3 analysis of IPC species isolated from the *elo3*Δ mutant (Oh *et al.*, 1997). This mutant lacks the enzymatic activity for elongating FA moieties to C26, and, therefore, produces IPC species predominantly comprising C22 amide-linked FAs (Oh *et al.*, 1997). Orbitrap analysis of an *elo3*Δ lipid extract detected the abundant ion with *m/z* 896.6260 corresponding to IPC 40:0;4 (data not shown). As expected, its orbitrap MS^2 fragmentation yielded an intense fragment with *m/z* 716.5590, corresponding to $[CerP - H_2O]^-$ (mass accuracy 1.4 ppm). Further orbitrap MS^3 analysis of $[CerP - H_2O]^-$ produced fragments with *m/z* 406.2365, 378.2409, 363.2303 and 360.2310, corresponding to the long chain base phosphate fragment ions $[LCBP18:0;3 - H_2O + CO]^-$ (mass accuracy 0.2 ppm); $[LCBP18:0;3 - H_2O]^-$ (mass accuracy 1.3 ppm); $[LCBP18:0;3 - H_3NO]^-$ (mass accuracy 0.6 ppm); and $[LCBP18:0;3 - 2H_2O]^-$ (mass accuracy 0.3 ppm), respectively (data not shown). Exactly the same fragment ions were detected upon orbitrap MS^3 of IPC 18:0;3/26:0;1 isolated from wild type *S. cerevisiae*. (Figure 24D). However, the fragment ion with *m/z* 355.3220 corresponding to an acyl anion of the FA moiety $[FA22:0;1 + O]^-$ (accuracy 0.6 ppm) was detected in the corresponding MS^3 spectrum of $[CerP - H_2O]^-$ from *elo3*Δ mutant (data not shown). Thus, the comparison of orbitrap MS^2 and MS^3 spectra acquired from IPC 18:0;3/26:0;1 (isolated from wild type) and IPC 18:0;3/22:0;1 (isolated from the *elo3*Δ mutant) species validated the chemical structure of major fragment ions, produced from IPC species comprising phytosphingosine long chain base and different amide-linked FAs with α-hydroxyl group.

We then set out to determine how hydroxyl groups in the long chain base and amide-linked FA moieties affected the fragmentation pathways of IPC species. Two enzyme activities in *S. cerevisiae*, encoded by SCS7 and SUR2 genes, are responsible for the hydroxylation of the ceramide backbone. Scs7p is the hydroxylase required for the α-hydroxylation of amide-linked FA moieties (Haak *et al.*, 1997) (Figure 23). Sphingolipids, synthesized by the *scs7*Δ mutant, comprise phytosphingosine and an amide-linked FA without an α-hydroxyl group. Sur2p is responsible for converting dihydrosphingosine to phytosphingosine, whereby a hydroxyl group is placed at position 4 of the long chain base (Haak *et al.*, 1997) (Figure 23). Thus, the ceramide backbone of sphingolipids from the *sur2*Δ mutant consists of dihydrosphingosine and an amide-linked FA with or without α-hydroxyl group. The double mutant *sur2*Δ*scs7*Δ is viable and synthesizes sphingolipids with a

ceramide backbone containing dihydrosphingosine and an amide-linked FA without α-hydroxyl group (Haak *et al.*, 1997).

Orbitrap MS and TOF MS spectra, acquired from a lipid extract of *scs7*Δ mutant, showed an abundant ion at *m/z* 936.6937, corresponding to IPC 44:0;3 (data not shown). Its orbitrap MS^2 analysis yielded intense ceramide phosphate fragments $[CerP - H_2O]^-$ with *m/z* 756.6262 (mass accuracy 2.0 ppm) and $[CerP]^-$ *m/z* 774.6369 (mass accuracy 1.7 ppm) (data not shown). In turn, MS^3 fragmentation of $[CerP - H_2O]^-$ produced two long chain base phosphate fragment ions with *m/z* 378.2412 and 360.2307, corresponding to $[LCBP18:0;3 - H_2O]^-$ (mass accuracy 0.1 ppm) and $[LCBP18:0;3 - 2H_2O]^-$ (mass accuracy 0.6 ppm), respectively (Figure 25A, B). Acyl anion of the amide-linked FA $[FA26:0;0 + O]^-$ was detected at *m/z* 395.3887 (mass accuracy 1.8 ppm) (Figure 3, panels A and B). Wild type IPC 44:0,4 and IPC 44:0;3 from *scs7*Δ were only different by a single hydroxyl group in the FA moiety (cp. Figure 24D with Figure 25B), yet several long chain base-specific fragments were missing in MS^3 spectra of IPC 44:0;3 from *scs7*Δ. Therefore, we speculate that the α-hydroxyl group enhanced the diversity of pathways of neutral loss of fragments of amide-linked FA moieties off the ceramide backbone. Nevertheless, it was possible to unambiguously assign fragments specific for the long chain base and amide-linked FA and thus identify IPC 44:0;3 from *scs7*Δ mutant as IPC 18:0:3/26:0;0.

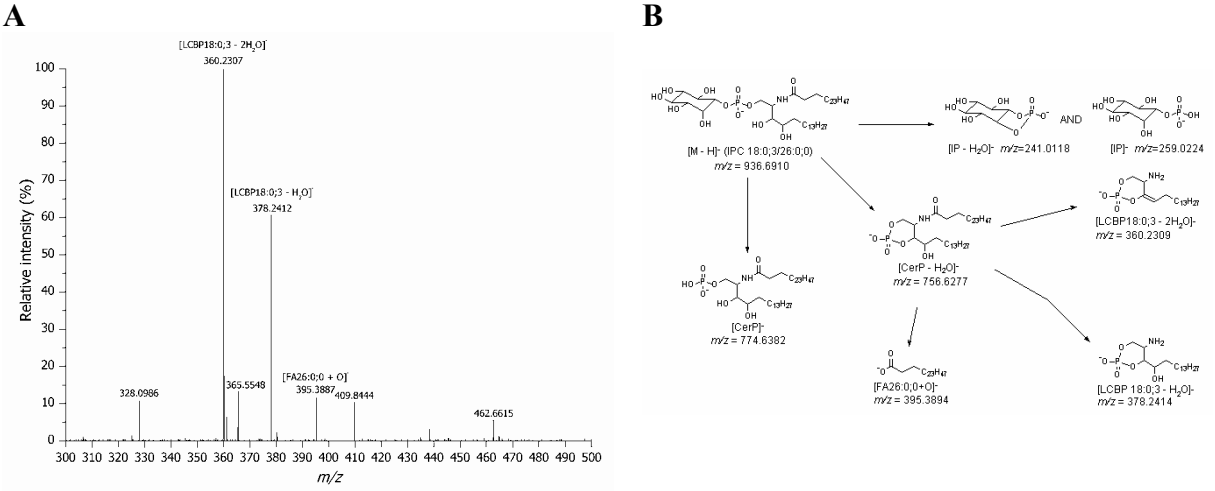

Figure 25. Fragmentation pathways of IPC 18:0;3/26:0;0 isolated from *scs7*Δ mutant. **(A)** Orbitrap MS^3 analysis of intermediate $[CerP - H_2O]^-$ fragment (*m/z* 756.6), which was obtained from the molecular anion of IPC 44:0;3 *via* its MS^2 fragmentation. Peaks with *m/z* 462.6826, 409.8589, 365.5548, 328.0986 originate from background and were not detectable in the ion trap MS^3 spectrum from the same precursor (data not shown). **(B)** Major fragmentation pathways of IPC 18:0;3/26:0;0 isolated from the *scs7*Δ mutant elucidated by QqTOF MS/MS and LTQ Orbitrap MS^n analysis.

We further compared the fragmentation pathways of the four IPCs with altered ceramide backbones: IPC 18:0:3/26:0;1 (wild type) (Figure 24D), IPC 18:0:3/26:0;0 (*scs7*Δ) (Figure 25B), IPC 18:0:2/26:0;1 (*sur2*Δ) (data not shown), and IPC 18:0:2/26:0;0

(*sur2*Δ*scs7*Δ) (data not shown). All four IPCs produced a common set of structure-specific fragments. [LCBP - H_2O]$^-$ and [LCBP - $2H_2O$]$^-$ were always produced from the long chain base, and the acyl anion [FA + O]$^-$ was produced from the amide-linked FA moiety (Table 5). If an α-hydroxyl group was present in the amide-linked FA (*e.g.* IPC 18:0:3/26:0;1, IPC 18:0:2/26:0;1), products of neutral loss of the FA related fragments [LCBP - H_2O + CO]$^-$ and [LCBP - H_3NO]$^-$ were typically observed, along with another FA related fragment [FA - CH_2O]$^-$ (Table 5; Figure 24D; Figure 25B). The relative intensities of structure-specific fragment ions varied between IPC species. Fragment ions comprising a long chain base phosphate moiety were, typically, more abundant than fragment ion(s) related to the FA moiety, although the α-hydroxyl group enhanced their intensity.

Thus we concluded that the fragmentation of molecular anions of IPCs on a QqTOF mass spectrometer predominantly produced head group specific fragments, whereas MS^2 fragmentation on the ion trap yielded abundant ceramide phosphate fragments [CerP - H_2O]$^-$, which served as a starting point for further ceramide backbone-specific fragmentation by MS^3. MS^3 analysis determined the number of carbon atoms, double bonds and hydroxyl groups in the long chain base and in the amide-linked FA of each fragmented IPC precursor and, hence, enabled their identification as individual molecular species.

Table 5. Structure specific fragment ions produced from inositol-containing sphingolipids upon MS^3 fragmentation of the intermediate [CerP - H_2O]$^-$ fragment ion

	Amide-linked fatty acid moiety	
Long chain base moiety	With α-hydroxyl group FA X:Y;1[a]	Without α-hydroxyl group FA X:Y;0
Phytos-phingosine LCB X:Y;3[a]	$[LCBP - H_2O]^-$ $[LCBP - 2H_2O]^-$ $[LCB - H_3NO]^-$ $[LCBP - H_2O + CO]^-$ $[FA + O]^-$ $[FA - CH_2O]^-$	$[LCBP - H_2O]^-$ $[LCBP - 2H_2O]^-$ $[FA + O]^-$
Dihydro-sphingosine LCB X:Y;2	$[LCBP - H_2O]^-$ $[LCBP - 2H_2O]^-$ $[LCB - H_3NO]^-$ $[LCBP - H_2O + CO]^-$ $[FA + O]^-$ $[FA - CH_2O]^-$	$[LCBP - H_2O]^-$ $[LCBP - 2H_2O]^-$ $[FA + O]^-$

[a] X and Y indicate the number of carbon atoms and double bonds in the long chain base or amide-linked fatty acid moiety, respectively.

3.3.2. Fragmentation pathways of MIPCs

The most abundant ions in the MIPC fraction were detected on a QqTOF mass spectrometer at *m/z* 1114.74 and 1142.79 and corresponded, respectively, to MIPC 44:0;4 and

MIPC 46:0;4 (data not shown), as was also previously observed (Gaigg *et al.*, 2001; Hechtberger *et al.*, 1994). Tandem mass spectrometry of MIPC species on a QqTOF instrument yielded fragments of the mannosyl-inositolphosphate (MIP) head group: $[MIP]^-$, $[MIP - H_2O]^-$, $[IP]^-$, $[IP - H_2O]^-$, and $[IP - 2H_2O]^-$ (Figure 26A, D). Two very low abundant fragment ions were detected at *m/z* 790.64 and 772.63, which corresponded to neutral loss of the head group as mannosyl-dehydroinositol (Δm = 324.11 Da), rendering ceramide phosphate fragments $[CerP]^-$ and $[CerP - H_2O]^-$, respectively. Higher collision energy (~80 eV) was required for complete dissociation of MIPCs, although the pattern of fragment ions was not altered considerably upon changing the collision energy offset.

Orbitrap MS^2 analysis of the MIPC 44:0;4 species demonstrated that fragment ions with *m/z* 790.6294, 772.6194, 421.0741 and 403.0643, were directly produced from the molecular anion (Figure 26B, D). Ion trap MS^3 analysis of $[MIP]^-$ with *m/z* 421.0 produced fragment ions with *m/z* 403.0, 258.8, and 241.1 that corresponded to $[MIP - H_2O]^-$, $[IP]^-$, and $[IP - H_2O]^-$, respectively (Figure 26C, D). Ion trap MS^3 fragmentation of $[MIP - H_2O]^-$ with *m/z* 403.1 produced fragment ions with *m/z* 241.1 and *m/z* 223.0, corresponding to $[IP - H_2O]^-$, and $[IP - 2H_2O]^-$ (Figure 26D), respectively (data not shown)

We concluded that head group ions of MIPCs were fragmented along several parallel pathways. However, at each stage the end products $[IP]^-$ and $[IP - H_2O]^-$ were produced. Yet their abundance was relatively low in the spectra acquired on a QqTOF machine, albeit they were dominating the spectra of IPCs (Figure 24A). This, presumably, reflected the stability of the glycosidic bond between the inositol and mannose residues in $[MIP]^-$ and $[MIP - H_2O]^-$ fragment ions. The fragment ion with *m/z* 421.07 ($[MIP]^-$) was highly abundant and, since masses of intact IPCs and MIPCs do not overlap, was suitable for class-specific profiling by PIS as described below.

Ion trap MS^3 spectrum of $[Cer - H_2O]^-$ with *m/z* 772.6 was similar to MS^3 spectra of the corresponding ceramide fragments of IPC species, described above (data not shown). long chain base phosphate fragment ions were detected at *m/z* 390.2, 362.3, 347.2 and 344.3 and corresponded to $[LCBP18:0;3 - H_2O + CO]^-$, $[LCBP18:0;3 - H_2O]^-$, $[LCBP18:0;3 - H_3NO]^-$ and $[LCBP18:0;3 - 2H_2O]^-$, respectively. Two FA related fragment ions were detected at *m/z* 411.3 and 365.4, corresponding to $[FA26:0;1 + O]^-$ and $[FA26:0;1 - CH_2O]^-$, respectively (data not shown). MS^3 analysis of MIPC species from the *sur2*Δ and *scs7*Δ mutants produced similar spectra as obtained for the IPC species from these mutants (data not shown). Thus, MS^3 analysis of the abundant $[Cer - H_2O]^-$ fragment elucidated the structure of the ceramide backbone of MIPC species in a similar way, as was demonstrated above for IPC species (Table 5).

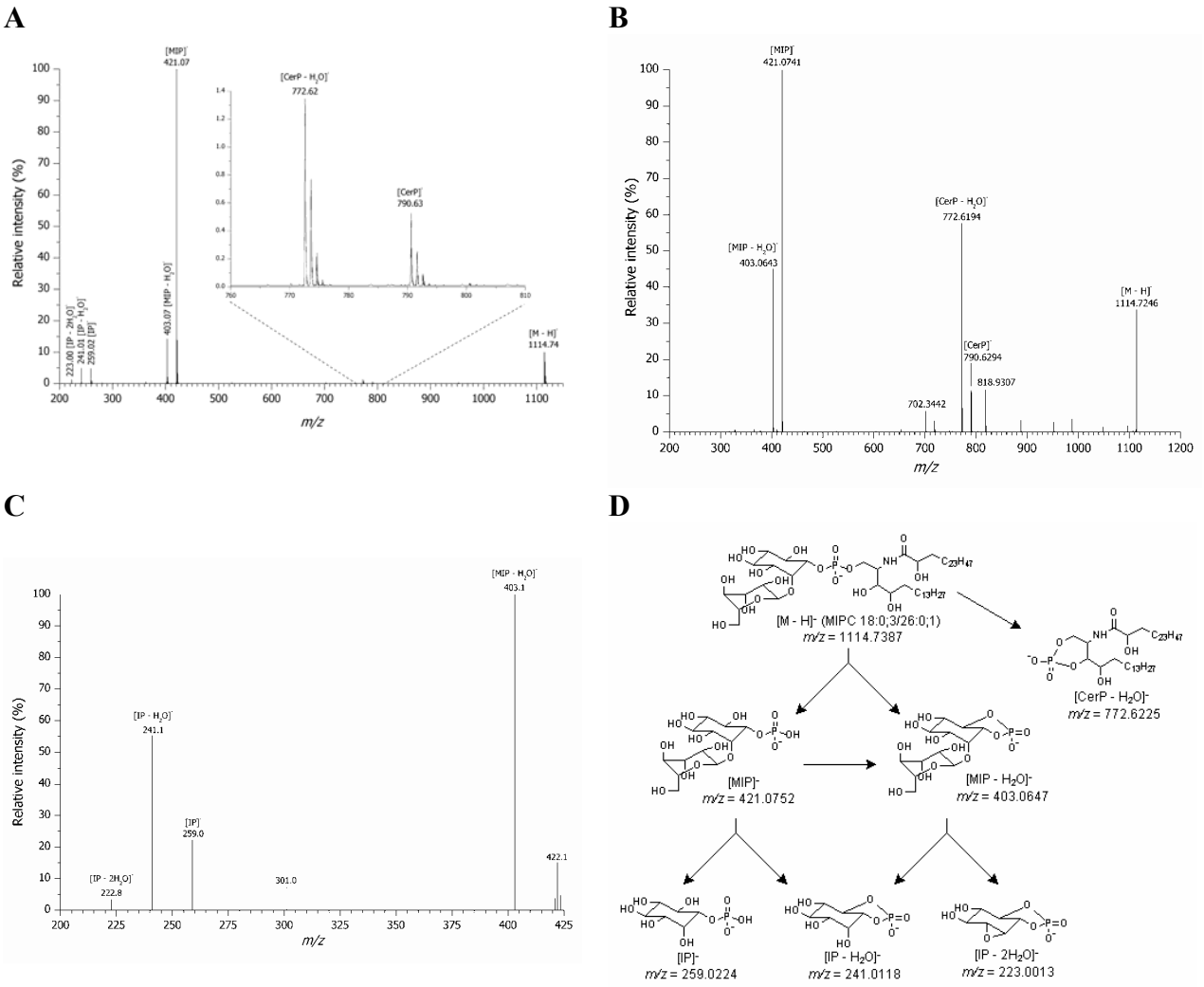

Figure 26. Fragmentation pathways of MIPC species. **(A)** QqTOF MS/MS spectrum of MIPC 44:0;4 ion of *m/z* 1114.7 ([M - H]$^-$) acquired at the collision energy of 80 eV. **(B)** Orbitrap MS^2 spectrum acquired from the same precursor. **(C)** Ion trap MS^3 spectrum of the head group fragment [MIP]$^-$ with *m/z* 421.1 **(D)** Major fragmentation pathways of MIPC 18:0;3/26:0;1 comprising fragments detected in QqTOF MS/MS and LTQ Orbitrap ion MS^n spectra. Note that MS^n fragmentation of *m/z* 772.6225 [CerP - H_2O]$^-$ proceeds according to the same pathways, as presented in Figure 24D and is therefore not shown.

3.3.3. Fragmentation pathways of M(IP)$_2$Cs

M(IP)$_2$C species contained two phosphate groups and therefore, in negative ion mode, they were mostly detected as doubly charged ions. Most abundant ions in the M(IP)$_2$C fraction were detected at *m/z* 677.88 and 691.90 and corresponded to M(IP)$_2$C 44:0;4 and M(IP)$_2$C 46:0;4 (data not shown), as was also observed by (Hechtberger *et al.*, 1994). Tandem mass spectra of M(IP)$_2$C species, acquired on a QqTOF instrument, were dominated by fragments of the mannosyl-diinositolphosphate (M(IP)$_2$) head group: [M(IP)$_2$]$^{2-}$, [M(IP)$_2$ - H_2O]$^{2-}$, [M(IP)$_2$ - I]$^{2-}$, [M(IP)$_2$ - P]$^-$, [MIP]$^-$, [MIP - H_2O]$^-$, [IP]$^-$, and [IP - H_2O]$^-$ (Figure 27A). At the lower collision energy offset, [M(IP)$_2$]$^{2-}$ (*m/z* 331.04) and [M(IP)$_2$ - P]$^-$ (*m/z* 583.13)

were most abundant (Figure 27B), whereas at the higher collision energy offset the fragmentation mainly yielded $[IP - H_2O]^-$ (*m/z* 241.01).

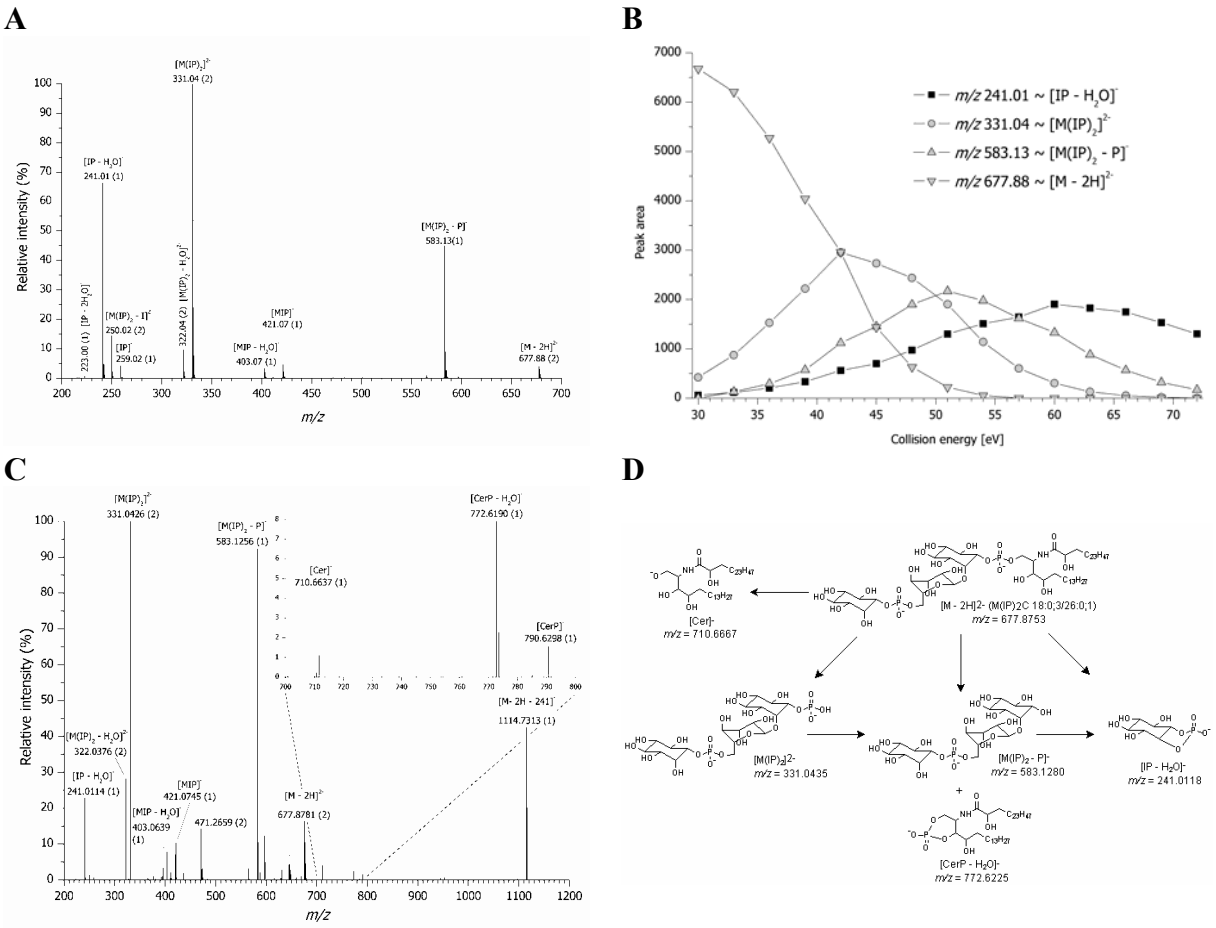

Figure 27. Fragmentation pathways of $M(IP)_2C$ species. **(A)** QqTOF MS/MS spectrum of $M(IP)_2C$ 44:0;4 ion having *m/z* 677.9 ($[M - 2H]^{2-}$) acquired at the collision energy of 52 eV. The charges of ions are indicated in brakets. **(B)** The intensity of fragment ions yielded from the $M(IP)_2C$ 44:0;4 species ($[M - 2H]^{2-}$) plotted against the collision energy offset. **(C)** Orbitrap MS^3 spectrum of $M(IP)_2C$ 44:0;4 species ($[M - 2H]^{2-}$) with *m/z* 677.8781. **(D)** Major fragmentation pathways of $M(IP)_2C$ species based on the fragments identified by QqTOF MS/MS and LTQ Orbitrap MS^n. MS^3 fragmentation of *m/z* 772.6225 $[CerP - H_2O]^-$ produced the same set of fragments as shown in Figure 24D. MS^3 fragmentation of $[Cer]^-$ yielded two FA specific fragment ions $[FA26:0;1 + O]^-$ and $[FA26:0;1 - CH_2O]^-$ (data not shown).

Orbitrap MS^2 and ion trap MS^2 spectra of the $M(IP)_2C$ species indicated that $[M(IP)_2 - P]^-$, $[M(IP)_2]^{2-}$, $[M(IP)_2 - H_2O]^{2-}$ and $[IP - H_2O]^-$ fragments were directly produced from the precursor (Figure 27C) by neutral loss of singly charged head group fragments. The fragment ion with *m/z* 1114.7316 was produced by cleaving $[IP - H_2O]^-$ (*m/z* 241.0114) fragment off the doubly charged precursor yielding $[M - 2H - 241]^-$. Loss of the head group as $[M(IP)_2 - P]^-$ (*m/z* 583.1256) and $[M(IP)_2 - H_2O]^-$ (*m/z* 645.0815) yielded the ceramide-phosphate *m/z* 772.6190 ($[CerP - H_2O]^-$) and the ceramide *m/z* 710.6637 ($[Cer]^-$) fragment ions, respectively (Figure 27C, D).

Further ion trap MS^3 fragmentation of $[M(IP)_2]^{2-}$ mainly produced $[M(IP)_2 - P]^-$ that subsequently yielded $[IP - H_2O]^-$ with *m/z* 241.0 (data not shown). Hence, $[M(IP)_2 - P]^-$ was produced *via* at least two independent pathways, which eventually produced the $[IP - H_2O]^-$

fragment (Figure 27D). MS^3 analysis of the ceramide backbone fragment ion $[CerP - H_2O]^-$ with *m/z* 772.6 produced long chain base phosphate and FA related fragments, similar to IPC and MIPC species (data not shown). MS^3 analysis of the $[Cer]^-$ fragment yielded an abundant acyl anion of the amide-linked FA with *m/z* 411.4 ($[FA26:0;1 + O]^-$) and its neutral loss product with *m/z* 365.4 ($[FA26:0;1 - CH_2O]^-$) (data not shown).

Taken together, we observed strong similarity between the fragmentation pathways of molecular anions of all three classes of inositol-containing sphingolipids and their subtypes. Collision-induced dissociation of precursors on a QqTOF instrument produced fragment ions in which charged phosphate group(s) was (were) attached to the inositol-containing head group, rather than to the ceramide backbone. In QqTOF spectra, ceramide-related fragments were hardly detectable at the collision energy offset required to cleave the precursor ions, although they were readily detectable in the corresponding ion trap spectra. In the linear collision cell of a QqTOF instrument, multiple-collision fragmentation promoted neutral loss of the ceramide backbone leaving a net negative charge at the head group. Therefore stable ceramide backbone fragments, such as $[FA26:0;1 + O]^-$, were abundant in ion trap mass spectra, however they were hardly detectable in spectra acquired on the QqTOF instrument. Importantly, ion trap MS^2 fragmentation of molecular anions of species of all three yeast sphingolipid classes yielded abundant $[CerP]^-$ and $[CerP - H_2O]^-$ fragments, paving the way for the characterization of their molecular composition *via* MS^3 fragmentation. Thus, molecular profiling of sphingolipids was most effectively achieved by combining the complementary mass spectrometric approaches: QqTOF MS/MS lent itself to rapid class-specific profiling, whereas ion trap MS^n enabled the structural elucidation of the ceramide backbone in individual molecular species (Table 5).

3.3.4. Profiling of sphingolipids in yeasts

We used *m/z* of the abundant fragment ions specific for each sphingolipid class for profiling lipid extracts by the method of MPIS (Ekroos *et al.*, 2002). The extracts were first subjected to mild alkaline hydrolysis, which destroyed glycerophospholipids. Within each sphingolipid class of *S. cerevisiae*, we detected several species that differed by the total number of carbon atoms and hydroxyl groups in their ceramide-backbone (Table 6). The ceramide backbone of the most abundant species of IPCs, MIPCs and $M(IP)_2Cs$ comprised 44 or 46 carbon atoms and four hydroxyl groups, which agreed well with previous observations (Gaigg *et al.*, 2001; Hechtberger *et al.*, 1994; Young *et al.*, 2002). Since $M(IP)_2C$ species were detected as doubly charged ions, unit mass resolution of the analytical quadrupole was insufficient to fully resolve their isotopic peaks. However, their identification was further

supported by the exact *m/z* of doubly charged precursor ions, which were easy to recognize in high-resolution TOF MS spectra.

Table 6. Detection of inositol-containing sphingolipids in various yeasts[a].

IPC species			MIPC species			$M(IP)_2C$ species		
Precursor ion (*m/z*)	Sum formula	Relative intensity[b] (%)	Precursor ion (*m/z*)	Sum formula	Relative intensity (%)	Precursor ion[c] (*m/z*)	Sum formula	Relative intensity (%)
S. cerevisiae								
924.7	42:0;4	11	1098.6	44:0;3	10	655.9	42:0;3	1
936.8	44:0;3	5	1114.6	44:0;4	100	661.9	44:0;2	3
952.7	44:0;4	100	1126.6	46:0;3	4	663.9	42:0;4	2
964.7	46:0;3	4	1130.6	44:0;5	8	669.9	44:0;3	14
968.7	44:0;5	38	1142.6	46:0;4	80	677.9	44:0;4	91
980.7	46:0;4	63	–	–	–	683.9	46:0;3	11
–	–	–	–	–	–	691.9	46:0;4	100
S. pombe								
952.7	44:0;4	100	1114.6	44:0;4	100	Not detected		
968.6	44:0;5	18	1130.6	44:0;5	3			
P. pastoris								
806.5	36:1;2	18	1058.6	40:0;4	3	655.9	42:0;3	12
808.5	36:0;2	24	1070.5	42:0;3	4	663.9	42:0;4	100
810.6	34:1;4	10	1072.6	40:1;5	4	671.9	42:0;5	13
822.6	36:1;3	32	1086.6	42:0;4	100	677.9	44:0;4	24
824.6	36:0;3	17	1100.6	42:1;5	11	685.9	44:0;5	4
908.7	42:0;3	26	1102.5	42:0;5	28	691.9	46:0;4	2
924.7	42:0;4	100	1114.6	44:0;4	27	–	–	–
936.7	44:0;3	10	1128.6	44:1;5	2	–	–	–
938.7	42:1;5	10	1130.5	44:0;5	7	–	–	–
940.5	42:0;5	56	1142.5	46:0;4	2	–	–	–
952.7	44:0;4	52	–	–	–	–	–	–
968.6	44:0;5	11	–	–	–	–	–	–

[a] IPC species were detected by precursor ion scanning for the fragments having *m/z* 241.0 ($[IP - H_2O]^-$) and 259.0 ($[IP]^-$) at the collision energy offset of 68 eV. MIPC species were detected by precursor ion scanning for the fragments having *m/z* 403.1 ($[MIP - H_2O]^-$) and 421.1 ($[MIP]^-$) at 80 eV. $M(IP)_2C$ species were detected by precursor ion scanning for the fragment ion having *m/z* 241.0 ($[IP - H_2O]^-$), 331.0 ($[M(IP)_2]^{2-}$), and 583.1 ($[M(IP)_2 - P]^-$) at the collision energy of 50 eV. All precursor ion scan spectra were acquired in parallel.
[b] Relative intensity within each sphingolipid class.
[c] Doubly charged ions ($z = -2$).

Since inositol-containing sphingolipids commonly occur in various fungi and plants (Dickson and Lester, 1999b; Sperling and Heinz, 2003), we further tested if their compositional difference could be characterized by MPIS in several fungi species. In the fission yeast *S. pombe* and the methylotrophic yeast *P. pastoris* both IPC and MIPC species were detectable, whereas $M(IP)_2C$ species were only identified in *P. pastoris* (Table 6). A ceramide backbone with 44 carbon atoms and 4 hydroxyl groups was typical for IPC and MIPC species in *S. pombe*. A previous study identified the long chain base of the most abundant species in *S. pombe* as C20 phytosphingosine (Garton *et al.*, 2003) and, therefore, their amide-linked monohydroxylated C24 FA moiety, *e.g.* IPC 20:0;3/24:0;1. It was also

reported that *S. pombe* synthesizes sphingolipids with monounsaturated C20 sphingosine long chain base (Garton *et al.*, 2003), however, no such species were detected among IPC and MIPC species in this work.

The sum formula of inositol-containing sphingolipids in *P. pastoris* strongly varied (Table 6), especially within the IPC class. *P. pastoris* mainly synthesized species with a ceramide backbone of 42 carbon atoms and four hydroxyl groups, whereas in *S. cerevisiae* and *S. pombe*, species with 44 carbon atoms and four hydroxyl groups were most abundant. Taken together, rapid and accurate profiling of the sphingolipid composition in several fungi organisms suggested that MPIS is a valuable tool for elucidating molecular details of sphingolipid biosynthesis.

3.3.5. Simultaneous profiling of sphingolipids and glycerophospholipids

Ion trapping capabilities (Chernushevich, 2000) of a QqTOF mass spectrometers enable the simultaneous acquisition of precursor ion spectra for a large number of fragment ions. We previously demonstrated that MPIS could rapidly decipher the molecular composition of glycerophospholipid species (Ekroos *et al.*, 2002; Ekroos *et al.*, 2003). Upon collision-induced dissociation, molecular anions of glycerophospholipids produced acyl anions of their FA moieties (Hsu and Turk, 2000a; Hsu and Turk, 2000b; Hsu and Turk, 2000c; Hsu and Turk, 2001). If masses of all possible acyl anions were selected for MPIS, individual lipid species would be detected in the two precursor ion scans, corresponding to their FA moieties. Since *m/z* of acyl anions of FAs do not overlap with *m/z* of characteristic fragments of sphingolipids, we reasoned that glycerophospholipids and sphingolipids could be simultaneously and independently detected in total lipid extracts.

As a case study, we analyzed a total lipid extract from *S. cerevisiae*. The *m/z* of six acyl anions of the most common saturated and monounsaturated FAs, with 14, 16 and 18 carbon atoms, and 11 yeast sphingolipid fragment ions were selected (Figure 28). Since optimal collision energy depends on the lipid class, we increased the collision energy linearly from 48 eV at *m/z* 650 to 82 eV at *m/z* 1150. 17 simultaneously acquired precursor ion scan spectra were interpreted by *Lipid Profiler* software and all prominent peaks automatically identified (Figure 28). Thus, MPIS enabled simultaneous and specific profiling of IPC, MIPC, $M(IP)_2C$ species, together with the identification of the molecular composition of individual species of PIs, PAs, PEs, PSs, and PCs. Similar results were obtained on total lipid extracts of *S. pombe* and *P. pastoris* (data not shown).

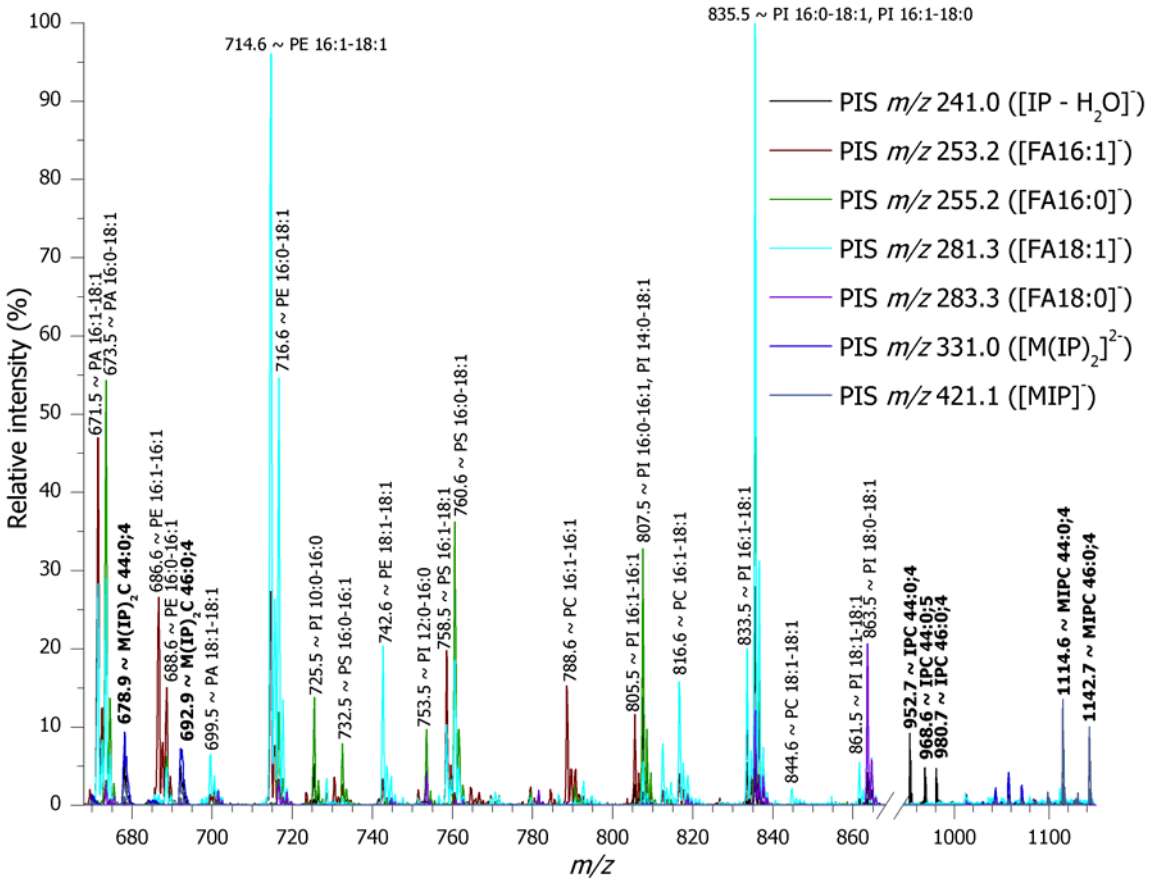

Figure 28. Simultaneous profiling of *S. cerevisiae* sphingolipids and glycerophospholipids from a total lipid extract by MPIS. Precursor ion spectra for 17 fragment ions corresponding to acyl anions of major FAs produced from glycerophospholipid species and 11 fragment ions produced from sphingolipid head groups (for presentation clarity, only 7 scans are presented in the figure). Peaks were identified by *Lipid Profiler* software. Detected sphingolipids and glycerophospholipids are annotated as described in the Materials and Methods section. Detected sphingolipid species are indicated in bold.

3.3.6. Discussion

We elucidated the fragmentation pathways of inositol-containing sphingolipids that are synthesized by plants and fungi. Upon collision-induced dissociation of their molecular anions on a QqTOF instrument, sphingolipids produced class-specific fragment ions, originating from their inositol-containing head groups. We further demonstrated that, by accounting for the number of carbon atoms, double bonds and hydroxyl groups at the corresponding amide-linked FA and the long chain base, ion trap MS^2 and MS^3 fragmentation provided important details on the structure of the ceramide backbone of sphingolipids. By comparing MS^3 spectra acquired from the $[CerP - H_2O]^-$ fragment obtained from IPC species with different ceramide backbones, we demonstrated that all inositol-containing sphingolipid species yielded a common set of fragment ions. Their unequivocal structural assignment was achieved by acquiring spectra on the LTQ Orbitrap machine with better than 3 ppm mass accuracy. The α-hydroxyl group in amide-linked FA moieties enhanced ceramide

fragmentation and produced additional fragments specific for their long chain bases (Table 5). The *m/z* of sphingolipid fragment ions, derived from their head groups, did not overlap with the *m/z* of acyl anions of common FAs, which enabled simultaneous profiling of sphingolipids and glycerophospholipids in total lipid extracts. As a case study, we compared the sphingolipid profiles in the yeasts *S. cerevisiae*, *S. pombe* and *P. pastoris,* which revealed that the composition of their ceramide backbones was remarkably diverse (Table 6).

3.4. AUTOMATED LIPID ANALYSIS BY ROBOTIC SAMPLE INFUSION

Sample infusion is a technically demanding and limiting factor for high throughput mass spectrometry-driven lipidomics. Several techniques based on (high) pressure delivery systems combined with electrospray ionization have been applied to automate and improve the analytical throughput. Two approaches are commonly used to deliver analytes for electrospray ionization and mass analysis; flow injection and liquid chromatography. By flow injection, sample material is automatically aspirated, transferred through a non-retaining transfer column to the electrospray capillary (Han and Gross, 1994; Han *et al.*, 2006; Kerwin *et al.*, 1994; Koivusalo *et al.*, 2001; Liebisch *et al.*, 1999; Liebisch *et al.*, 2004). By liquid chromatography, aspirated sample material is transferred through a chromatographic column which can separate lipids into classes or species prior to the subsequent electrospray ionization (Hermansson *et al.*, 2005; Merrill *et al.*, 2005). Common to the flow injection and liquid chromatography systems are the need for high flow rates (μl/min) and high ionization voltages (2-4 kV), which inherently reduce sensitivity and promote in-source fragmentation of analytes. Furthermore, these systems require time-consuming washing and pre-conditioning of the columns to minimize sample carryover.

Recently, an automated nanoelectrospray robot, the NanoMate, was developed (Schultz *et al.*, 2000). This robotic infusion device consists of a conventional 96-well plate, a rack of 96 disposable and conductive pipette tips, and an ESI Chip (Figure 29). The ESI Chip is fabricated from a monolithic silicon substrate, and today contains a 20x20 array of nozzles offering 400 analyses per microchip. The robotic infusion device is capable of sampling from the 96-well plate and infusing each sample in rapid succession, providing relatively high sample throughput. The low nanoliter/minute flow rates allow for very small sample consumption and improved sensitivity compared to devices operating with higher flow rates. Furthermore, a dedicated pipette tip and nozzle are used for each sample, thus eliminating the potential for carryover. This device has been applied in the fields of proteomics (Zhang and

Van Pelt, 2004), metabolomics (Staack *et al.*, 2005; Yu *et al.*, 2005) and lipidomics (Linden *et al.*, 2006; Schwudke *et al.*, 2006; Zamfir *et al.*, 2004).

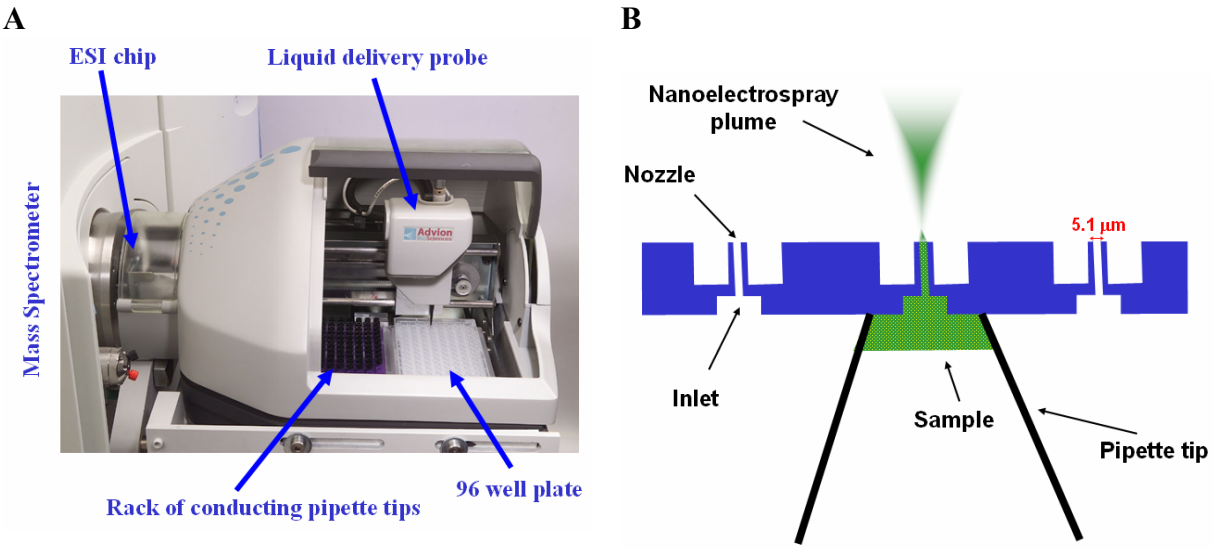

Figure 29. **(A)** Picture of the NanoMate HD System mounted onto a mass spectrometer. This robotic ion source is contains a 96-well plate with loaded sample material, a rack of conducting pipette tips, a liquid delivery probe which aspirates sample using a pipette tip and delivers it to the ESI chip positioned at the orifice of the mass spectrometer. **(B)** Depiction of the pipette tip to ESI chip contact. The liquid delivery probe carrying the aspirated sample in a pipette tip docks to the ESI chip and forms an air tight contact. Voltage and a backpressure are applied through the liquid delivery probe and promote the ionization of sample material through the nozzle on the ESI chip.

This section outlines analytical properties of the nanoelectrospray robot NanoMate operated together with a QqTOF mass spectrometer. The dynamic quantification range of this instrumental combination was evaluated and validated by comparison to established methodology based on a flow injection system and triple quadrupole mass spectrometer (Liebisch *et al.*, 2006; Liebisch *et al.*, 1999; Liebisch *et al.*, 2004). Furthermore, optimizing the negative ion mode infusion conditions demonstrated a significant increase in the sensitivity for anionic glycerophospholipid and sphingolipid analysis. Finally, sensitive cholesterol quantification was achieved by acetyl chloride derivatization in 96-well plates followed by targeted MRM analysis of cholesterol acetate ammonium adducts using the NanoMate and QqTOF instrumentation. These results set the basis for the combination of robotic sample infusion by the NanoMate system, mass analysis by the QqTOF mass spectrometer and spectral data analysis by dedicated Lipid Profiler software as a powerful tool for comprehensive and quantitative lipidome analysis.

3.4.1. Method validation

Installation of the NanoMate on a QSTAR mass spectrometer requires modification of the orifice (*i.e.* the region where ions enter the mass spectrometer). The main difference compared to the orifice design used for the conventional nanoelectrospray ion source is the

2.5 cm ion guide (cylindrical metal tubing) that is placed onto the existing orifice plate. This extension increases the distance ions have to travel before entering the mass spectrometer and potentially compromises sensitivity.

To compare the sensitivity of conventional nanoelectrospray operated manually with capillaries and the NanoMate system, we infused 500 nM synthetic PC 16:0/22:6 in positive ion mode using both ion sources. No significant difference was observed in the intensity of the PC 16:0/22:6 precursor at *m/z* 806.57 as detected by TOF MS (data not shown). Additionally, compared to the conventional nanoelectrospray ion source, the NanoMate system produced lower intensities of sodium adducts of PC, SM, ceramide and PE species in positive ion mode, and lower intensities of chloride adducts of PC and PA species in negative ion mode (data not shown). The NanoMate system allowed reproducible and stable ion spray at a flow rate of approximately 160-250 nl/min.

To evaluate the quantification dynamic range of the NanoMate operated together with the QqTOF mass spectrometer, we performed PIS *m/z* 184.1 analysis of solutions of synthetic PC 16:0/18:1 within the concentration range of 1.5 nM to 150 µM, and synthetic PC 18:1/18:1 at a fixed concentration of 200 nM. Within the concentration range of 1.5 nM to 15 µM PC 16:0/18:1, the response was linear and with a slope value of approximately one (Figure 30). At 150 µM PC 16:0/18:1, the response leveled off due to saturation of the TOF analyzer (data not shown). Similar results were obtained by MPIS analysis in negative ion mode (*q.v.* section 3.1.7. page 32).

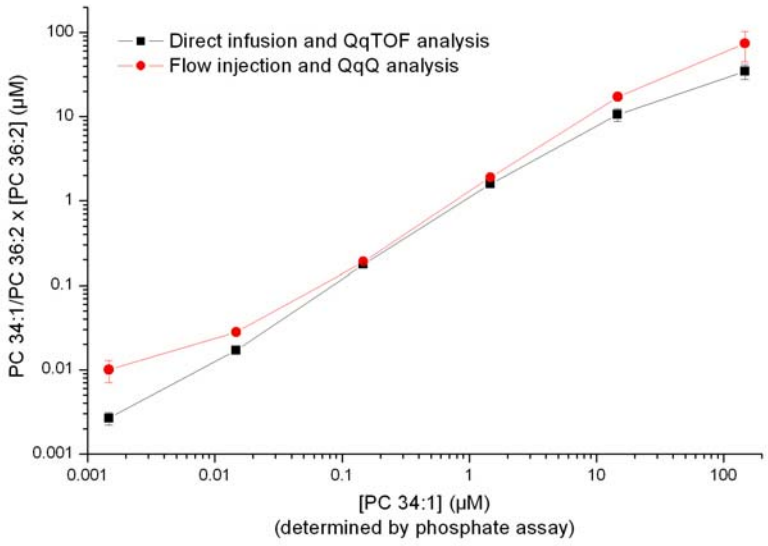

Figure 30. Quantification dynamic range of PIS *m/z* 184.1 performed by direct infusion using the NanoMate operated together with the QqTOF mass spectrometer (■), and flow injection using an Aligent pump operated together with a triple quadrupole instrument (QqQ, ●). Solutions of synthetic PC 16:0/18:1 (PC 34:1) within the concentration range of 1.5 nM to 150 µM, and synthetic PC 18:1/18:1 (PC 36:2) at 200 nM were analyzed by both instrumentations. For each sample the concentration of PC 34:1 was estimated by dividing the PC 34:1 precursor peak intensity (*m/z* 760.6) with the PC 36:2 peak intensity (*m/z* 786.6) and multiplication with the PC 36:2 concentration (y-axis). Each sample was analyzed in triplicate. The concentration of synthetic PC 16:0/18:1 (PC 34:1) and PC 18:1/18:1 was determined by phosphate assay.

To validate the performance of the NanoMate and QqTOF instrumentation and prove its efficacy for mass spectrometry-driven lipidomics, we analyzed the solutions of synthetic PC 16:0/18:1 and PC 18:1/18:1 on a triple quadrupole mass spectrometer equipped with a flow injection system (Liebisch *et al.*, 2004). The quantification dynamic range of these two instrumentations showed similar responses (Figure 30). However, discrepancies were apparent at the lowest and highest concentration of PC 16:0/18:1 (*i.e.* 1.5 nM and 150 μM, respectively). Importantly, the direct infusion by the NanoMate and QqTOF instrumentation had a 10-fold extended dynamic range and detection limit to 1.5 nM PC 16:0/18:1 compared to the flow injection system and the triple quadrupole mass spectrometer (Figure 30). This result was attributed to the higher levels of spectral noise in PIS *m/z* 184.1 spectra acquired on the triple quadrupole instrument and the carryover effects of the flow injection system (data not shown). In contrast, the PIS *m/z* 184.1 analysis using the flow injection system and the triple quadrupole mass spectrometer had a 10-fold extended dynamic range at the higher PC 16:0/18:1 concentrations analyzed (Figure 30). This discrepancy between the two instrumentations was explained by the saturation of the TOF analyzer on the QqTOF mass spectrometer. Similar results were obtained with the analysis of synthetic SM, PE and PS (data not shown).

3.4.2. Selective ionization of lipid classes

Han *et al* (Han and Gross, 2005; Han *et al.*, 2004) have demonstrated the efficacy of adapting the solvent composition used for electrospray ionization to selectively ionize certain lipid classes within total lipid extracts. The technique of selective ionization of lipid classes has been termed "intrasource separation" (Han and Gross, 2003) since it takes place in the ion source and because of its analogy to chromatographic techniques previously employed for separation of lipid classes (Gross and Sobel, 1980).

NanoMate infusion parameters were originally optimized for positive ion mode analysis of synthetic lipid standards and lipid extracts dissolved in 5 mM ammonium acetate in chloroform/methanol (1:2). The most significant parameters identified for producing reproducible and stable ion spray were the ion spray voltage, the backpressure, the curtain gas flow rate, and distance of the ESI Chip to the orifice (of the ion guide). Further method optimization demonstrated that the solvent system 7.5 mM ammonium acetate in chloroform/methanol/2-propanol (1:2:4) produced the most reproducible and stable ion spray with the lowest incidence of total ion spray failures (~3%). The utilization of this solvent system was the prerequisite for successful application of data-dependent acquisition for

lipidome analysis since this method cannot tolerate pronounced fluctuations and premature breakdown of the ion spray (Schwudke *et al.*, 2006).

For negative ion mode MPIS analysis, 7.5 mM ammonium acetate in chloroform/methanol/2-propanol (1:2:4) produced reproducible and stable ion spray, which allowed the non-selective ionization of PA, PE, PS, PG, PI and PC as acetate adducts (*q.v.* Figure 13A page 34). However, compared to the sensitive analysis of PC species in positive ion mode, the inclusion of ammonium acetate reduced the sensitivity of negative ion mode analysis of PC species 21-fold (data not shown). Hence, various solvent compositions without ammonium salts and applicable infusion conditions were sought to improve the sensitivity and allow the selective ionization of lipid classes.

Three solvent systems without ammonium salts were found to significantly improve the sensitivity of the negative ion mode analysis, allow the selective ionization of lipid classes, and produce reproducible ion spray: i) chloroform/methanol/2-propanol (1:2:4), ii) 0.05% saturated methylamine (CH_3NH_2) in chloroform/methanol/2-propanol (1:2:4) and iii) 0.05% saturated methylamine in methanol. Saturated methylamine solutions were prepared by purging gaseous methylamine into methanol.

A systematic comparison of ionization efficiencies of glycerophospholipid and sphingolipid classes was performed by infusing a comprehensive mixture of the glycerophospholipid species; PA 17:0/17:0, PS 17:0/17:0, PI 17:0/17:0, PG 17:0/17:0, cardiolipin (Car) 14:0/14:0/14:0/14:0, PE 17:0/17:0 and PC 18:3/18:3, and sphingolipid species; Cer 18:1;2/17:0;0, galactosylceramide (GalCer) 18:1;2/12:0;0, SM 18:1;2/17:0;0, IPC 18:0;2/26:0;0, MIPC 18:0;2/26:0;0 and $M(IP)_2C$ 18:0;2/26:0;0 dissolved in the above-mentioned solvent systems (Figure 31).

Infusing the comprehensive lipid mixture dissolved in chloroform/methanol/2-propanol (1:2:4) improved the ionization efficiency of the anionic glycerophospholipid classes PA, PS, PI, PG and cardiolipin, but had no impact on the ionization efficiency of PE, and reduced the ionization efficiency of PC compared to the conventional infusion with 7.5 mM ammonium acetate in chloroform/methanol/2-propanol (1:2:4) (Figure 31B). This solvent composition increased the ionization efficiency of the PG and cardiolipin species 30-fold, and increased the ionization efficiency of PA, PS and PI species 11-fold. The ionization efficiencies of sphingolipids were also improved; most significant were the 11-fold increase in IPC and $M(IP)_2C$ ionization efficiency, and the 6-fold increase in MIPC ionization efficiency (Figure 31C).

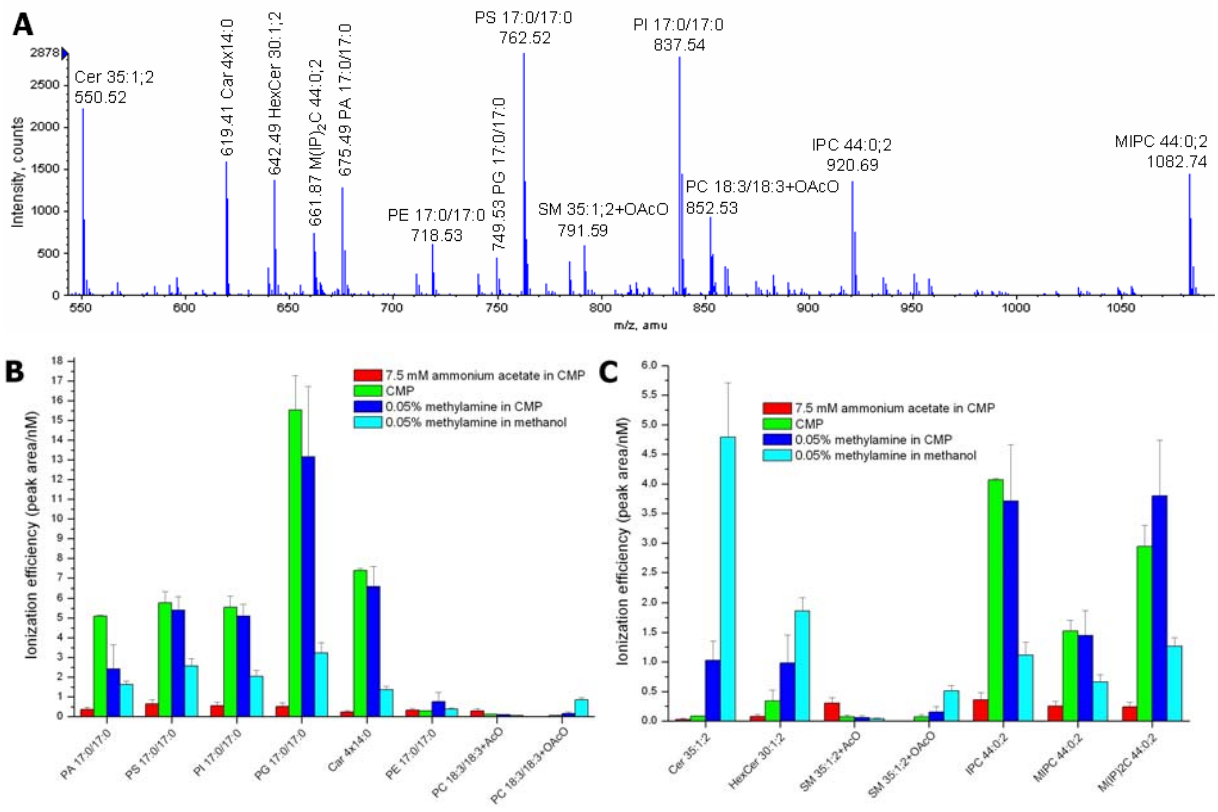

Figure 31. Comparison of ionization efficiencies of glycerophospholipid and sphingolipid species. **(A)** TOF MS spectrum of a mixture of glycerophospholipid and sphingolipid species (*q.v.* spectral annotation) dissolved and infused in 0.05% saturated methylamine in methanol. Ion spray voltage and backpressure were -0.95 kV and 0.6 psi, respectively. In addition, the glycerophospholipid and sphingolipid mixture was dissolved and infused in 7.5 mM ammonium acetate in chloroform/methanol/2-propanol (1:2:4) (CMP) using -0.95 kV and 1.25 psi, dissolved and infused in only CMP using -0.75 kV and 1.4 psi, and dissolved and infused 0.05% saturated methylamine in CMP using -0.75 kV and 1.4 psi. Notice that the lipid mixture was not equimolar. **(B)** Comparison of ionization efficiencies of glycerophospholipid species. Ionization efficiency was calculated as the analyte peak area divided its concentration. Notice that ionization efficiency is an arbitrary value. **(C)** Comparison of ionization efficiencies of sphingolipid species. Analysis was performed in triplicate. Notice that the infusion with methylamine gives rise to PC and SM methyl carbonate adduct ions (CH_3OCOO^-, abbreviated as +OAcO).

The infusion with chloroform/methanol/2-propanol (1:2:4) did not improve the ionization efficiency of the weak anionic PE class, which is in agreement with the observations made by Han *et al.* using electrospray ionization at a flow rate of ~8 µl/min (Han *et al.*, 2006). Han et al. demonstrated a 3-fold increase in the ionization efficiency of PE class lipids by infusing samples in alkaline conditions with 30 µM LiOH. Lithium ions are known to promote severe contamination of the mass spectrometer orifice and quadrupole analyzers by the precipitation of lithium salt, whereby the instrumental performance is compromised. Hence, the gaseous base methylamine was applied instead of LiOH to promote the ionization efficiency of PE class lipid and avoid comprising the instrumental longevity. Infusing samples with 0.05% saturated methylamine (~50 µM) in chloroform/methanol/2-propanol (1:2:4) improved the ionization efficiency of PE by 2-fold compared to both chloroform/methanol/2-propanol (1:2:4) and 7.5 mM ammonium acetate in chloroform/methanol/2-propanol (1:2:4)

(Figure 31B). More remarkable was the 40-fold and 12-fold increase in ionization efficiency of ceramide and galactosylceramide, respectively, compared to the 7.5 mM ammonium acetate in chloroform/methanol/2-propanol (1:2:4) (Figure 31C).

Further optimization of the ionization conditions prompted infusion of sample material dissolved in 0.05% saturated methylamine in methanol. Using this solvent composition showed a striking 188-fold and 24-fold increase in the ionization efficiency of ceramide and galactosylceramide, respectively, compared to infusion in 7.5 mM ammonium acetate in chloroform/methanol/2-propanol (1:2:4) (Figure 31C). The ionization efficiencies of all other glycerophospholipid and sphingolipid classes in 0.05% saturated methylamine in methanol were superior to those of infusing with 7.5 mM ammonium acetate in chloroform/methanol/2-propanol (1:2:4), but produce approximately 2-fold lower ionization efficiencies than infusion in chloroform/methanol/2-propanol (1:2:4) with or without methylamine (Figure 31B,C).

Interestingly, the infusion in the presence of methylamine rendered PC and SM species detectable as methyl carbonate (CH_3OCOO^-) adduct ions (Figure 31B,C) (Zhang and Reid, 2006). The alkaline conditions created by the methylamine induced the chemical reaction where atmospheric CO_2 reacts with methanol (CH_3OH) to form methyl carbonate. Compared to the ionization efficacy of PC and SM acetate adduct ion obtained by infusion with 7.5 mM ammonium acetate, the ionization efficiency of PC and SM methyl carbonate adduct were 2-fold higher in the methylamine containing infusate. Further evaluation of the properties of the infusion with 0.05% saturated methylamine in methanol demonstrated that neutral DAG species formed methyl carbonate adduct ions applicable for molecular profiling by MPIS (data not shown).

3.4.3. Cholesterol quantification by MRM analysis

Cholesterol is an abundant and essential component of mammalian cell membranes. Recently, structural characterization of this poorly ionizable neutral lipid species by electrospray ionization mass spectrometry was achieved indirectly by chemically acetylating cholesterol to form cholesterol acetate, which subsequently allowed the sensitive ionization of cholesterol acetate as an ammonium adduct (Liebisch *et al.*, 2006). MS/MS analysis of the cholesterol acetate ammonium adduct ion produced a single structure-specific fragment with *m/z* 369.36 through the neutral loss of acetic acid and ammonia (Figure 32A). Spiking total lipid extracts with stable isotope labeled cholesterol (*i.e.* D_7 or D_6) and performing MRM analysis on a triple quadrupole instrument allowed the absolute quantification of cholesterol in biological extracts (Liebisch *et al.*, 2006). The conversion of cholesterol into cholesterol

acetate was performed by harsh acetyl chloride (CH_3COCl) derivatization in sealed glass tubes.

This cholesterol quantification method was further optimized for MRM analysis using the NanoMate and QqTOF instrumentation. Infusion of synthetic cholesterol acetate dissolved in 7.5 mM ammonium acetate in chloroform/methanol/2-propanol (1:2:4) rendered cholesterol acetate detectable as an ammonium adduct with *m/z* 446.40 which upon collision-induced dissociation released the structure specific-fragment ion with *m/z* 369.36 (Figure 32A). MRM analysis was performed by repeated MS/MS analysis of the ammonium adducts of cholesterol acetate (*m/z* 446.4) and internal standard cholesterol-D6 acetate (*m/z* 452.4) produced by acetyl chloride derivatization (Figure 32B). The absolute quantification of cholesterol was performed by dividing the peak intensity of the cholesterol acetate fragment ion at *m/z* 369.36 with the peak intensity of the cholesterol-D6 acetate fragment ion at *m/z* 375.40 followed by multiplication with the spiked amount of cholesterol-D6 (similar to the quantification of glycerophospholipids, *q.v.* section 3.1.7. page 32).

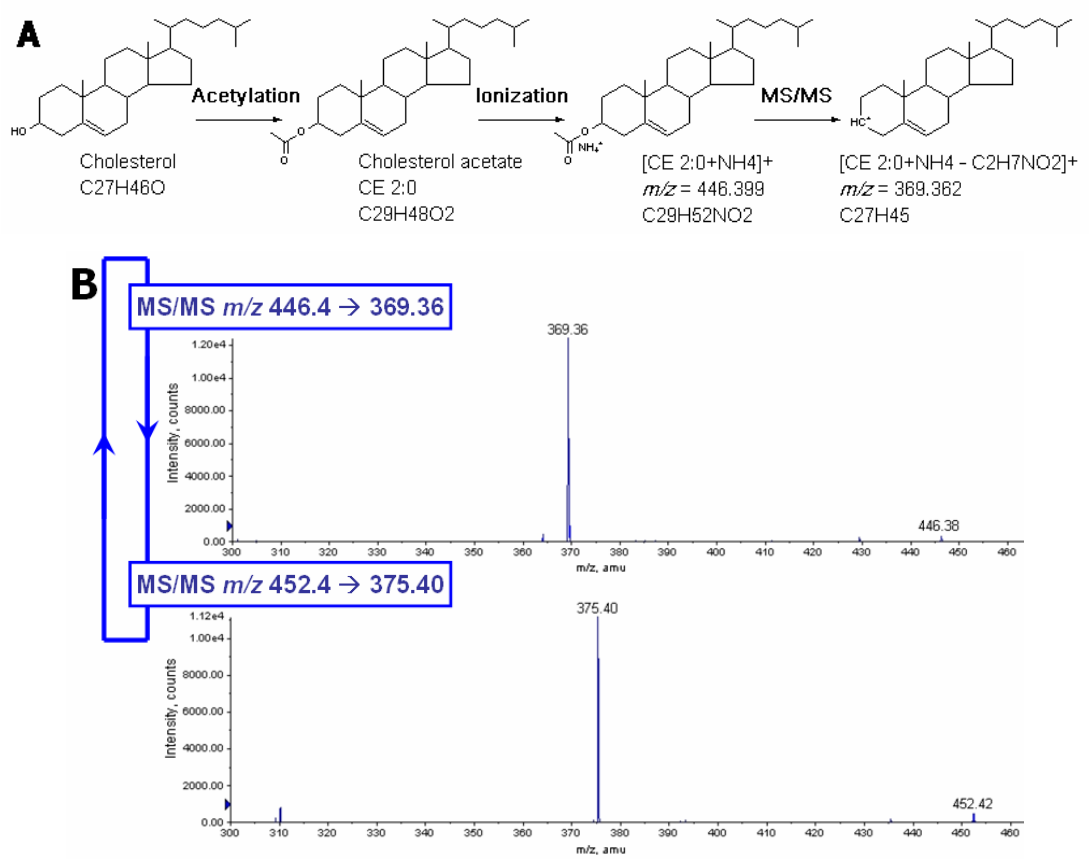

Figure 32. **(A)** Outline of the cholesterol quantification procedure. Cholesterol was converted to cholesterol acetate by acetyl chloride derivatization, followed by sample infusion in positive ion mode which allowed the ionization of cholesterol acetate as an ammonium adduct having *m/z* 446.40. Collision-induced dissociation of the cholesterol acetate ammonium adduct produced the structure specific fragment ion with *m/z* 369.36 **(B)** MS/MS spectra of ammonium adducts of cholesterol acetate (*m/z* 446.4) and cholesterol-D_6 acetate (*m/z* 452.4) obtained by MRM analysis of a derivatizised mixture of cholesterol and cholesterol-D_6 (both at 1 µM in the original sample). MRM analysis was performed by repeated MS/MS analysis of *m/z* 446.4 and MS/MS analysis *m/z* 452.4. Each MS/MS experiment was recorded for 1 second, thereby producing a cycle time of 2 seconds. In total, 300 cycles were acquired (*i.e.* 10 minutes of analysis) for the shown TOF MS spectra.

A major disadvantage of acetyl chloride derivatization is the concomitant production of hydrogen chloride (HCl) which corrodes the expensive vacuum centrifugation apparatus used for evaporating the derivatization reagent prior to the mass spectrometric analysis. This disadvantage could in principle be circumvented by evaporating the derivatization reagent using a stream of nitrogen. However, this approach limits the sample throughput since no suitable device exists for evaporating more than 20 samples at a time. This prompted the evaluation of the efficacy of performing the acetyl chloride derivatization in the polypropylene-based 96-well plates used for storing samples prior to infusion by the NanoMate (Figure 29A page 67).

The acetyl chloride derivatization method was performed in 96-well plates by adding 50 µl of acetyl chloride/chloroform (1:5) to dried sample material, and leaving the reaction mixture unsealed at room temperature in the fume hood. The reaction mixture was evaporated after 2 hours. Sample material was dissolved in 7.5 mM ammonium acetate in chloroform/methanol/2-propanol (1:2:4) and subjected to MRM analysis as outlined above. Initial experiments demonstrated no significant difference in the production of cholesterol acetate by the acetyl chloride derivatization in 96-well plates or in glass vials (data not shown). To evaluate the dynamic quantification range of this adapted cholesterol quantification method, we performed MRM analysis of solutions of cholesterol-D_6 within the concentration range of 1 nM to 10 µM subjected to acetyl chloride derivatization either in a 96-well plate or glass vials (Figure 33). After the derivatization, samples were dried by vacuum centrifugation, and dissolved in 7.5 mM ammonium acetate in chloroform/methanol/2-propanol (1:2:4) containing synthetic cholesterol acetate at a fixed concentration of 1 µM. The response of the cholesterol-D_6 acetate fragment ion with *m/z* 375.40 was linear within the concentration range of 1 nM to 10 µM (Figure 33), and showed that the detection limit of the method to was approximately 1 nM cholesterol, which equal the detection limit for sterols achieved using atmospheric pressure photoionization (Lembcke *et al.*, 2005). In comparison, a detection limit of 500 nM cholesterol was previously reported for this method when operated on a triple quadrupole instrument (Liebisch *et al.*, 2006). The improved sensitivity of the QqTOF-based MRM analysis primarily reflects the high mass resolution of the TOF analyzer which allows specific detection of the cholesterol acetate derived fragment ion, and secondarily a longer acquisition time. Importantly, the dynamic quantification range was independent of whether acetyl chloride derivatization was performed in a 96-well plate or in glass vials (Figure 33). Furthermore, comparing the peak intensities of the cholesterol-D_6 and cholesterol acetate fragment ions at *m/z* 375.40 and 369.38, respectively, showed that 93% of cholesterol-D_6 was converted into cholesterol-D_6 acetate.

In conclusion, the cholesterol quantification method previously developed by Liebisch et al. (Liebisch *et al.*, 2006) was successfully adapted to the 96-well plate format applicable for the NanoMate infusion device. Equally important, performing the acetyl chloride derivatization in a 96-well plate allowed the remaining sample material after PIS *m/z* 184.1 and MPIS analysis to be used for cholesterol analysis, thus reducing the sample amount required for total lipidome analysis (*q.v.* section 3.5.).

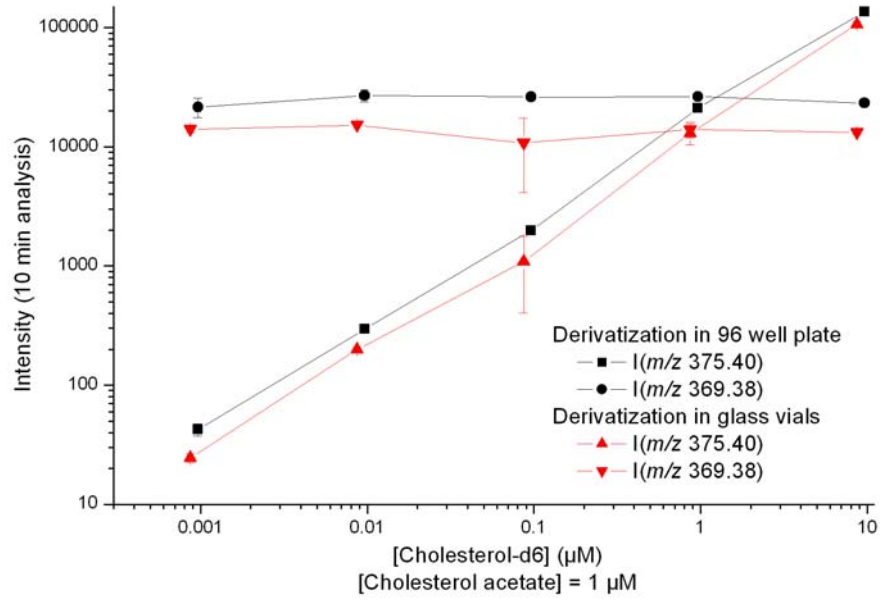

Figure 33. Quantification dynamic range the MRM analysis of derivatized cholesterol. 50 µl aliquots of solutions of cholesterol-D_6 within the concentration range of 1 nM to 10 µM were loaded in either a 96-well plate or in glass vials. Samples in the 96-well plate were evaporated by vacuum centrifugation, whereas samples in glass vials were evaporated using a stream of nitrogen. Dried samples were added 50 µl acetyl chloride/chloroform (1:5). Samples in 96-well plates were left unsealed at room temperature for 2 hours. Samples in glass vials were left at room temperature for 1 hour followed by evaporation using a stream of nitrogen. Dried sample were dissolved in 50 µl of 7.5 mM ammonium acetate in chloroform/methanol/2-propanol (1:2:4) containing 1 µM synthetic cholesterol acetate. Samples were automatically analyzed by 10 minutes MRM analysis (*q.v.* Figure 32B). Absolute peak intensities of cholesterol-D_6 and cholesterol acetate fragment ions with *m/z* 375.40 and 369.38, respectively, are plotted as a function of cholesterol-D_6 concentration. Sample analysis was performed in triplicate.

3.4.4. Discussion

The basis for a novel high-throughput orientated lipid analysis methodology has been established by combining an automated nanoelectrospray robot, the NanoMate, with mass analysis by a QqTOF mass spectrometer and spectral data analysis by dedicated Lipid Profiler software. It was demonstrated that this method design allowed sensitive mass analysis in both positive and negative ion mode equivalent to established methodology based on flow injection system and triple quadrupole mass spectrometry (Figure 30) (Liebisch *et al.*, 2004). The robotic infusion device allowed the selective ionization of lipid classes with a concomitant increase in sensitivity by modification of the solvent composition, the ion spray voltage and

backpressure (Figure 31), which could not be achieved by conventional nanoelectrospray operated with capillaries (personal observation). The combined NanoMate and QqTOF instrumentation offered direct quantification of the molecular constituents of a wide range of lipid classes with detection limits in the order of 1-10 nM (Figure 30, Figure 33 and Figure 14 page 36). Notably, a preferential and enhanced ionization of all anionic glycerophospholipid and sphingolipid species was achieved by omitting ammonium acetate in the infusate, or replacing ammonium acetate with methylamine (3.4.2. page 69). Interestingly, the alkaline infusion conditions with methylamine resulted in the specific ionization of ceramide and hexosylceramide species, a 2-fold increase in the PE ionisation, and promoted the detection of PC, SM and DAG species methyl carbonate adduct ions.

The total analysis time for the PIS *m/z* 184.1 (and MRM analysis of cholesterol acetate) was 1.3 minute per sample by the flow injection system and triple quadrupole mass spectrometer (Liebisch *et al.*, 2004). Although this instrumental setup allowed rapid mass analysis of lipid extracts and was high-throughput orientated, this technique required multiple injections of the same lipid extract to separately analyze each lipid class by lipid class-specific precursor ion scans (PE, PG, PI, etc.). Typically, 20 µl sample was required per injection (Liebisch *et al.*, 2004). In addition, the poor resolution power of the triple quadrupole instrument may complicate the analysis of complex sample material where the presence of isobaric lipid species, matrix-derived precursor ions and elevated noise levels may reduce the efficacy of the methodology.

In comparison, the time for PIS *m/z* 184.1 analysis by the combination of the NanoMate and the QqTOF mass spectrometer was set to 18 minutes per sample, thus providing a lower analytical throughput for the PIS *m/z* 184.1 analysis than the flow injection system and triple quadrupole instrumentation. However, the PIS *m/z* 184.1 analysis by the QqTOF instrumentation allowed precursor ion scans to be recorded with high mass resolution thereby producing almost noise-free precursor ion scans and improving the specificity and sensitivity (Ekroos *et al.*, 2002). Importantly, the direct infusion by the NanoMate and a 30 minutes QqTOF-driven MPIS analysis in negative ion mode allowed the molecular glycerophospholipid species of all classes (PA, PG, PI, PS, PE, PC) to be quantified from a single injection of 10 µl sample (*q.v.* Figure 31, and section 3.1. page 21). In addition, sensitive cholesterol analysis was achieved by acetyl chloride derivatization followed by targeted MRM analysis of cholesterol acetate ammonium adducts. Furthermore, the targeted MRM analysis was applicable for the quantification of low abundant ceramide, hexosylceramide and lactosylceramide species in total lipid extract (data not shown, *q.v.* section 3.5. below).

In summary, the analytical throughput of the two instrumentations for lipid analysis, *i.e.* flow injection analysis by the triple quadrupole mass spectrometer and the direct infusion by the NanoMate and mass analysis by the QqTOF mass spectrometer, are similar, but produced different data formats of the lipid species and classes present in total lipid extracts.

3.5. AUTOMATED AND QUANTITATIVE LIPIDOME ANALYSIS OF T CELL RECEPTOR SIGNALLING DOMAINS

T lymphocytes are crucial for both humoral and cell-mediated immune responses. Common to all T lymphocyte subpopulations is the expression of the T cell antigen receptor (TCR)-CD3 membrane complex (Figure 34) which mediates signals essential for the development and maturation of T cell in the thymus, as well as the activation and differentiation of mature T cells into effector and memory cells in the periphery. The TCR exists predominantly as a transmembrane αβ heterodimer (Davis, 2002; Rudolph *et al.*, 2006). The TCR subunits belong to the immunoglobulin superfamily possessing extracellular variable and constant domains structurally homologous to immunoglobulins. Distinct regions in the variable domains of the TCR exhibit specificity for the engagement with a cognate peptide-major histocompatibility complex (MHC) expressed on the surface on antigen-presenting cells (Figure 34). Upon this engagement, the TCR-CD3 complex and other downstream effectors organize distinct TCR signaling domains in T cell plasma membrane which subsequently induces a physiological T lymphocyte response (Figure 34).

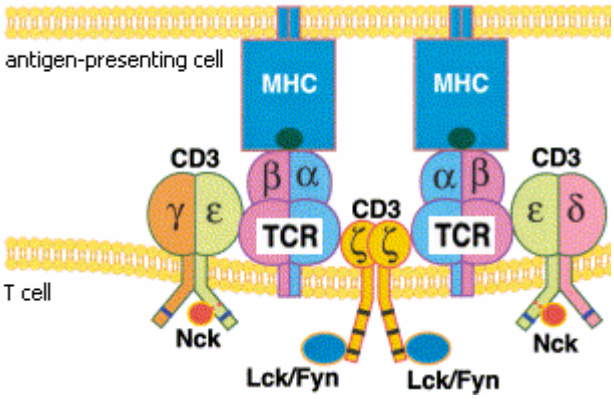

Figure 34. Schematic overview of the organization of the TCR-CD3 membrane complex and its interaction with MHC. TCR is composed of a transmembrane αβ heterodimer. CD3 is a complex of five transmembrane proteins that associate for form three dimers: a γε heterodimer, a δε heterodimer and a ζζ homodimer. All CD3 subunits contain immunoreceptor tyrosine-based activation motifs which become phosphorylated by tyrosine kinases Lck and Fyn upon receptor activation. Adapted from (Davis, 2002).

Several studies have implicated lipid rafts in the formation of TCR signaling domains. Lipid rafts are envisaged as lateral assemblies enriched in cholesterol and sphingolipids that form liquid-ordered membrane microdomains into which specific classes of proteins can partition (Simons and Vaz, 2004). Biochemical studies of the composition of detergent-resistant membranes from T cells have indicated several effectors of the TCR signaling machinery to be lipid raft-associated, including the TCR ζ-chain and protein tyrosine kinases (Montixi *et al.*, 1998; Zhang *et al.*, 1998). However, the analysis of detergent-resistant membranes is prone to artifacts due to the unspecific detergent extraction of membrane and non-equilibrium density gradient centrifugation. Thus, an alternative method based on immunoisolation using antibody-labeled magnetic beads was developed for the isolation of TCR signaling machinery (Harder and Kuhn, 2000). This method showed that effectors of the TCR signaling machinery were specifically recruited into TCR signaling domains in a time dependent manner (Harder and Kuhn, 2000; Hartgroves *et al.*, 2003). Further evidence for a functional significance of specific lipid-lipid interactions mediating a putative lipid raft environment within the TCR signaling domains was obtained by two-photon laser scanning microscopy of the membrane-order probe Laurdan. This approach revealed an elevated order of the T cell plasma membrane in the vicinity of activated TCRs (Gaus *et al.*, 2005). However, these biochemical and microscopy-based methods have provided no insight into the specific molecular lipid composition assumed to compose the TCR signaling domains in living cells.

To specifically address the molecular lipid composition of TCR signaling domains, we immunoisolated plasma membrane fragments enriched in activated TCR-CD3 complexes from Jurkat cells as previously described (Harder and Kuhn, 2000; Hartgroves *et al.*, 2003). Immunoisolates were subjected to lipid extraction and analyzed using a repertoire of the developed mass spectrometric methodology presented throughout this thesis. This methodology revealed a specific lipid composition with elevated levels of cholesterol, SM species, and PC species with short chain and saturated FA moieties in the immunoisolated TCR signaling domains.

3.5.1. Overview of analytical strategy

Plasma membrane fragments enriched in the TCR-CD3 complex were immunoisolated by forming conjugates between αCD3 antibody-coated magnetic beads and Jurkat cells, an immortalized T lymphoma cell line. Conjugates were warmed to 37°C for 10 min, inducing the formation of TCR signaling domains as previously described (Harder and Kuhn, 2000; Hashemi *et al.*, 1996; Lowin-Kropf *et al.*, 1998). Subsequently, the conjugates were

homogenized using nitrogen cavitation, and the beads were retrieved and washed. This procedure showed a strong accumulation of TCR ζ-chain, CD3ε and other effector proteins (data not shown, (Harder and Kuhn, 2000)). Plasma membrane fragments were retrieved in parallel from αTfR antibody-coated beads conjugated to Jurkat cells in order to control the specific recovery of TCR signaling domains. αTfR immunoisolates showed accumulation of TfR and depletion of TCR ζ-chain and CD3ε (data not shown). The two populations of immunoisolated membrane fragments bound to antibody-coated beads were washed, suspended in water, spiked with a mixture of synthetic lipid standards (Table 7), and subjected to lipid extraction. In addition, lipid extraction of Jurkat cells was performed.

Comprehensive and quantitative lipid analysis of total lipid extract was performed by four automatic injections per sample designed to determine the i) PC and SM composition by PIS *m/z* 184.1 analysis, ii) PA, PE, PS, PG and PI composition by MPIS analysis, iii) targeted MRM analysis of low abundant ceramide, hexosylceramide and lactosylceramide species, and iv) cholesterol analysis by MRM analysis (Table 7). The total analysis time was 1 hour and 50 minutes per sample. Each recorded spectral data array was processed by Lipid Profiler software for the automatic identification and quantification of detected lipid species, followed by compiling all data sets for graphical display.

Table 7. Overview of monitored lipid classes and applied methodology.

Lipid class	Method	Internal standard	Analysis time
PC	+PIS *m/z* 184.1	PC 18:3/18:3	30 min
SM		SM 18:1;2/17:0;0	
PA	–MPIS	PA 17:0/17:0	35 min
PE		PE 17:0/17:0	
PS		PS 17:0/17:0	
PG		PG 17:0/17:0	
PI		PI 17:0/17:0	
Cer	+MRM[a]	Cer 18:1;2/17:0;0	30 min
HexCer		GalCer 18:1;2/12:0;0	
LacCer		LacCer 18:1;2/12:0;0	
Cholesterol	Acetylation, +MRM[b]	Cholesterol-D_6	15 min

[a]MRM analysis of precursors Cer 34:1;2, Cer 42:1;2, Cer 42:2;2, Cer 35:1;2 (IS), HexCer 34:1;2, HexCer 42:1;2, HexCer 42:2;2, HexCer 30:1;2 (IS), LacCer 34:1;2, LacCer 42:1;2, LacCer 42:2;2 and LacCer 30:1;2 (IS). Quantification of the lipid species was performed by monitoring the intensities of long chain base specific fragment ions at *m/z* 252.3, 264.3 and 282.3

[b]MRM analysis of *m/z* 446.4 (cholesterol acetate) → 369.35, *m/z* 452.4 (cholesterol-D_6 acetate) → 375.35

3.5.2. Comparison of lipid class composition

The quantitative lipid analysis of whole Jurkat cells, αTfR and αCD3 immunoisolates demonstrated subtle, yet specific differences in both the composition of lipid class and molecular lipid species. The lipid class composition of Jurkat cells showed PC to be the most abundant lipid class making up 42 mol% of all identified lipid species (Figure 35).

Cholesterol was the second most abundant lipid species/class constituting 20 mol% of all identified lipid species. The other lipid classes PE, PI, PS and SM constituted between 6 and 13 mol% of all the identified lipid species (Figure 35). Ceramides, hexosylceramides and lactosylceramides were less abundant and together constituted 0.12 mol%. This lipid class composition agreed well with the lipid composition of another immortalized T lymphoma cell line MT-4 (Brugger *et al.*, 2006).

The lipid composition of the αCD3 immunoisolate differed significantly from that of Jurkat cells. Cholesterol was the most abundant lipid species/class in the αCD3 immunoisolate; representing 37 mol% the all identified lipid species (Figure 35). In comparison, the αCD3 immunoisolate had 1.9-fold higher concentration of cholesterol molecules compared to that of Jurkat cells. Similarly, compared to that of the Jurkat cells, SM levels were increased 1.7-fold to 10 mol% in the αCD3 immunoisolate. Furthermore, the lipid class composition of the αCD3 immunoisolate showed PC to be the second most abundant lipid class composing 31 mol%. Interestingly, the molecular PC species composition showed significant differences compared to that of Jurkat cells (see below, Figure 36). The abundance of PI and PE class lipids in the αCD3 immunoisolate were reduced compared to that of Jurkat cells. PI lipids were reduced from 8 mol% in the Jurkat cells to 1 mol% in the αCD3 immunoisolate (Figure 35). PE lipids were reduced from 13 mol% in the Jurkat cells to 8 mol% in the αCD3 immunoisolate (Figure 35). Despite being low abundant, the levels of ceramides, hexosylceramides and lactosylceramides showed pronounced differences; ceramides were 2.7-fold more abundant in Jurkat cells than in the αCD3 immunoisolate; in contrast, hexosylceramides and lactosylceramides were 2.3-fold and 50-fold, respectively, more abundant in the αCD3 immunoisolate (Figure 35).

The lipid class composition of the αTfR immunoisolate, the control for specific recovery of TCR signaling domains, showed a distinct lipid class composition different from that of both the αCD3 immunoisolate and the Jurkat cells. Similar to Jurkat cells, PC was the most abundant lipid class constituting 45 mol% of all identified lipid species (Figure 35) albeit with a different molecular PC species composition (see below, Figure 36). Interestingly, the level of cholesterol was 28 mol% in the αTfR immunoisolate, which was equal to the average of that of Jurkat cells and the αCD3 immunoisolate (Figure 35). Furthermore, SM, PE and PI levels of the αTfR immunoisolate equaled that of the αCD3 immunoisolate. Interestingly, the level of PS in the αTfR immunoisolate was 2-fold less than that of both the αCD3 immunoisolate and the Jurkat cells.

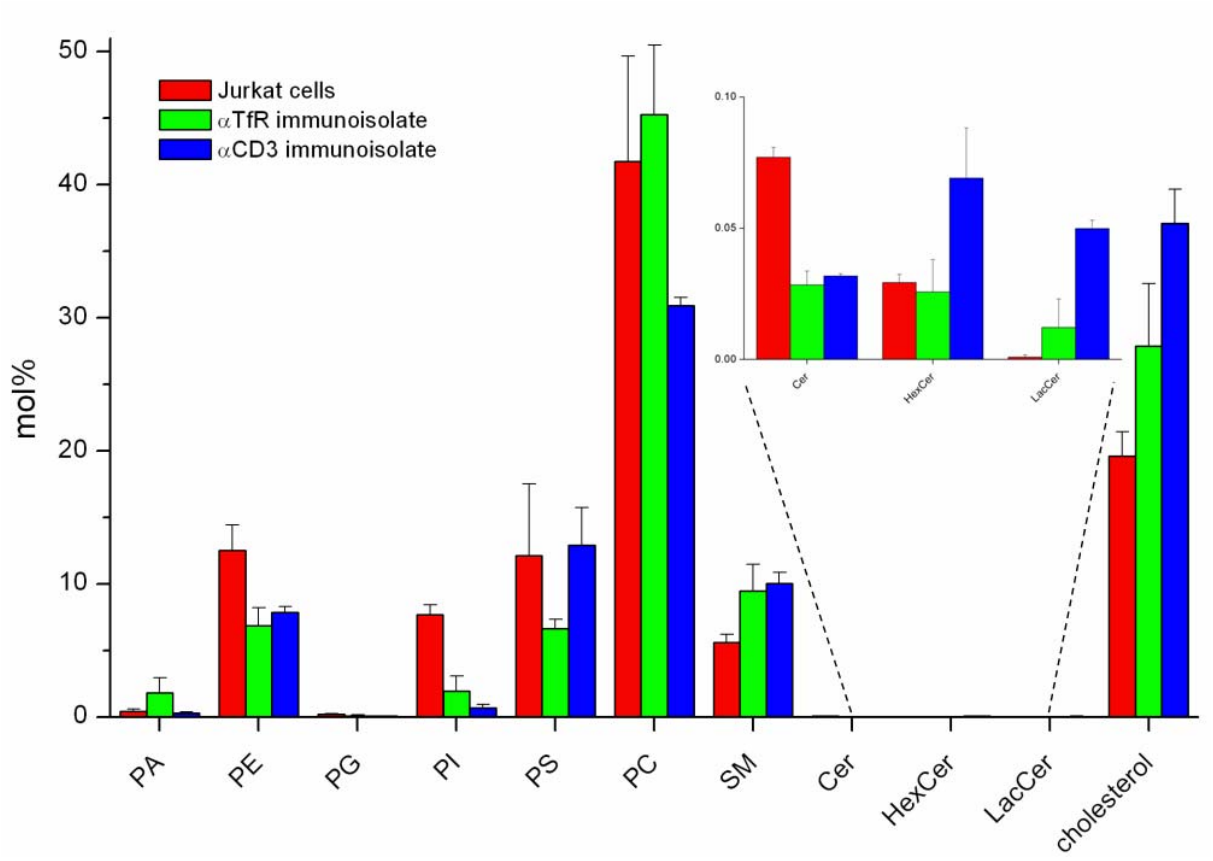

Figure 35. Lipid class composition of Jurkat cells, αTfR and αCD3 immunoisolates. Quantitative lipid analysis was performed as outlined in Table 7. Lipid analysis of three independent replicates was performed.

3.5.3. Comparison of molecular lipid species composition

The comparison of the molecular lipid species composition of Jurkat cells, αTfR and αCD3 immunoisolates showed the molecular PC species composition to display the most pronounced differences (Figure 36A). Automatic processing of PIS *m/z* 184.1 data by Lipid Profiler software identified 76 molecular PC species. The 5 most abundant molecular PC species in Jurkat cells were PC 34:1 (16:0-18:1) > PC 34:2 (16:1-18:1) > PC 32:1 (16:0-16:1) ≈ PC 36:2 (18:1-18:1) > PC 32:0 (16:0-16:0). These molecular PC species were also the most abundant in the αTfR and αCD3 immunoisolates albeit with altered ratios. The αCD3 immunoisolate showed similar levels of PC 34:1 (16:0-18:1), and the short-chain and saturated PC 32:0 (16:0-16:0) (Figure 36A). The αTfR immunoisolate showed a molecular PC species composition intermediate of the Jurkat cells and the αCD3 immunoisolate (Figure 36A). This observation prompted the quantification of double bond composition of the molecular PC species (Figure 36B). This comparison demonstrated that the αCD3 immunoisolate had a systematic increase in PC species with 0 or 1 double bond within the FA moieties. In contrast, Jurkat cells displayed higher levels of molecular PC species having FA moieties with 2 or more double bonds. Interestingly, the PC species double bond composition

of the αTfR immunoisolate was consistently intermediate of the αCD3 immunoisolate and the Jurkat cells, thus emphasizing molecular specificity of the αCD3 immunoisolate. Quantitative evaluation of the distribution of FA chain-length in molecular PC species showed minor, but systematic differences. PC species of the αCD3 and αTfR immunoisolate had shorter FA chain-lengths compared to that of Jurkat cells (Figure 36C).

The automatic processing of PIS *m/z* 184.1 data by Lipid Profiler software identified 16 molecular SM species; the most abundant having the sum composition 34:1;2 corresponding to the species SM 18:1;2/16:0;0 (Figure 36A). Comparison of the molecular SM composition showed SM 34:1;2 to be specifically enriched in the αCD3 and αTfR immunoisolates compared to that of Jurkat cells (Figure 36A).

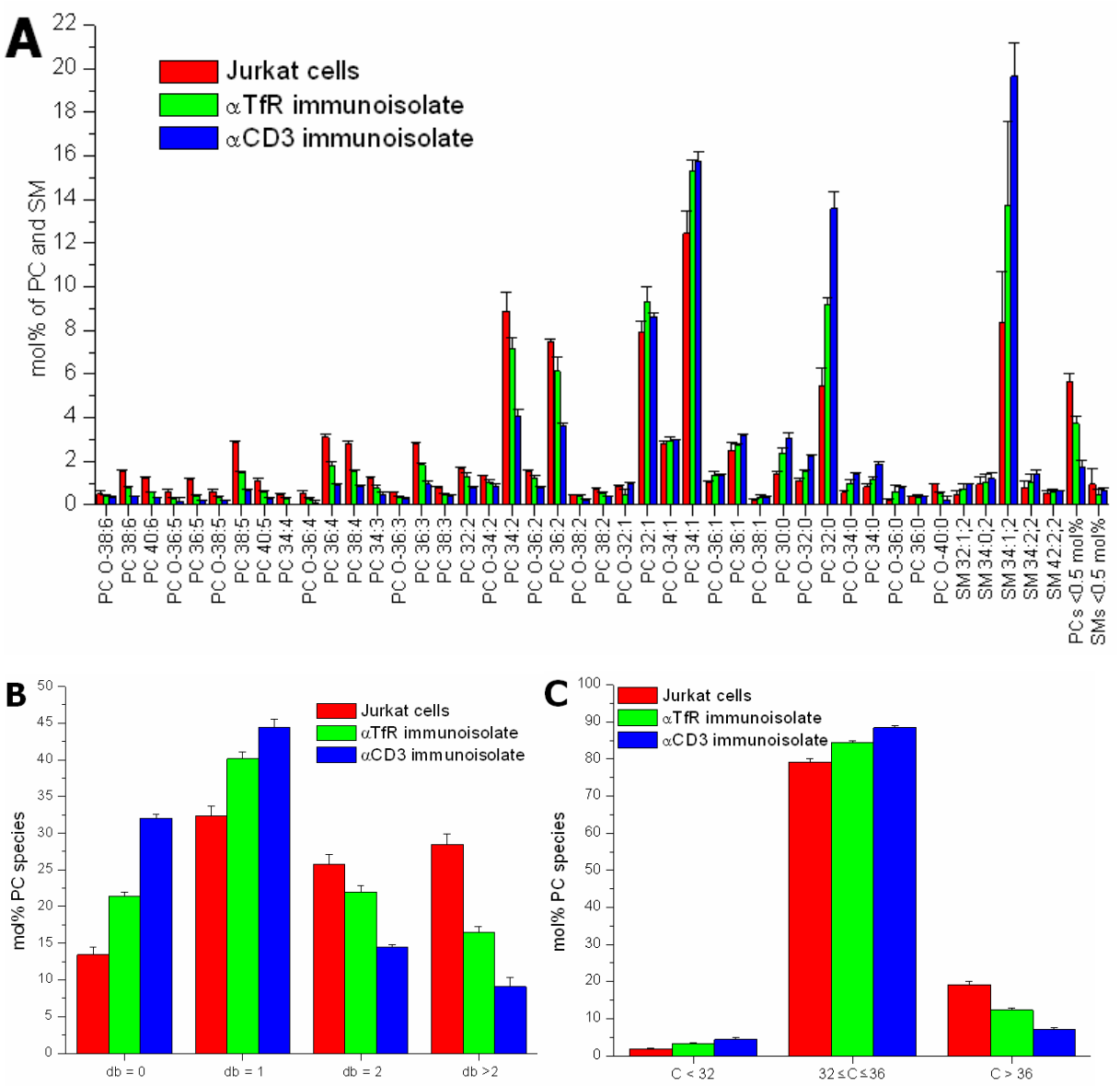

Figure 36. **(A)** Molecular composition of PC and SM species. **(B)** Double bond (db) composition of PC species. **(C)** Composition of total FA chain-length of PC species. All data was compiled from PIS *m/z* 184.1 analysis of three independent replicates.

The results of the MPIS analysis of anionic glycerophospholipid species in negative ion mode showed differences mainly in lipid class composition (see above, Figure 35). The automatic processing of MPIS data by Lipid Profiler software identified 29 molecular PE species (Figure 37A) and 11 molecular PS species (Figure 37B). In-depth analysis of the molecular PE species composition showed that PE 18:0-18:2 and PE 18:0-18:1 were the major species in Jurkat cells, αCD3 and αTfR immunoisolates (Figure 37A). The Jurkat cells, αCD3 and αTfR immunoisolates displayed subtle differences in the PE species composition. Similar to the PC species of the αCD3 immunoisolate, the molecular PE species showed a tendency for higher concentrations of species with saturated or mono-unsaturated FA residues compared to both the Jurkat cells and the αTfR immunoisolate (Figure 37A). Interestingly, both immunoisolates displayed elevated levels of ether PE species having a polyunsaturated FA moiety (Figure 37A), similar to that observed in the lipidome of HIV (Brugger *et al.*, 2006).

The analysis of the molecular PS species composition of Jurkat cells, αCD3 and αTfR immunoisolates displayed subtle differences (Figure 37B). The species PS 18:0-18:2 and PS 18:0-18:1 were the most abundant, similar to that of the PE class lipids.

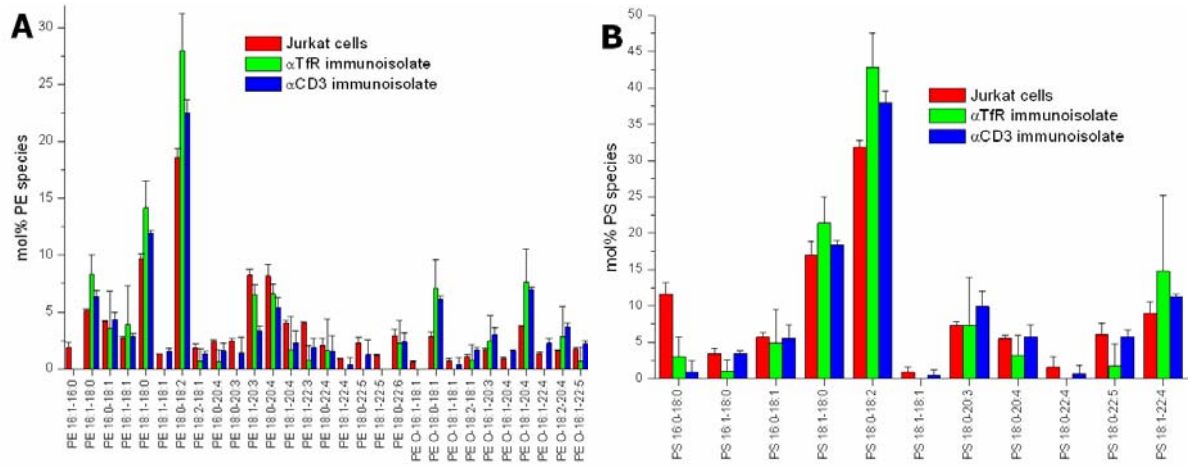

Figure 37. **(A)** Molecular composition of PE species. **(B)** Molecular composition of PS species. Data was obtained by negative ion mode MPIS analysis.

3.5.4. Discussion

This study indicated that TCR signaling complexes comprise a unique lipid composition reminiscent of lipid rafts (Simons and Vaz, 2004). TCR signaling complexes, isolated as αCD3 immunoisolate, were found to be specifically enriched in cholesterol, SM species and PC species having short- and saturated FA moieties compared to that of Jurkat

cells and the αTfR immunoisolate (Figure 35 and Figure 36). In addition, the isolated TCR signaling complexes displayed significant levels of PS species, and depletion in PI species and glycerophospholipid species containing polyunsaturated FA moieties. Of particular note was the finding that TCR signaling domains were not highly enriched in SM species, which was compensated by increased levels of PC species having short- and saturated FA moieties (Figure 36). This finding corroborates biophysical results indicating that liquid-ordered domains can exist in the absence of SM with only cholesterol and PC species having low and high phase transition temperatures (Veatch and Keller, 2003). The determined lipid composition of the TCR signaling domains also corroborates recent results demonstrating an increased order of the plasma membrane in vicinity of activated TCRs (Gaus *et al.*, 2005). Interestingly, a time-course analysis of the lipid composition of the αCD3 immunoisolate indicated a specific time-dependent reorganization of lipid species within the TCR signaling domains (data not shown).

TCR/CD3 signaling is central to the initiation of antigen-specific T cell responses to pathogens, vaccines, transplanted tissues, tumors, and autoantigens. Hence, elucidating the earliest events in T cell signaling is critical for a basic understanding of these responses and thereby advancing efforts to enhance or attenuate T cell responses *in vivo*. In summary, the results presented in this section demonstrated the efficacy of the developed mass spectrometric methodology for advancing our basic understanding of membrane function and architecture.

4. CONCLUSIONS

During my thesis study, I established methodology for automated and quantitative analysis of molecular lipid species based on mass spectrometry. From this work a novel high-throughput methodology for lipidome analysis emerged (Figure 38). The main assets of this methodology are the use of powerful hybrid mass spectrometers with high mass resolution combined with the sensitive and automated sample analysis by a nanoelectrospray robot and dedicated Lipid Profiler software (Figure 38). Comprehensive characterization and quantification of molecular lipid species was achieved by spiking total lipid extracts with unique lipid standards, utilizing selective ionization conditions for sample infusion, and performing structure-specific mass analysis by hybrid QqTOF and linear ion trap-orbitrap mass spectrometers. The analytical routine allowed the comprehensive characterization and quantification of molecular glycerophospholipid species, molecular diacylglycerol species

(data not shown), molecular sphingolipid species including ceramides, glycosphingolipids and inositol-containing sphingolipids, and the sterol lipid cholesterol and its acylated derivatives (data not shown).

The performance of the analytical routine was validated by comparing its dynamic quantification range to that of established methodology based on triple quandrupole mass spectrometry (section 3.4.1. page 67). Furthermore, its efficacy for lipidomics projects was demonstrated by the successful quantitative deciphering of the lipid composition of TCR signaling domains (section 3.5.), its capacity as tracer technology tool for identifying low abundant lipid species with unique structural features (Kuerschner *et al.*, 2005), and its analytical flexibility by charting lipidomes of bacteria, yeast and viruses (data not shown).

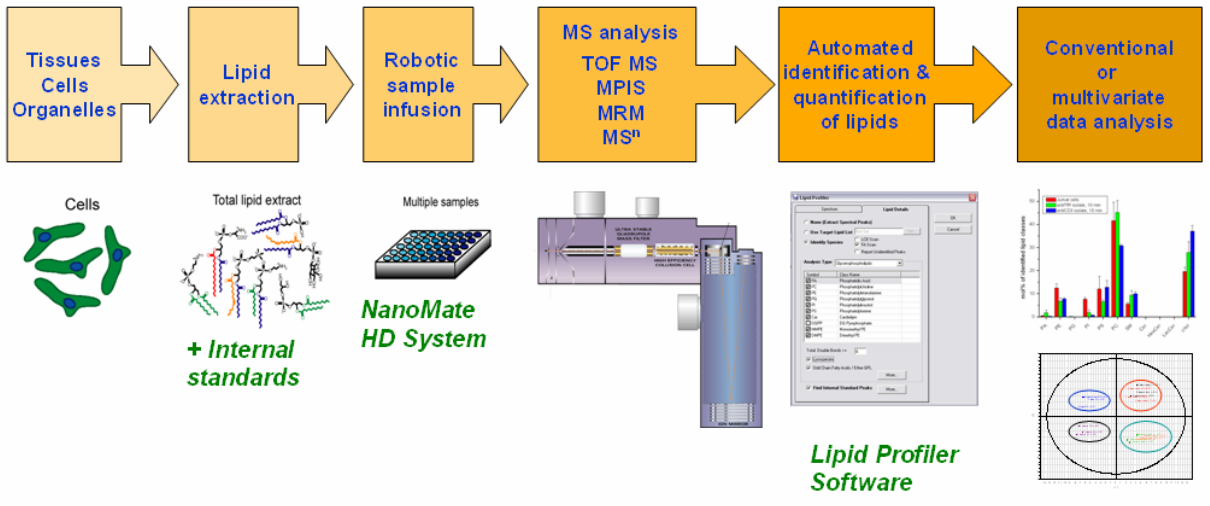

Figure 38. Overview of the methodology developed for automated and quantitative lipid analysis.

The developed methodology comprises six consecutive procedures (Figure 38). 1) sample preparation, 2) two phase lipid extraction to isolate a total lipid extract, 3) automatic sample infusion by the robotic ion source NanoMate, 4) lipid species specific mass analysis by either QqTOF or ion trap mass spectrometry, 5) automated identification and quantification of detected lipid species by Lipid Profiler software, and 6) export of compiled data arrays for interpretation by conventional or multivariate data analysis.

Although not discussed in detail in this thesis, the initial sample preparation and lipid extraction often represent the limiting factor for successful and accurate lipidome analysis. Of particular importance is the use of lipid class-specific internal standards for correcting biased losses of lipid classes during the extraction procedure and to correct for perturbations of ionization efficiencies during sample infusion. Equally important is to minimize the co-extraction of sample matrix components (*e.g.* sodium salts, protease inhibitors) which can compromise ion spray stability, impose ion suppression, and promote detection of unspecific

precursor ions. For example, the successful characterization and quantification of polar and low abundant lipid classes such as phosphoinositides and complex sphingolipids relied on stringent evaluation of the applied lipid extraction conditions for optimizing recovery and detection (Pettitt *et al.*, 2006). Furthermore, the analysis of highly complex lipidomes, where the identification and quantification of certain molecular species are ambiguous, can be improved by reducing sample complexity by preparative TLC or liquid chromatography (DeLong *et al.*, 2001; Sommer *et al.*, 2006).

The analytical throughput of the methodology was enhanced by integrating the chip-based nanoelectrospray robot NanoMate and the development of Lipid Profiler software. The performance of the robotic nanoelectrospray ionization source was optimized to allow reproducible and sensitive analysis of total lipid extracts (section 3.4.). Equally important, for negative ion mode analysis the robotic infusion device demonstrated the capacity to selectively ionize certain lipid classes with enhanced sensitivity upon modification of the solvent composition used for infusion (section 3.4.2.). The chip-based nanoelectrospray ionization source allowed low sample consumption (5-10 μl total lipid extract per injection) and eliminated the potential for carryover effects, inherent to flow injection and liquid chromatography systems, by infusing each sample with a dedicated pipette tip and nozzle.

A hybrid QqTOF mass spectrometer served as the primary tool for structure-specific analysis of lipid species. MPIS and targeted MRM analysis were successfully applied for charting molecular lipid species in total lipid extracts of mammalian, yeast and bacterial sources. Negative ion mode MPIS analysis was highly efficient and specific for the comprehensive characterization of molecular glycerophospholipid and diacylglycerol species based on their release of structure-specific fragment ions upon collision-induced dissociation (section 3.1.). This approach also allowed the absolute quantification of molecular lipid species by spiking total lipid extracts with synthetic lipid standards having heptadecanoyl (17:0)-containing FA moieties, and was demonstrated to have a linear quantification range from 10 nM to 100 μM. Furthermore, the MPIS method increased the number of detected species in all lipid classes by an average factor of 1.8, compared to the conventional lipid class-specific precursor ion scans (Table 1 page 27). The acquisition time was within 35 min per sample and the approach lent itself to high-throughput lipidomics. The MPIS methodology increased the scope and precision of the characterization of glycerophopholipidomes without limiting the analysis throughput, since all required structure-specific scans were acquired in parallel and rapidly deciphered by the dedicated Lipid Profiler software. However, the most comprehensive characterization and quantification of individual glycerophospholipid species, including *sn-1/sn-2* positional isomers, required the combination

of QqTOF and ion trap mass spectrometry (section 3.2.), which potentially can be complemented by orifice ozonolysis to determine the localization of double bond in FA moieties (Thomas *et al.*, 2006). The targeted MRM analysis was an efficient approach for quantification of cholesterol (after acetyl chloride derivatization) and low abundant sphingolipid species. This method was used to improve the analytical sensitivity by optimizing the acquisition time used for detection of structure-specific fragment ions derived from the targeted lipid precursors.

The most comprehensive characterization of glycerophospholipid species was achieved by the combination of QqTOF and ion trap mass spectrometry. It was demonstrated that ion trap MS^3 analysis allowed quantification of positional isomeric PC species in total lipid extracts without prior chromatographic separation (section 3.2.). Similarly, the MS^n analysis on a novel high mass resolution linear ion trap-orbitrap mass spectrometer was used to unravel structure-specific fragmentation pathways of inositol-containing sphingolipids which in turn allowed their molecular characterization directly from total lipid extracts (*q.v.* section 3.3.).

The prerequisite for rendering the MPIS and MRM-based methodologies applicable for high-throughput orientated lipidomics projects was the development of Lipid Profiler software. Lipid Profiler software was designed for the automated identification and quantification of detected lipid species. Importantly, applying a novel algorithm for the isotopic correction of peak intensities that was adjusted to the specific features of MPIS spectra was implemented for accurate identification and quantification of lipid species (section 3.1.6.). Currently, Lipid Profiler software allows the identification of species from numerous lipid classes, including glycerophospholipid and their lyso-species, sphingolipids including sulphatides and gangliosides, glycerolipids including diacylglycerols, triacylglycerols and diacylglycerolglycosides, and sterol lipids. In addition to its efficient data handling properties, Lipid Profiler software was designed for visual inspection of acquired spectra with automated annotation of precursors, overlay of MPIS spectra from single experiments or the overlay of spectra recorded of different samples (data not shown). Various spectral normalization modes were implemented (*e.g.* to maximal peak intensity in a spectrum, to defined internal standard peak) together with spectral subtraction plots which assisted the identification of perturbed lipid precursors in the sample material.

In conclusion, the novel high-throughput methodology for automated, comprehensive and quantitative lipidome analysis was successfully applied in several lipidomics projects thereby defining it as an efficient venue for investigating the molecular architecture of biological membranes.

5. MATERIALS AND METHODS

5.1.1. Chemicals, cell media and lipid standards

All common chemicals were purchased from Sigma Chemicals (St. Louis, MO) or Merck (Darmstadt, Germany). Synthetic lipid standards (expect for PI 17:0/17:0) and lipid extracts were purchased from Avanti Polar Lipids, Inc. (Alabaster, AL). The concentration of lipid species in stock solutions was determined by phosphate assay (Rouser *et al.*, 1970). Phospholipase A_2 from *Crotalus atrox* venom, cholesterol and cholesterol acetate was from Sigma Chemical Company, (St. Louis MO). [2,2,3,4,4,6-D_6]-cholesterol was obtained from Cambridge Isotope Laboratories (Andover, MA, USA) with isotope purity higher than 98 %. Yeast extract, peptone and dextrose were purchased from Difco Laboratories (BD GmbH, Heidelberg, Germany). Cell media was from Gibco BRL (Rockville MD) and foetal calf serum from PAA Laboratories GmbH (Cölbe, Germany). Nanoelectrospray capillaries (brand "short") were purchased from Proxeon Biosystems A/S (Odense, Denmark). T

5.1.2. Synthesis of PI 17:0/17:0

1,2-diheptadecanoyl-*sn*-glycero-3-phosphoinisitol (PI 17:0/17:0) was synthesized according to the procedure of Filthuth and Eibl(Filthuth and Eibl, 1992). The phosphoramidite of 2,3,4,5,6-penta-*O*-acetyl-DL-myo-inositol was coupled to 1,2-di-heptadecanoyl-*sn*-glycerol (obtained by acylation of *sn*-3-*O*-benzyl-glycerol with heptadecanoylchloride followed by hydrogenolysis), followed by oxidation and deprotection(Filthuth and Eibl, 1992). The final product was purified using a silica column and eluted with a gradient of $CHCl_3$/MeOH/aqueous ammonia 90:9:1 to 60:36:4 (v/v/v), yielding the ammonium salt of PI 17:0/17:0. The purity and identity of the compound was assessed by thin layer chromatography, quantitative determination of phosphorus content (Rouser *et al.*, 1970) and tandem mass spectrometry.

5.1.3. Hydrolysis of PC standards by phospholipase A_2

Synthetic PC standards and their mixtures were hydrolysed by phospholipase A_2 as described by Kates et al. (Kates, 1986). Briefly, 500 nmol of dried PC standard was dissolved in 800 µL diethyl ether/MeOH 99:1 (v/v) and mixed with 450 µL of aqueous solution containing 40 mM calcium chloride, 20 mM Tris-HCl pH 8.0 and 7 µg phospholipase A_2. Mixtures were vigorously vortexed for 5 hours and then dried in a vacuum concentrator. Dried samples were extracted and prepared for mass spectrometric analysis as described below.

5.1.4. Yeast strains, growth conditions and lipid extraction

Yeast strains used in this work were *Saccharomyces cerevisiae* RH690-15D (wild type); mutant strains *elo3*Δ, *sur2*Δ, and *scs7*Δ produced in the BY4741 background were obtained from Euroscarf (Frankfurt, Germany); the double null mutant *scs7*Δ*sur2*Δ was kindly provided by Dr. Teresa Dunn; *Schizosaccharomyces pombe* strain FY254 and *Pichia pastoris* strain SmdII 684. Yeast cells were grown at 30°C to log phase in rich medium (yeast extract/peptone/dextrose) prepared as previously described(Sherman, 1991).

Yeasts were harvested by centrifugation for 5 min at 1000 g, and washed twice in a cold lysis buffer (25 mM Tris, 5 mM EDTA, pH 8.5). Pelleted yeast was stored at -80°C until used. Upon thawing, the pellet was re-suspended in a cold lysis buffer to a density of 4 OD_{600} unit/ml. Cells were lysed by vortexing their suspension with glass beads for 5 min at 4°C (Serrano, 1988). The cell lysate was then cleared of glass beads by centrifugation for 5 min at 500 g and 4°C. The cell lysate was then mixed with chloroform/methanol/water/pyridine (60:30:6:1) and extracted at 60°C for 2 hours (Hechtberger and Daum, 1995). The extract was dried in a vacuum centrifuge, followed by either mild alkaline hydrolysis or resuspension in chloroform/methanol/water (16:16:5) and stored at -20°C.

To hydrolyze glycerophospholipids, the pelleted cell lysate was taken up in methanol containing 0.1 M NaOH and vortexed at 30°C for 2 hours (Hechtberger *et al.*, 1994; Smith and Lester, 1974). 1 M acetic acid and 0.5% (w/w) EDTA were added to adjust the pH of the reaction mixture to neutral. Chloroform was added to induce phase separation and the organic phase was recovered and evaporated to dryness in a vacuum centrifuge. Extracted sphingolipids were re-dissolved in chloroform/methanol/water (16:16:5) and stored at -20°C

5.1.5. Fractionation of yeast sphingolipids by TLC

Preparative TLC was carried out on aluminium-back silica 60 high-performance plates (Camag, Muttenz, Switzerland) essentially as described by Hetchberger *et al.*(Hechtberger *et al.*, 1994). Total lipid extracts dissolved in chloroform/methanol/water (16:16:5) were loaded as 5 cm lane in the center of a silica plate and developed in chloroform/methanol/4.2 M ammonia (9:7:2) or chloroform/methanol/acetic acid/water (16:6:4:1.6). Developed silica plates were dried, cut in half, and one half was subjected to sulphuric acid staining. Subsequently, the two parts were aligned, and strips containing $M(IP)_2C$, MIPC and IPC sphingolipids were excised from an un-stained part of the TLC plate. Silica strips were extracted with chloroform/methanol/water (16:16:5) for 1 hour, and the obtained sphingolipid class fractions stored at -20°C.

5.1.6. Mammalian cell culture, sample preparation and lipid extraction

MDCK II cells were cultured and subjected to lipid extraction as previously described (Ekroos *et al.*, 2002; Ekroos *et al.*, 2003). Jurkat cells were cultured as previously described (Harder and Kuhn, 2000), and prepared for lipid extraction by two times washing in phosphate buffered saline (PBS) followed by pelleting of 200.000 Jurkat cells. αCD3 and αTfR immunoisolates from Jurkat cells were prepared as previously described (Harder and Kuhn, 2000), and washed two times washing in PBS. Jurkat cells, αCD3 and αTfR immunoisolates were added 200 µL water and spiked with 10 µL internal standard solution, containing defined amounts of PA 17:0/17:0, PS 17:0/17:0, PI 17:0/17:0, PG 17:0/17:0, PE 17:0/17:0, PC 18:3/18:3, ceramide 18:1;2/17:0;0, galactosylceramide 18:1;2/12:0;0, SM 18:1;2/17:0;0, and cholesterol-D_6. Then 495 µL chloroform/methanol (3:1) was added and the resultant mixture was vortexed for 15 minutes. Phase separation was induced by 2 minutes centrifugation at 1000 g. The lower (organic) phase was transferred to a new tube. The samples were dried by vacuum centrifugation and dissolved in 50 µL methanol.

5.1.7. Acetyl chloride derivatization of cholesterol

Lipid standards and total lipid extracts were loaded in 96-well plates (Eppendorf AG, Hamburg, Germany) and evaporated using a vacuum centrifuge. Dried samples were dissolved in 50 µL acetyl chloride/chloroform (1:5) (Liebisch *et al.*, 2006) and left unsealed at room temperature for 2 hours to produce cholesterol acetate. Dried and acetylated samples were dissolved in 7.5 mM ammonium acetate in chloroform/methanol/2-propanol and subjected to MRM analysis (see below).

5.1.8. Sample preparation for mass spectrometric analysis

Standards and lipid extracts were prepared in specified concentrations and in specific solvent systems depending on the infusion device and the mode of analysis. Table 8 summarizes the applied solvent systems and concomitant ion spray settings. Solvents systems containing methylamine were prepared diluting a saturated methylamine solution obtained by purging gaseous methylamine into methanol.

Table 8. Overview of the applied solvent systems and concomitant ion spray settings

Infusion device	Solvent composition	Ion mode	Ion spray settings
Nanoelectrospray ion source [a]	5 mM chloroform/methanol (1:2)	±	IS = ±0.9 kV GS1 = 3
NanoMate HD System[b]	7.5 mM ammonium acetate in chloroform/methanol/2-propanol (1:2:4)	±	Voltage = ±0.95 kV Pressure = 1.25 psi
NanoMate HD System[b]	Chloroform/methanol/2-propanol (1:2:4)	–	Voltage = -0.75 kV Pressure = 1.4 psi
NanoMate HD System[b]	0.05% saturated methylamine in chloroform/methanol/2-propanol (1:2:4)	–	Voltage = -0.75 kV Pressure = 1.4 psi
NanoMate HD System[b]	0.05% saturated methylamine in methanol	–	Voltage = -0.95 kV Pressure = 0.6 psi

[a]Ion spray settings were controlled by Analyst QS software

[a]Ion spray settings were controlled by Chipsoft 6.3.2 software

5.1.9. Quadrupole time-of-flight mass spectrometry

Lipid extracts and synthetic lipid standards were analyzed in negative and positive ion modes on a modified QSTAR® Pulsar *i* quadrupole time-of-flight mass spectrometer (Applied Biosystems/MDS Sciex, Concord, Canada) equipped with a nanoelectrospray ion source (Proxeon Biosystems A/S, Odense, Denmark) as previously described (Ekroos *et al.*, 2002) or the robotic nanoflow ion source NanoMate HD System (Advion Biosciences Inc, Ithaca NJ). The instrument was calibrated in MS/MS mode using a synthetic lipid standard 1-palmitoyl-2-docosahexaenoyl-*sn*-glycero-3-phosphocholine as previously described (Ekroos and Shevchenko, 2002).

The characteristic fragment ion of phosphorylcholine, *m/z* 184.1, was selected for PIS analysis of SM, PC and LPC species in positive ion mode. Negative ion mode MPIS was performed as previously described (Ekroos *et al.*, 2002). The analytical quadrupole Q1 was operated under the unit mass resolution settings with 30 msec dwell time and step size of 0.2 Da. Collision energy was linearly ramped from 45 eV at *m/z* 620 to 60 eV at *m/z* 920. The *m/z* of fragment ions selected for MPIS are listed in the Appendix Table 1A. The *m/z* of fragment ions were selected within a mass range of 0.15 Da. Peak enhancement (Chernushevich, 2000) (trapping of fragment ions in the collision cell) was applied according to the instructions of the manufacturer and controlled by Analyst® QS 1.1 software (Applied Biosystems/MDS Sciex).

MRM analysis was performed in positive ion mode by repeated MS/MS analysis of targeted precursor ions. Each cycle of MS/MS experiments were set to 1 second per precursor ion. All MS/MS spectra were recorded at unit resolution of the analytical quadrupole Q1 and peak enhancement applied according to the instructions of the manufacturer. The quantification of cholesterol performed by monitoring the fragmentations of *m/z* 446.4 to *m/z*

369.38 (cholesterol acetate) and *m/z* 452.4 to *m/z* 375.40 (cholesterol-D_6 acetate). Quantification of targeted ceramide, hexosylceramides and lactosylceramides were performed by monitoring the common long chain base-specific fragment ions with *m/z* 252.3, 264.3 and 282.3.

5.1.10. Mass spectrometry on ion trap and hybrid LTQ Orbitrap instruments

MS^n fragmentation was performed on a quadrupole ion trap mass spectrometer LCQ (ThermoElectron Corp., San Jose, CA) as previously described (Ekroos *et al.*, 2003), and a hybrid linear ion trap - orbitrap mass spectrometer (LTQ Orbitrap)(Hu *et al.*, 2005; Olsen *et al.*, 2005) from the same company equipped with the NanoMate HD ion source (Advion BioSciences Ltd, Ithaca NJ). MS analysis was performed in negative ion mode. The instrument was calibrated externally according to the instructions of the manufacturer. MS^2 and MS^3 spectra were acquired under operator control. MS^2 and MS^3 spectra were recorded with a mass resolution of R = 30.000 (FWHM) at *m/z* 400 and an acquisition time period of 0.5 sec/scan. For MS^2 and MS^3 experiments the normalized collision energy of 20% and 26%, respectively, was applied. The activation time was set at 30 ms with the activation parameter q = 0.25. For MS^2 and MS^3 analysis, precursor ions were isolated within the range of 3 Da and 5 Da, respectively. The mass accuracy was better than 3 ppm for MS and MS^n experiments.

5.1.11. Annotation of glycerophospholipid species

Detected glycerophospholipid species were be annotated by their molecular composition or by their sum formula depending on the mode of analysis. For sum formula annotations the following convention was applied: <lipid class> <total number of carbon atoms in the FA moieties>:<total number of double bonds in the FA moieties> (*e.g.* PE 36:2 as detected by the PE head group scan PIS *m/z* 196.0, Figure 8A page 23).

The molecular composition of glycerophospholipid species detected by MPIS was annotated as: <lipid class> <number of carbon atoms in the first FA moiety>:<number of double bonds in the first FA moiety>-<number of carbon atoms in the second FA moiety>:<number of double bonds in the second FA moiety>. For example, PE 18:0-18:2 is an asymmetric diacyl PE comprising a FA moiety with 18 carbon atoms and no double bonds and another FA moiety with 18 carbon atoms and two double bonds. This annotation was chosen to reflect the limitation of the MPIS analysis in accurately determining the position of the FA moieties (*sn-1* or *sn-2*) on the glycerol phosphate backbone, and the position or *cis-trans* configuration of double bonds.

Lipid species with the known or accurately determined position of FA moieties were annotated as: <lipid class> <number of carbon atoms in the *sn*-1 positioned FA moiety>:<number of double bonds in the *sn*-1 positioned FA moiety>/<number of carbon atoms in the *sn*-2 positioned FA moiety >:<number of double bonds in the *sn*-2 positioned FA moiety > (*e.g.* PE 18:0/18:2). Detected ether species were annotated with the prefix *O*- (*e.g.* PC *O*-34:2 or PC *O*-16:1/18:1).

5.1.12. Annotation of sphingolipid species

Yeast sphingolipid species were annotated either by their molecular composition or by sum formula, depending on the method of their structural characterization. To denote the molecular composition the following convention was applied: <Lipid class> <Number of carbon atoms in the long chain base moiety>:<Number of double bonds in the long chain base moiety >;<Number of hydroxyl groups in the long chain base moiety >/<Number of carbon atoms in the FA moiety>:<Number of double bonds in the FA moiety >;<Number of hydroxyl groups in the FA moiety>. For example, a peak at *m/z* 952.7 was identified as IPC 18:0;3/26:0;1 (Figure 24 page 54), *i.e.* as an inositolphosphoceramide, whose long chain base consisted of C18 phytosphingosine with no double bonds and 3 hydroxyl groups. Its amide-linked FA moiety comprised 26 carbon atoms, no double bonds and one hydroxyl group. If the composition of the FA moiety and long chain base were not separately determined, sphingolipids were characterized by the sum formula of their ceramide backbone: <Lipid class> <Number of carbon atoms in the ceramide backbone>:<Number of double bonds in the ceramide backbone>;<Number of hydroxyl groups in the ceramide backbone>. For example, a peak detected at *m/z* 938.7 was identified as IPC 42:1;5, *i.e.* as an inositolphosphoceramide containing a total of 42 carbon atoms, one double bond, and five hydroxyl groups in its entire ceramide backbone.

5.1.13. Lipid Profiler prototype software

Lipid Profiler software was developed in collaboration with MDS Sciex. The software operates together with Analyst software (MDS Sciex) to identify and quantify lipid species detected by MPIS. Optionally, it could also process spectra acquired on triple quadrupole and linear ion trap mass spectrometers (data not shown). It was written in Visual Basic and uses a stand-alone lipid database (Microsoft Access), which stores information on the *m/z* and fragment specificity of lipid classes and the applied precursor ion scans (*q.v.* Appendix). Lipid species were identified by matching, within a user-defined tolerance, the *m*/*z* of precursor ions detected in MPIS spectra to the candidate *m*/*z* calculated using the database. Lipid Profiler

software employed two isotopic correction algorithms to calculate the intensity of lipid precursors within overlapping isotopic clusters which are explained in (Ejsing *et al.*, 2006).

Absolute quantification of identified species relied upon a spiked mixture of synthetic internal standards having two diheptadecanoyl FA moieties: PA 17:0/17:0, PE 17:0/17:0, PG 17:0/17:0, PS 17:0/17:0, PC 17:0/17:0 and PI 17:0/17:0. The concentration of an endogenous lipid species of the PX class with the FA moieties FA_i and FA_j was calculated as:

$$[\mathrm{PX\ FA_i - FA_j}] = \frac{\mathrm{I(PX\ FA_i - FA_j)}}{\mathrm{I(PX\,17:0/17:0)}} \cdot [\mathrm{PX\,17:0/17:0}] \cdot \frac{\rho_{\mathrm{PX\,17:0/17:0}}}{\rho_{\mathrm{PX\ FAi-FAj}}},$$

where [PX 17:0/17:0] stands for the concentration of the internal standard of the same PX class; I(PX FA_i-FA_j) is the sum of intensities (or the areas) of the monoisotopic peaks of the corresponding precursor detected in the precursor ion scans specific for the FA moieties FA_i and FA_j; I(PX 17:0/17:0) is the intensity (area) of the monoisotopic peak of the precursor ion of the internal standard detected in the precursor ion scan specific for FA 17:0. The intensities (areas) of monisotopic peaks were adjusted to represent the total intensity of the isotopic cluster. To this end, they were multiplied by a factor equal to 1 / ρ, where ρ is the intensity of the monoisotopic peak relative to the total intensity of all peaks in the isotopic cluster calculated from the theoretical isotopic distribution of the corresponding lipid species.

The mol% of the quantified lipid species relative to all identified lipid species in the analyzed sample was calculated as:

$$\eta(\mathrm{PX\ FA_i - FA_j}) = \frac{[\mathrm{PX\ FA_i - FA_j}]}{\sum_{X,i,j} [\mathrm{PX\ FA_i - FA_j}]},$$

A workflow diagram of MPIS data processing by Lipid Profiler software is presented in Figure 39.

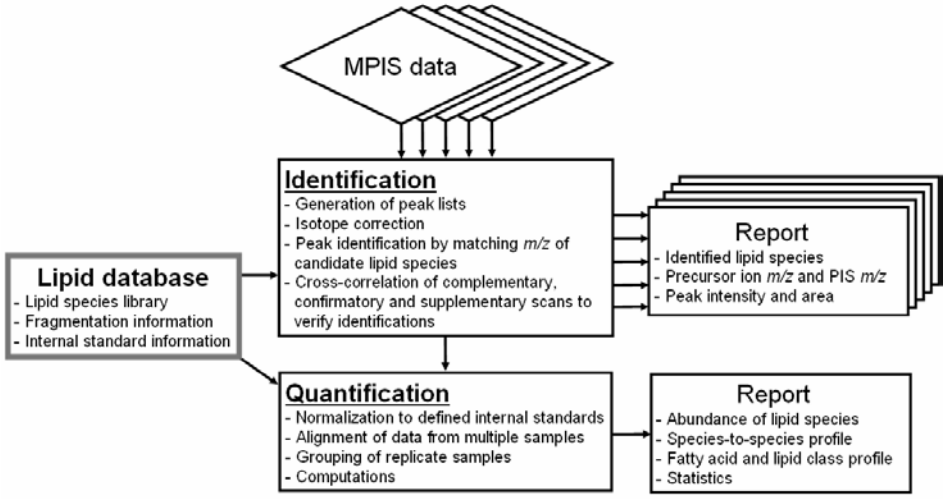

Figure 39. The workflow of automated processing of MPIS data by Lipid Profiler.

6. REFERENCES

AKESSON, B., J. ELOVSON, and G. ARVIDSON. 1970. Initial incorporation into rat liver glycerolipids of intraportally injected (9,10-3H2)palmitic acid. *Biochim Biophys Acta*. 218:44-56.

ARVIDSON, G.A. 1968. Biosynthesis of phosphatidylcholines in rat liver. *Eur J Biochem*. 5:415-21.

BABURINA, I., and S. JACKOWSKI. 1998. Apoptosis triggered by 1-O-octadecyl-2-O-methyl-rac-glycero-3-phosphocholine is prevented by increased expression of CTP:phosphocholine cytidylyltransferase. *J Biol Chem*. 273:2169-73.

BAGNAT, M., A. CHANG, and K. SIMONS. 2001. Plasma membrane proton ATPase Pma1p requires raft association for surface delivery in yeast. *Mol Biol Cell*. 12:4129-4138.

BAGNAT, M., S. KERANEN, A. SHEVCHENKO, and K. SIMONS. 2000. Lipid rafts function in biosynthetic delivery of proteins to the cell surface in yeast. *Proc Natl Acad Sci U S A*. 97:3254-3259.

BAGNAT, M., and K. SIMONS. 2002. Cell surface polarization during yeast mating. *Proc Natl Acad Sci U S A*. 99:14183-14188.

BECKEDORF, A.I., C. SCHAFFER, P. MESSNER, and J. PETER-KATALINIC. 2002. Mapping and sequencing of cardiolipins from Geobacillus stearothermophilus NRS 2004/3a by positive and negative ion nanoESI-QTOF-MS and MS/MS. *J Mass Spectrom*. 37:1086-94.

BLANK, M.L., M. ROBINSON, V. FITZGERALD, and F. SNYDER. 1984. Novel Quantitative Method for Determination of Molecular-Species of Phospholipids and Diglycerides. *Journal of Chromatography*. 298:473-482.

BLOM, T.S., M. KOIVUSALO, E. KUISMANEN, R. KOSTIAINEN, P. SOMERHARJU, and E. IKONEN. 2001. Mass spectrometric analysis reveals an increase in plasma membrane polyunsaturated phospholipid species upon cellular cholesterol loading. *Biochemistry*. 40:14635-14644.

BOUMANN, H.A., M.J.A. DAMEN, C. VERSLUIS, A.J.R. HECK, B. DE KRUIJFF, and A. DE KROON. 2003. The two biosynthetic routes leading to phosphatidylcholine in yeast produce different sets of molecular species. Evidence for lipid remodeling. *Biochemistry*. 42:3054-3059.

BOUMANN, H.A., B. DE KRUIJFF, A.J. HECK, and A.I. DE KROON. 2004. The selective utilization of substrates in vivo by the phosphatidylethanolamine and phosphatidylcholine biosynthetic enzymes Ept1p and Cpt1p in yeast. *FEBS Lett*. 569:173-7.

BROOKS, S., G.T. CLARK, S.M. WRIGHT, R.J. TRUEMAN, A.D. POSTLE, A.R. COSSINS, and N.M. MACLEAN. 2002. Electrospray ionisation mass spectrometric analysis of lipid restructuring in the carp (Cyprinus carpio L.) during cold acclimation. *J Exp Biol*. 205:3989-97.

BRUGGER, B., G. ERBEN, R. SANDHOFF, F.T. WIELAND, and W.D. LEHMANN. 1997. Quantitative analysis of biological membrane lipids at the low picomole level by nanoelectrospray ionization tandem mass spectrometry. *Proc Natl Acad Sci U S A*. 94:2339-2344.

BRUGGER, B., G. ERBEN, R. SANDHOFF, F.T. WIELAND, and W.D. LEHMANN. 1999. Quantitative analysis of biological membrane lipids at the low picomole level by nano-electrospray ionization tandem mass spectrometry (vol 94, pg 2339, 1997). *Proceedings of the National Academy of Sciences of the United States of America*. 96:10943-10943.

BRUGGER, B., B. GLASS, P. HABERKANT, I. LEIBRECHT, F.T. WIELAND, and H.G. KRASSLICH. 2006. The HIV lipidome: A raft with an unusual composition. *Proceedings of the National Academy of Sciences of the United States of America*. 103:2641-2646.

BRUGGER, B., C. GRAHAM, I. LEIBRECHT, E. MOMBELLI, A. JEN, F. WIELAND, and R. MORRIS. 2004. The membrane domains occupied by glycosylphosphatidylinositol-anchored prion protein and Thy-1 differ in lipid composition. *Journal of Biological Chemistry*. 279:7530-7536.

CASSERLY, I., and E. TOPOL. 2004. Convergence of atherosclerosis and Alzheimer's disease: inflammation, cholesterol, and misfolded proteins. *Lancet*. 363:1139-1146.

CHERNUSHEVICH, I. 2000. Duty cycle improvement for a quadrupole time-of-flight mass spectrometer and its use for precursor ion scans. *Eur J Mass Spectrom*. 6:471-479.

CHERNUSHEVICH, I., A. LOBODA, and B. THOMSON. 2001. An introduction to quadrupole time-of-flight mass spectrometry. *J Mass Spectrom*. 36:849-865.

COLE, R.B. 2000. Some tenets pertaining to electrospray ionization mass spectrometry. *J Mass Spectrom*. 35:763-772.

CONNOR, W.E., D.S. LIN, G. THOMAS, F. EY, T. DELOUGHERY, and N. ZHU. 1997. Abnormal phospholipid molecular species of erythrocytes in sickle cell anemia. *J Lipid Res*. 38:2516-2528.

CUI, Z., M. HOUWELING, M.H. CHEN, M. RECORD, H. CHAP, D.E. VANCE, and F. TERCE. 1996. A genetic defect in phosphatidylcholine biosynthesis triggers apoptosis in Chinese hamster ovary cells. *J Biol Chem*. 271:14668-71.

CUI, Z., J.E. VANCE, M.H. CHEN, D.R. VOELKER, and D.E. VANCE. 1993. Cloning and expression of a novel phosphatidylethanolamine N- methyltransferase. A specific biochemical and cytological marker for a unique membrane fraction in rat liver. *J Biol Chem*. 268:16655-63.

CUNNINGHAM, B.A., A.D. BROWN, D.H. WOLFE, W.P. WILLIAMS, and A. BRAIN. 1998. Ripple phase formation in phosphatidylcholine: Effect of acyl chain relative length, position, and unsaturation. *Phys Rev E*. 58:3662-3672.

DAVIS, M.M. 2002. A new trigger for T cells. *Cell*. 110:285-287.

DELONG, C.J., P.R.S. BAKER, M. SAMUEL, Z. CUI, and M.J. THOMAS. 2001. Molecular species composition of rat liver phospholipids by ESI-MS/MS: the effect of chromatography. *J Lipid Res*. 42:1959-1968.

DELONG, C.J., Y.J. SHEN, M.J. THOMAS, and Z. CUI. 1999. Molecular distinction of phosphatidylcholine synthesis between the CDP- choline pathway and phosphatidylethanolamine methylation pathway. *J Biol Chem*. 274:29683-8.

DICKSON, R.C., and R.L. LESTER. 1999a. Metabolism and selected functions of sphingolipids in the yeast *Saccharomyces cerevisiae*. *Biochim Biophys Acta*. 1438:305-321.

DICKSON, R.C., and R.L. LESTER. 1999b. Yeast sphingolipids. *Biochim Biophys Acta*. 1426:347-357.

DICKSON, R.C., and R.L. LESTER. 2002. Sphingolipid functions in *Saccharomyces cerevisiae*. *Biochim Biophys Acta*. 1583:13-25.

EATON, S. 2006. Release and trafficking of lipid-linked morphogens. *Current Opinion in Genetics & Development*. 16:17-22.

EISENKOLB, M., C. ZENZMAIER, E. LEITNER, and R. SCHNEITER. 2002. A specific structural requirement for ergosterol in long-chain fatty acid synthesis mutants important for maintaining raft domains in yeast. *Mol Biol Cell*. 13:4414-28.

EJSING, C.S., E. DUCHOSLAV, J. SAMPAIO, K. SIMONS, R. BONNER, C. THIELE, K. EKROOS, and A. SHEVCHENKO. 2006. Automated identification and quantification of glycerophospholipid molecular species by multiple precursor ion scanning. *Analytical Chemistry*. 78:6202-6214.

EKROOS, K., I.V. CHERNUSHEVICH, K. SIMONS, and A. SHEVCHENKO. 2002. Quantitative profiling of phospholipids by multiple precursor ion scanning on a hybrid quadrupole time-of-flight mass spectrometer. *Anal Chem*. 74:941-9.

EKROOS, K., C.S. EJSING, U. BAHR, M. KARAS, K. SIMONS, and A. SHEVCHENKO. 2003. Charting molecular composition of phosphatidylcholines by fatty acid scanning and ion trap MS3 fragmentation. *J Lipid Res*. 44:2181-2192.

EKROOS, K., and A. SHEVCHENKO. 2002. Simple two-point calibration of hybrid quadrupole time-of-flight instruments using a synthetic lipid standard. *Rapid Commun Mass Spectrom*. 16:1254-1255.

FAHY, E., S. SUBRAMANIAM, H.A. BROWN, C.K. GLASS, A.H. MERRILL, R.C. MURPHY, C.R.H. RAETZ, D.W. RUSSELL, Y. SEYAMA, W. SHAW, T. SHIMIZU, F. SPENER, G. VAN MEER, M.S. VANNIEUWENHZE, S.H. WHITE, J.L. WITZTUM, and E.A. DENNIS. 2005. A comprehensive classification system for lipids. *Journal of Lipid Research*. 46:839-861.

FILTHUTH, E., and H. EIBL. 1992. Synthesis of Enantiomerically Pure Lysophosphatidylinositols and Alkylphosphoinositols. *Chemistry and Physics of Lipids*. 60:253-261.

FRIDRIKSSON, E.K., P.A. SHIPKOVA, E.D. SHEETS, D. HOLOWKA, B. BAIRD, and F.W. MCLAFFERTY. 1999. Quantitative analysis of phospholipids in functionally important membrane domains from RBL-2H3 mast cells using tandem high-resolution mass spectrometry. *Biochemistry*. 38:8056-8063.

FUNATO, K., B. VALLEE, and H. RIEZMAN. 2002. Biosynthesis and trafficking of sphingolipids in the yeast *Saccharomyces cerevisiae*. *Biochemistry*. 41:15105-15114.

FUTERMAN, A.H., and Y.A. HANNUN. 2004. The complex life of simple sphingolipids. *Embo Reports*. 5:777-782.

GAIGG, B., T.B.F. NEERGAARD, R. SCHNEITER, J.K. HANSEN, N.J. FAERGEMAN, N.A. JENSEN, J.R. ANDERSEN, J. FRIIS, R. SANDHOFF, H.D. SCHRODER, and J. KNUDSEN. 2001. Depletion of acyl-coenzyme A-binding protein affects sphingolipid synthesis and causes vesicle accumulation and membrane defects in *Saccharomyces cerevisiae*. *Mol Biol Cell*. 12:1147-1160.

GARTON, S., L.V. MICHAELSON, F. BEAUDOIN, M.H. BEALE, and J.A. NAPIER. 2003. The dihydroceramide desaturase is not essential for cell viability in *Schizosaccharomyces pombe*. *FEBS Lett*. 538:192-196.

GAUS, K., E. CHKLOVSKAIA, B.F.S. GROTH, W. JESSUP, and T. HARDER. 2005. Condensation of the plasma membrane at the site of T lymphocyte activation. *Journal of Cell Biology*. 171:121-131.

GLISH, G.L., and R.W. VACHET. 2003. The basics of mass spectrometry in the twenty-first century. *Nat Rev Drug Discov*. 2:140-150.

GRIFFITHS, W.J. 2003. Tandem mass spectrometry in the study of fatty acids, bile acids, and steroids. *Mass Spectrometry Reviews*. 22:81-152.

GROSS, R.W., and B.E. SOBEL. 1980. Isocratic High-Performance Liquid-Chromatography Separation of Phosphoglycerides and Lysophosphoglycerides. *Journal of Chromatography*. 197:79-85.

GU, M., J.L. KERWIN, J.D. WATTS, and R. AEBERSOLD. 1997. Ceramide profiling of complex lipid mixtures by electrospray ionization mass spectrometry. *Anal Biochem*. 244:347-356.

HAAK, D., K. GABLE, T. BEELER, and T. DUNN. 1997. Hydroxylation of *Saccharomyces cerevisiae* ceramides requires Sur2p and Scs7p. *J Biol Chem*. 272:29704-29710.

HAINES, T.H. 2001. Do sterols reduce proton and sodium leaks through lipid bilayers? *Progress in Lipid Research*. 40:299-324.

HAN, X. 2002. Characterization and direct quantitation of ceramide molecular species from lipid extracts of biological samples by electrospray ionization tandem mass spectrometry. *Anal Biochem*. 302:199-212.

HAN, X., and R.W. GROSS. 1994. Electrospray ionization mass spectroscopic analysis of human erythrocyte plasma membrane phospholipids. *Proc Natl Acad Sci U S A*. 91:10635-9.

HAN, X., and R.W. GROSS. 2003. Global analyses of cellular lipidomes directly from crude extracts of biological samples by ESI mass spectrometry: a bridge to lipidomics. *J Lipid Res*. 44:1071-9.

HAN, X., K. YANG, J. YANG, K.N. FIKES, H. CHENG, and R.W. GROSS. 2006. Factors influencing the electrospray intrasource separation and selective ionization of glycerophospholipids. *J Am Soc Mass Spectrom*. 17:264-74.

HAN, X.L., and R.W. GROSS. 1995. Structural determination of picomole amounts of phospholipids via electrospray ionization tandem mass spectrometry. *J Am Soc Mass Spectrom*. 6:1202-1210.

HAN, X.L., and R.W. GROSS. 2005. Shotgun lipidomics: Electrospray ionization mass spectrometric analysis and quantitation of cellular lipidomes directly from crude extracts of biological samples. *Mass Spectrometry Reviews*. 24:367-412.

HAN, X.L., J.Y. YANG, H. CHENG, H.P. YE, and R.W. GROSS. 2004. Toward fingerprinting cellular lipidomes directly from biological samples by two-dimensional electrospray ionization mass spectrometry. *Analytical Biochemistry*. 330:317-331.

HARDER, T., and M. KUHN. 2000. Selective accumulation of raft-associated membrane protein LAT in T cell receptor signaling assemblies. *Journal of Cell Biology*. 151:199-207.

HARDMAN, M., and A.A. MAKAROV. 2003. Interfacing the orbitrap mass analyzer to an electrospray ion source. *Anal Chem*. 75:1699-1705.

HARTGROVES, L.C., J. LIN, H. LANGEN, T. ZECH, A. WEISS, and T. HARDER. 2003. Synergistic assembly of linker for activation of T cells signaling protein complexes in T cell plasma membrane domains. *Journal of Biological Chemistry*. 278:20389-20394.

HASHEMI, B.B., J.P. SLATTERY, D. HOLOWKA, and B. BAIRD. 1996. Sustained T cell receptor-mediated Ca2+ responses rely on dynamic engagement of receptors. *Journal of Immunology*. 156:3660-3667.

HECHTBERGER, P., and G. DAUM. 1995. Intracellular-transport of inositol-containing sphingolipids in the yeast *Saccharomyces cerevisiae*. *FEBS Lett*. 367:201-204.

HECHTBERGER, P., E. ZINSER, R. SAF, K. HUMMEL, F. PALTAUF, and G. DAUM. 1994. Characterization, quantification and subcellular localization of inositol-containing sphingolipids of the yeast Saccharomyces cerevisiae. *Eur J Biochem*. 225:641-649.

HEIKINHEIMO, L., and P. SOMERHARJU. 2002. Translocation of phosphatidylthreonine and -serine to mitochronida diminishes exponentially with increasing molecular hydrophobicity. *Traffic*. 3:367-377.

HERMANSSON, M., A. UPHOFF, R. KAKELA, and P. SOMERHARJU. 2005. Automated quantitative analysis of complex lipidomes by liquid chromatography/mass spectrometry. *Analytical Chemistry*. 77:2166-2175.

HSU, F.F., and J. TURK. 2000a. Characterization of phosphatidylinositol, phosphatidylinositol-4- phosphate, and phosphatidylinositol-4,5-bisphosphate by electrospray ionization tandem mass spectrometry: a mechanistic study. *J Am Soc Mass Spectrom*. 11:986-99.

HSU, F.F., and J. TURK. 2000b. Charge-driven fragmentation processes in diacyl glycerophosphatidic acids upon low-energy collisional activation. A mechanistic proposal. *J Am Soc Mass Spectrom*. 11:797-803.

HSU, F.F., and J. TURK. 2000c. Charge-remote and charge-driven fragmentation processes in diacyl glycerophosphoethanolamine upon low-energy collisional activation: a mechanistic proposal. *J Am Soc Mass Spectrom*. 11:892-9.

HSU, F.F., and J. TURK. 2001. Studies on phosphatidylglycerol with triple quadrupole tandem mass spectrometry with electrospray ionization: Fragmentation processes and structural characterization. *J Am Soc Mass Spectrom*. 12:1036-1043.

HSU, F.F., and J. TURK. 2002. Characterization of ceramides by low energy collisional-activated dissociation tandem mass spectrometry with negative-ion electrospray ionization. *J Am Soc Mass Spectrom*. 13:558-70.

HU, Q.Z., R.J. NOLL, H.Y. LI, A. MAKAROV, M. HARDMAN, and R.G. COOKS. 2005. The Orbitrap: a new mass spectrometer. *J Mass Spectrom*. 40:430-443.

HUNT, A.N., G.T. CLARK, J.R. NEALE, and A.D. POSTLE. 2002. A comparison of the molecular specificities of whole cell and endonuclear phosphatidylcholine synthesis. *FEBS Lett*. 530:89-93.

HVATTUM, E., G. HAGELIN, and A. LARSEN. 1998. Study of mechanisms involved in the collision-induced dissociation of carboxylate anions from glycerophospholipids using negative ion electrospray tandem quadrupole mass spectrometry. *Rapid Commun Mass Spectrom*. 12:1405-9.

IKONEN, E., and M. HOLTTA-VUORI. 2004. Cellular pathology of Niemann-Pick type C disease. *Seminars in Cell & Developmental Biology*. 15:445-454.

IUPAC-IUB. 1978. Nomenclature of Lipids - (Recommendations 1976) - Iupac-Iub-Commission-on-Biochemical-Nomenclature. *Biochemical Journal*. 171:21-35.

KATES, M. 1986. Techniques of lipidology . In RH Burdon & PH van Knippenberg (eds), Laboratory Techniques in Biochemistry and Molecular Biology. A.E.S. B.V., editor.

KAWAI, K., M. FUJITA, and M. NAKAO. 1974. Lipid components of two different regions of an intestinal epithelial cell membrane of mouse. *Biochim Biophys Acta*. 369:222-33.

KELLER, S.L., A. RADHAKRISHNAN, and H.M. MCCONNELL. 2000. Saturated phospholipids with high melting temperatures form complexes with cholesterol in monolayers. *J Phys Chem B*. 104:7522-7527.

KENT, C. 1995. Eukaryotic phospholipid biosynthesis. *Annu Rev Biochem*. 64:315-43.

KERWIN, J.L., A.R. TUININGA, and L.H. ERICSSON. 1994. Identification of molecular species of glycerophospholipids and sphingomyelin using electrospray mass spectrometry. *J Lipid Res*. 35:1102-14.

KOIVUSALO, M., P. HAIMI, L. HEIKINHEIMO, R. KOSTIAINEN, and P. SOMERHARJU. 2001. Quantitative determination of phospholipid compositions by ESI-MS: effects of acyl chain length, unsaturation, and lipid concentration on instrument response. *J Lipid Res*. 42:663-72.

KUERSCHNER, L., C.S. EJSING, K. EKROOS, A. SHEVCHENKO, K.I. ANDERSON, and C. THIELE. 2005. Polyene-lipids: A new tool to image lipids. *Nature Methods*. 2:39-45.

KUYPERS, F.A., P. BUTIKOFER, and C.H.L. SHACKLETON. 1991. Application of Liquid-Chromatography Thermospray Mass-Spectrometry in the Analysis of Glycerophospholipid Molecular-Species. *Journal of Chromatography-Biomedical Applications*. 562:191-206.

LANDS, W.E.M., and P. HART. 1965. Metabolism of glycerolipids. 6. Specificities of acyl coenzyme A - phospholipid acyltransferases. *J Biol Chem*. 240:1905-&.

LARSEN, A., S. URAN, P.B. JACOBSEN, and T. SKOTLAND. 2001. Collision-induced dissociation of glycero phospholipids using electrospray ion-trap mass spectrometry. *Rapid Commun Mass Spectrom*. 15:2393-8.

LEMBCKE, J., U. CEGLAREK, G.M. FIEDLER, S. BAUMANN, A. LEICHTLE, and J. THIERY. 2005. Rapid quantification of free and esterified phytosterols in human serum using APPI-LC-MS/MS. *Journal of Lipid Research*. 46:21-26.

LIEBISCH, G., M. BINDER, R. SCHIFFERER, T. LANGMANN, B. SCHULZ, and G. SCHMITZ. 2006. High throughput quantification of cholesterol and cholesteryl ester by electrospray ionization tandem mass spectrometry (ESI-MS/MS). *Biochim Biophys Acta*.

LIEBISCH, G., W. DROBNIK, M. REIL, B. TRUMBACH, R. ARNECKE, B. OLGEMOLLER, A. ROSCHER, and G. SCHMITZ. 1999. Quantitative measurement of different ceramide species from crude cellular extracts by electrospray ionization tandem mass spectrometry (ESI-MS/MS). *J Lipid Res*. 40:1539-1546.

LIEBISCH, G., B. LIESER, J. RATHENBERG, W. DROBNIK, and G. SCHMITZ. 2004. High-throughput quantification of phosphatidylcholine and sphingomyelin by electrospray ionization tandem mass spectrometry coupled with isotope correction algorithm. *Biochimica Et Biophysica Acta-Molecular and Cell Biology of Lipids*. 1686:108-117.

LINDEN, D., L. WILLIAM-OLSSON, A. AHNMARK, K. EKROOS, C. HALLBERG, H.P. SJOGREN, B. BECKER, L. SVENSSON, J.C. CLAPHAM, J. OSCARSSON, and S. SCHREYER. 2006. Liver-directed overexpression of mitochondrial glycerol-3-phosphate acyltransferase results in hepatic steatosis, increased triacylglycerol secretion and reduced fatty acid oxidation. *Faseb J*. 20:434-43.

LOWIN-KROPF, B., V.S. SHAPIRO, and A. WEISS. 1998. Cytoskeletal polarization of T cells is regulated by an immunoreceptor tyrosine-based activation motif-dependent mechanism. *Journal of Cell Biology*. 140:861-871.

LU, Y., S. HONG, E. TJONAHEN, and C.N. SERHAN. 2005. Mediator-lipidomics: databases and search algorithms for PUFA-derived mediators. *Journal of Lipid Research*. 46:790-802.

MAKAROV, A. 2000. Electrostatic axially harmonic orbital trapping: A high-performance technique of mass analysis. *Anal Chem*. 72:1156-1162.

MARCH, R.E. 1997. An introduction to quadrupole ion trap mass spectrometry. *J Mass Spectrom*. 32:351-369.

MERRILL, A.H., M.C. SULLARDS, J.C. ALLEGOOD, S. KELLY, and E. WANG. 2005. Sphingolipidomics: High-throughput, structure-specific, and quantitative analysis of sphingolipids by liquid chromatography tandem mass spectrometry. *Methods*. 36:207-224.

MONTIXI, C., C. LANGLET, A.M. BERNARD, J. THIMONIER, C. DUBOIS, M.A. WURBEL, J.P. CHAUVIN, M. PIERRES, and H.T. HE. 1998. Engagement of T cell receptor triggers its recruitment to low-density detergent-insoluble membrane domains. *Embo Journal*. 17:5334-5348.

MURPHY, R.C., J. FIEDLER, and J. HEVKO. 2001. Analysis of nonvolatile lipids by mass spectrometry. *Chemical Reviews*. 101:479-526.

NAGAN, N., and R.A. ZOELLER. 2001. Plasmalogens: biosynthesis and functions. *Progress in Lipid Research*. 40:199-229.

OH, C.S., D.A. TOKE, S. MANDALA, and C.E. MARTIN. 1997. ELO2 and ELO3, homologues of the Saccharomyces cerevisiae ELO1 gene, function in fatty acid elongation and are required for sphingolipid formation. *J Biol Chem*. 272:17376-17384.

OKUYAMA, H., K. YAMADA, and H. IKEZAWA. 1975. Accepton concentration effect in the selectivity of acyl coenzyme A: U aclglycerylphosphorylcholine acyltransferase system in rat liver. *J Biol Chem*. 250:1710-3.

OLSEN, J.V., L.M. DE GODOY, G. LI, B. MACEK, P. MORTENSEN, R. PESCH, A. MAKAROV, O. LANGE, S. HORNING, and M. MANN. 2005. Parts per million mass accuracy on an orbitrap mass spectrometer via lock-mass injection into a C-trap. *Mol Cell Proteomics*.

PETTITT, T.R., S.K. DOVE, A. LUBBEN, S.D.J. CALAMINUS, and M.J.O. WAKELAM. 2006. Analysis of intact phosphoinositides in biological samples. *Journal of Lipid Research*. 47:1588-1596.

PULFER, M., and R.C. MURPHY. 2003. Electrospray mass spectrometry of phospholipids. *Mass Spectrometry Reviews*. 22:332-364.

RENOOIJ, W., L.M. VAN GOLDE, R.F. ZWAAL, and L.L. VAN DEENEN. 1976. Topological asymmetry of phospholipid metabolism in rat erythrocyte membranes. Evidence for flip-flop of lecithin. *Eur J Biochem*. 61:53-8.

RODEMER, C., T.P. THAI, B. BRUGGER, T. KAERCHER, H. WERNER, K.A. NAVE, F. WIELAND, K. GORGAS, and W.W. JUST. 2003. Inactivation of ether lipid biosynthesis causes male infertility, defects in eye development and optic nerve hypoplasia in mice. *Human Molecular Genetics*. 12:1881-1895.

ROUSER, G., S. FKEISCHER, and A. YAMAMOTO. 1970. Two dimensional thin layer chromatographic separation of polar lipids and determination of phospholipids by phosphorus analysis of spots. *Lipids*. 5:494-6.

RUDOLPH, M.G., R.L. STANFIELD, and I.A. WILSON. 2006. How TCRs bind MHCs, peptides, and coreceptors. *Annual Review of Immunology*. 24:419-466.

SCHNEITER, R. 1999. Brave little yeast, please guide us to Thebes: sphingolipid function in *S. cerevisiae*. *Bioessays*. 21:1004-1010.

SCHNEITER, R., B. BRUGGER, R. SANDHOFF, G. ZELLNIG, A. LEBER, M. LAMPL, K. ATHENSTAEDT, C. HRASTNIK, S. EDER, G. DAUM, F. PALTAUF, F.T. WIELAND, and S.D. KOHLWEIN. 1999. Electrospray ionization tandem mass spectrometry (ESI-MS/MS) analysis of the lipid molecular species composition of yeast subcellular membranes reveals acyl chain-based sorting/remodeling of distinct molecular species en route to the plasma membrane. *J Cell Biol*. 146:741-754.

SCHULTZ, G.A., T.N. CORSO, S.J. PROSSER, and S. ZHANG. 2000. A fully integrated monolithic microchip electrospray device for mass spectrometry. *Anal Chem*. 72:4058-63.

SCHWUDKE, D., J. OEGEMA, L. BURTON, E. ENTCHEV, J.T. HANNICH, C.S. EJSING, T. KURZCHALIA, and A. SHEVCHENKO. 2006. Lipid profiling by multiple precursor and neutral loss scanning driven by the data-dependent acquisition. *Anal Chem*. 78:585-95.

SERHAN, C.N. 2005. Mediator lipidomics. *Prostaglandins & Other Lipid Mediators*. 77:4-14.

SERHAN, C.N., and J. SAVILL. 2005. Resolution of inflammation: The beginning programs the end. *Nature Immunology*. 6:1191-1197.

SERRANO, R. 1988. H+-ATPase from plasma membranes of *Saccharomyces cerevisiae* and *Avena sativa* roots - purification and reconstitution. *Methods Enzymol*. 157:533-544.

SHERMAN, F. 1991. Getting started with yeast. *Methods Enzymol*. 194:3-21.

SIMONS, K., and R. EHEHALT. 2002. Cholesterol, lipid rafts, and disease. *Journal of Clinical Investigation*. 110:597-603.

SIMONS, K., and W.L.C. VAZ. 2004. Model systems, lipid rafts, and cell membranes. *Annual Review of Biophysics and Biomolecular Structure*. 33:269-295.

SIMS, K.J., S.D. SPASSIEVA, E.O. VOIT, and L.M. OBEID. 2004. Yeast sphingolipid metabolism: clues and connections. *Biochem. Cell Biol.* 82:45-61.

SMITH, S.W., and R.L. LESTER. 1974. Inositol phosphorylceramide, a novel substance and the chief member of a major group of yeast sphingolipids containing a single inositol phosphate. *J Biol Chem*. 249:3395-3405.

SOMMER, U., H. HERSCOVITZ, F.K. WELTY, and C.E. COSTELLO. 2006. LC-MS-based method for the qualitative and quantitative analysis of complex lipid mixtures. *Journal of Lipid Research*. 47:804-814.

SPERLING, P., and E. HEINZ. 2003. Plant sphingolipids: structural diversity, biosynthesis, first genes and functions. *Biochim Biophys Acta*. 1632:1-15.

STAACK, R.F., E. VARESIO, and G. HOPFGARTNER. 2005. The combination of liquid chromatography/tandem mass spectrometry and chip-based infusion for improved screening and characterization of drug metabolites. *Rapid Communications in Mass Spectrometry*. 19:618-626.

STEEN, H., B. KUSTER, M. FERNANDEZ, A. PANDEY, and M. MANN. 2001. Detection of tyrosine phosphorylated peptides by precursor ion scanning quadrupole TOF mass spectrometry in positive ion mode. *Anal Chem*. 73:1440-8.

THOMAS, M.C., T.W. MITCHELL, and S.J. BLANKSBY. 2006. Ozonolysis of phospholipid double bonds during electrospray ionization: A new tool for structure determination. *Journal of the American Chemical Society*. 128:58-59.

VAN HEUSDEN, G.P., C.P. REUTELINGSPERGER, and H. VAN DEN BOSCH. 1981. Substrate specificity of lysophospholipase-transacylase from rat lung and its action on various physical forms of lysophosphatidylcholine. *Biochim Biophys Acta*. 663:22-33.

VAN MEER, G. 2005. Cellular lipidomics. *Embo Journal*. 24:3159-3165.

VANCE, D., and J. VANCE. 1996. New Comprehensive Biochemistry Volume 31: Biochemistry of Lipids, Lipoproteins and Membranes. *Amsterdam: Elsevier Science B.V*.

VEATCH, S.L., and S.L. KELLER. 2003. Separation of liquid phases in giant vesicles of ternary mixtures of phospholipids and cholesterol. *Biophysical Journal*. 85:3074-3083.

WAITE, K.A., and D.E. VANCE. 2000. Why expression of phosphatidylethanolamine N-methyltransferase does not rescue Chinese hamster ovary cells that have an impaired CDP-choline pathway. *J Biol Chem*. 275:21197-202.

WALKEY, C.J., L. YU, L.B. AGELLON, and D.E. VANCE. 1998. Biochemical and evolutionary significance of phospholipid methylation. *J Biol Chem*. 273:27043-6.

WENK, M.R. 2005. The emerging field of lipidomics. *Nature Reviews Drug Discovery*. 4:594-610.

WENK, M.R., L. LUCAST, G. DI PAOLO, A.J. ROMANELLI, S.F. SUCHY, R.L. NUSSBAUM, G.W. CLINE, G.I. SHULMAN, W. MCMURRAY, and P. DE CAMILLI. 2003. Phosphoinositide profiling in complex lipid mixtures using electrospray ionization mass spectrometry. *Nature Biotechnology*. 21:813-817.

YAMASHITA, A., T. SUGIURA, and K. WAKU. 1997. Acyltransferases and transacylases involved in fatty acid remodeling of phospholipids and metabolism of bioactive lipids in mammalian cells. *J Biochem (Tokyo)*. 122:1-16.

YOUNG, M.E., T.S. KARPOVA, B. BRUGGER, D.M. MOSCHENROSS, G.K. WANG, R. SCHNEITER, F.T. WIELAND, and J.A. COOPER. 2002. The Sur7p family defines novel cortical domains in *Saccharomyces cerevisiae*, affects sphingolipid metabolism, and is involved in sporulation. *Mol Cell Biol*. 22:927-934.

YU, L.J., Y. CHEN, M.P. DENINNO, T.N. O'CONNELL, and C. HOP. 2005. Identification of a novel glutathione adduct of diclofenac, 4 '-hydroxy-2 '-glutathion-deschloro-diclofenac, upon incubation with human liver microsomes. *Drug Metabolism and Disposition*. 33:484-488.

ZAMFIR, A., Z. VUKELIC, L. BINDILA, J. PETER-KATALINIC, R. ALMEIDA, A. STERLING, and M. ALLEN. 2004. Fully-automated chip-based nanoelectrospray tandem mass spectrometry of gangliosides from human cerebellum. *Journal of the American Society for Mass Spectrometry*. 15:1649-1657.

ZEMSKI BERRY, K.A., and R.C. MURPHY. 2004. Electrospray ionization tandem mass spectrometry of glycerophosphoethanolamine plasmalogen phospholipids. *J Am Soc Mass Spectrom*. 15:1499-508.

ZHANG, S., and C.K. VAN PELT. 2004. Chip-based nanoelectrospray mass spectrometry for protein characterization. *Expert Rev Proteomics*. 1:449-68.

ZHANG, W.G., R.P. TRIBLE, and L.E. SAMELSON. 1998. LAT palmitoylation: Its essential role in membrane microdomain targeting and tyrosine phosphorylation during T cell activation. *Immunity*. 9:239-246.

ZHANG, X., and G.E. REID. 2006. Multistage tandem mass spectrometry of anionic phosphatidylcholine lipid adducts reveals novel dissociation pathways. *International Journal of Mass Spectrometry*. 252:242-255.

7. APPENDIX: LIST OF FRAGMENT IONS

Table 1A. FA and lipid class-specific fragment ions commonly used for MPIS in negative ion mode.

Fragment ion	*m/z*	Specific detection of
[Glycerolphosphate – H_2O]$^-$	153.0	PA/PG/PS/PI
[Cholinephosphate – 15]$^-$	168.0	PC/LPC
FA 10:0	171.1	glycerophospholipid species
FA 11:0	185.2	glycerophospholipid species
[ethanolaminephosphate – H_2O]$^-$	196.0	PE/LPE
FA 12:0	199.2	glycerophospholipid species
FA 13:1	211.2	glycerophospholipid species
O-14:1	211.2	plasmenyl species
FA 13:0	213.2	glycerophospholipid species
[Inositolphosphate – $2H_2O$]$^-$	223.0	PI
[dimethylethanolaminephosphate – H_2O]$^-$	224.1	PC/LPC/dimethylphosphoethanolamine
FA 14:1	225.2	glycerophospholipid species
FA 14:0	227.2	glycerophospholipid species
FA 15:2	237.2	glycerophospholipid species
O-16:2	237.2	plasmenyl species
FA 15:1	239.2	glycerophospholipid species
O-16:1	239.2	plasmenyl species
[Inositolsphophate – H_2O]$^-$	241.0	PI
FA 15:0	241.2	glycerophospholipid species
FA 16:2	251.2	glycerophospholipid species
FA 16:1	253.2	glycerophospholipid species
FA 16:0	255.2	glycerophospholipid species
FA 20:5-CO_2	257.2	glycerophospholipid species
[Inositolphosphate]$^-$	259.0	PI
FA 20:4-CO_2	259.2	glycerophospholipid species
FA 17:2	265.2	glycerophospholipid species
O-18:2	265.3	plasmenyl species
FA 17:1	267.2	glycerophospholipid species
O-18:1	267.3	plasmenyl species
FA 17:0	269.3	glycerophospholipid species
FA 18:3	277.2	glycerophospholipid species
FA 18:2	279.2	glycerophospholipid species
FA 18:1	281.3	glycerophospholipid species
FA 22:6-CO_2	283.2	glycerophospholipid species
FA 18:0	283.3	glycerophospholipid species
FA 22:5-CO_2	285.3	glycerophospholipid species
FA 22:4-CO_2	287.3	glycerophospholipid species
FA 19:2	293.3	glycerophospholipid species
O-20:2	293.3	plasmenyl species
O-20:1	295.3	plasmenyl species
FA 19:1	295.3	glycerophospholipid species
FA 19:0	297.3	glycerophospholipid species
FA 20:5	301.2	glycerophospholipid species
FA 20:4	303.2	glycerophospholipid species
FA 20:3	305.2	glycerophospholipid species
FA 20:2	307.3	glycerophospholipid species
FA 20:1	309.3	glycerophospholipid species
FA 20:0	311.3	glycerophospholipid species
FA 22:6	327.2	glycerophospholipid species
FA 22:5	329.2	glycerophospholipid species
FA 22:4	331.3	glycerophospholipid species
FA 22:3	333.3	glycerophospholipid species
FA 22:2	335.3	glycerophospholipid species
FA 22:1	337.3	glycerophospholipid species
FA 22:0	339.3	glycerophospholipid species
FA 26:0	395.4	glycerophospholipid species

8. PUBLICATIONS

- Ekroos K, **Ejsing CS**, Bahr U, Karas M, Simons K, Shevchenko A.

  Charting molecular composition of phosphatidylcholines by fatty acid scanning and ion trap MS^3 fragmentation

  J Lipid Res. 2003 Nov;44(11):2181-92

  Equal contributions by Ekroos and Ejsing.

- Kuerschner L, **Ejsing CS**, Ekroos K, Shevchenko A, Anderson KI, Thiele C.

  Polyene-lipids: a new tool to image lipids

  Nat Methods. 2005 Jan;2(1):39-45

- **Ejsing CS**, Moehring T, Bahr U, Duchoslav, Karas M, Simons K, Shevchenko A.

  Collision-induced dissociation pathways of yeast sphingolipids and their molecular profiling in total lipid extracts: a study by quadrupole TOF and linear ion trap-orbitrap mass spectrometry

  J Mass Spectrom. 2006 Mar;41(3):372-89.

- **Ejsing CS**, Duchoslav E, Simons K, Thiele C, Ekroos K, Shevchenko A.

  Automated identification and quantification of glycerophospholipid molecular species by multiple precursor ion scanning

  Anal Chem. 2006 Sep 1;78(17):6202-14.

- Özcan N, **Ejsing CS**, Lipski A, Morbach S, Shevchenko A, Krämer R

  Activitiy modulation of the betaine transporter BetP from *Corynebacterium glutamicum* by changes in osmolality, temperature and lipid surrounding

  Submitted

9. ACKNOWLEDGMENTS

I thank my advisors Kai Simons and Andrej Shevchenko for providing the facilities and resources I needed throughout this thesis study, for their educational conversations and putting their trust in me.

I am indebted to my friends and colleagues; Kim Ekroos, Robin Klemm, Vineeth Surendranath, Julio Sampaio for their collaboration, kind support and advice in many aspects of life and the work I carried out. I thank all group members of the Simons and Shevchenko laboratories for their expert advice, critical discussions and assistance. Thanks to Michel Bagnat and Tomasz Proszynski for providing me with yeast strains. I thank Ms. Judith Nicholls and Dominik Schwudke for their critical reading of manuscripts.

I especially thank Eva Duchoslav and Ron Bonner for the indispensable collaboration which fostered the Lipid Profiler software. I am grateful to Igor Chernushevich and Lyle Burton for their expert advice on quadrupole time-of-flight mass spectrometry and data processing.

I am grateful to Christoph Thiele for synthesizing PI 17:0/17:0 and his constructive comments. I thank Lars Kuerschner for the interesting and fruitful collaboration on the metabolism of polyene-lipids. I thank Gerhard Liebisch for his technical assistance with the cholesterol quantification and the comparison of our methodologies. Thanks to Uta Bahr and Thomas Möhring for their kind assistance with ion trap mass spectrometry. A special thanks to Reinaldo Almeida and Mark Baumert for their expert advice on NanoMate HD System operation.

I thank Tobias Zech and Thomas Harder for the collaboration on charting the lipid composition of TCR signaling domains. I thank Nuran Özcan, Reinhard Krämer, Ching-Ju Tsai and Christine Ziegler for the collaborative studies on activity modulation and crystallization of the betaine transporter BetP from *Corynebacterium glutamicum*.

I am grateful to Bernard Hoflack and Michael Karas for reviewing my thesis.

Finally, I would like to thank my parents, my brother and my grandparents for supporting me throughout my life, for providing me the foundation for what I have accomplished today. And, thank you, Dalma, for loving me!

10. DECLARATION ACCORDING TO § 5.5

I herewith declare that I have produced this paper without the prohibited assistance of third parties and without making use of aids other than those specified; notions taken over directly or indirectly from other sources have been identified as such. This paper has not previously been presented in identical or similar form to any other German or foreign examination board.

The thesis work was conducted from 1.10.2003 to 16.10.2006 under the supervision of Kai Simons and Andrej Shevchenko at the Max Planck Institute of Molecular Cell Biology and Genetics, Dresden.

Dresden, 16. October 2006

Christer Stenby Ejsing